Seeding Properties of Amyloid-beta and Tau in the Cerebrospinal Fluid

Inauguraldissertation

zur

Erlangung der Würde eines Doktors der Philosophie

vorgelegt der

Philosophisch-Naturwissenschaftlichen Fakultät

der Universität Basel

von

Zhiva Kalinova Skachokova

von Bulgarien

Zürich, 2018

Genehmigt von der Philosophisch-Naturwissenschaftlichen Fakultät auf Antrag von

Prof. Markus Rüegg
Dr. Dr. David Winkler
Prof. Bernhard Bettler

Basel, 24.05.2016

Prof. Dr. J. Schibler

Preface

The following dissertation was written by the author. The 'Results' part consists of two published manuscripts, a manuscript in preparation and additional preliminary data. In (Skachokova et al. 2015) the author executed the experiments, analysis and writing of the manuscript. In (Ozcelik, Sprenger, Skachokova et al. 2016) the author contributed with some of the experiments, analysis and final writing, as additionally stated (see 'Results' part). The additional data is a result of own work.

Basel, May 2016

Table of Contents

Summary

Alzheimer's disease (AD) is the most common neurodegenerative disorder, and its prevalence is still increasing. However, currently there are no treatment options available, nor reliable presymptomatic biomarkers for its diagnosis. Neuropathologically, AD is characterized by aggregates (plaques and cerebrovascuar deposits; and tangles) composed of two different proteins: amyloid-β (Aβ) and tau, respectively. Brain derived Aβ and tau exhibit prion-like properties, as based on recent studies.

Small and soluble Aβ species have been identified as the most potent Aβ seeds, and they may be present in the CSF which could be of a diagnostic value. Injection of CSF obtained from AD patients into APP23 transgenic mice however did not result into induction or acceleration of amyloidosis, indicating that human CSF Aβ is not seed competent, in contrast to brain Aβ (Fritschi et al. 2014). In order to test this hypothesis further, we injected susceptible mice with APP23 mice' CSF, containing Aβ at higher amounts than the human CSF, and sacrificed the mice after longer seeding time. As a result, we did not see a significant seeding effect, confirming that CSF Aβ does not show relevant prion-like properties *in vivo*.

Next, we looked at the prion-like properties of tau in the CSF. Since tau concentration in the CSF increases with progression of AD, unlike Aβ levels, it is possible that seeding competent tau species might reach the CSF compartment. For this purpose, we collected CSF from aged, tangle-bearing P301S mice and injected it into young, pretangle stage P301S mice. As a result, we observed significantly higher number of hyperphosphorylated tau inclusions in the injected hippocampus, indicating that CSF tau can induce tau hyperphosphorylation in the host mice. This could be indicative of an early prion-like seeding response. We then investigated whether CSF obtained from human tauopathy patients could induce tau aggregation using the same methodology. The collection of human CSF samples as well as the analysis of human CSF seeded mice is still ongoing.

Tau protein fragments have been identified in both the CSF and the brain of AD patients, however it is not clear what is their role in the progression of the disease. Recent studies suggest that tau fragmentation, rather than aggregation per se, may play an important role in neurodegeneration. To study the relation between truncated and full-length tau *in vivo* and shed more light on this question, we used an inducible mouse line expressing truncated 3R tau, and crossed it with full-length tau-expressing mice (3R, or 4R with and without a mutation). As a result, mice exhibited severe neuronal loss and motor palsy in the absence of tau aggregation. However, they recovered once the expression of fragmented tau was ceased, except for the 3R-expressing mice. This shows the importance of fragmented tau for toxicity and points at new therapeutic targets in the treatment of tauopathies.

Taken together, the results presented here point at the possible use of CSF tau in the development of future AD diagnostic essays, and implicate tau truncation as a potential pharmacological target in tauopathies.

Introduction

Alzheimer's disease is a progressive neurodegenerative disorder with an increasing prevalence and deleterious life consequences. It was first described by Alois Alzheimer more than a century ago, and even though our understanding of the disease has grown substantially since then, current treatment option is still lacking (Fig. 1). This, together with AD's better mechanistic understanding, presymptomatic diagnosis and finally prevention, is one of the challenges facing contemporary biomedical research and our society, as a whole.

Alzheimer's disease

Epidemiology and risk factors

There are currently 40 million people living with dementia worldwide, and this number is expected to double every 20 years, as developing countries are at increasing risk with their younger populations (Prince et al. 2013). Alzheimer's disease (AD) is the most common type of dementia, with roughly 30% of early onset dementia cases (before 65 years of age) being attributed to AD (Lambert et al. 2014). In Switzerland alone, there are more than 100 000 AD patients at present, and 3 times more are expected by 2050 (Blankman et al. 2012). Also, there is a trend for decreasing age-specific incidence of dementia during the last years, probably explained by lowering vascular risk factors among others, indicating the complexity of the disease. There are few known genes implicated in a small subpopulation of cases, however the majority of AD cases are sporadic, due to yet unknown cause(s).
Age is the main risk factor for dementia and AD, however, a variety of lifestyle factors have been implicated in the disease pathogenesis as well. Those include cardiovascular health, diabetes, obesity, physical and mental activity, depression, smoking and level of education. However, their exact roles in the disease are yet to be elucidated as AD develops over a long preclinical period of several decades and those may be rather causalities (Scheltens et al. 2016).

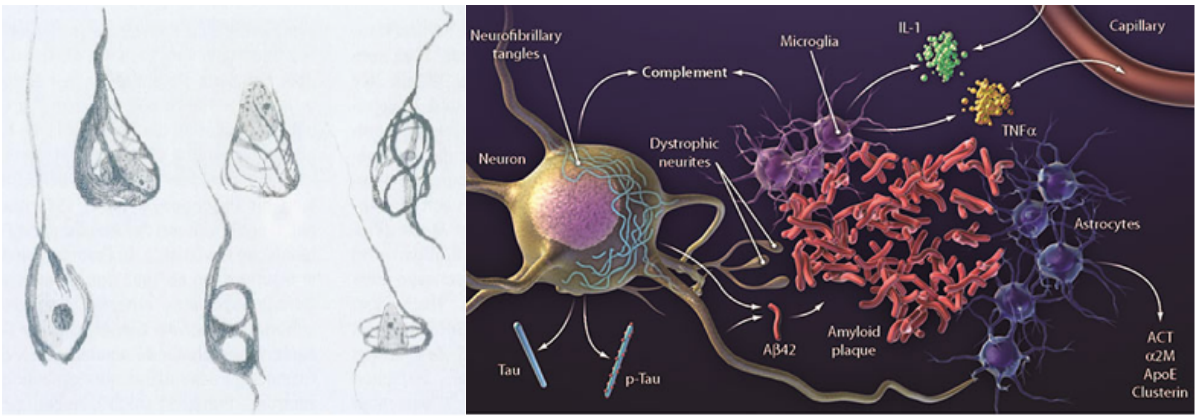

Figure 1. Original drawing by Alois Alzheimer (left) from 1907 showing the neurofibrillary lesions present in the brain of his patient, and a schematic drawing illustrating most molecules and cellular processes involved in AD known today (right; adapted from (Holtzman et al. 2011)). Despite increased understating of the mechanisms and risk factors involved, the exact cause leading to AD is still unknown.

Symptoms

The first ever described AD patient, Auguste Deter, died in the year 1907 while exhibiting no sense of time and place, impaired episodic memory, delusions, disrupted sleep and temporary vegetative states, and became ultimately completely dependent on others (Alzheimer et al. 1907). A century later she was diagnosed as a carrier of presenilin 1 (PSEN1) mutation and so exhibited a rare form of an early, genetic AD (Muller et al. 2013). In current clinical practice aged individuals with (sporadic) AD can have similar complaints, mainly memory disturbances and executive dysfunction, but also in some atypical cases language and visual problems which may precede memory impairment. Current clinical diagnosis depends not only on neuropsychological testing, but also on a set of criteria including brain imaging (MRI, PET) and CSF biomarkers (McKhann et al. 2011).

Genetic risk factors

A few mutations have been linked to the rare familial forms of AD, implicating amyloid beta and tau as the main mediators in the disease (Fig. 2). Amyloid precursor protein (APP) is the precursor of Aβ, and different mutations in the gene affect Aβ production and aggregation (Scheltens et al. 2016). PSEN1 and PSEN2 regulate gamma-secretase, which cleaves APP. Mutations in PSEN lead to the generation of longer Aβ peptides, and have been associated with early disease onset and more rapid progression (Scheuner et al. 1996). Mutations in *Tau* gene cause neurodegeneration without the formation of amyloid plaques, as seen in patients with Frontotemporal dementia. The interplay of Aβ and tau is still a matter of debate, most likely they both act in parallel causing AD (Small & Duff 2008).
In the sporadic AD, the major genetic risk factors known so far is the APOE4 allele, as in homozygous individuals it increases the risk of AD by 50% (Genin et al. 2011). APOE has been implicated in Aβ clearance (Castellano et al. 2011). In addition, genes involved in immune system and inflammation, together with lipid metabolism have been identified as linked to AD (Guerreiro & Hardy 2014).

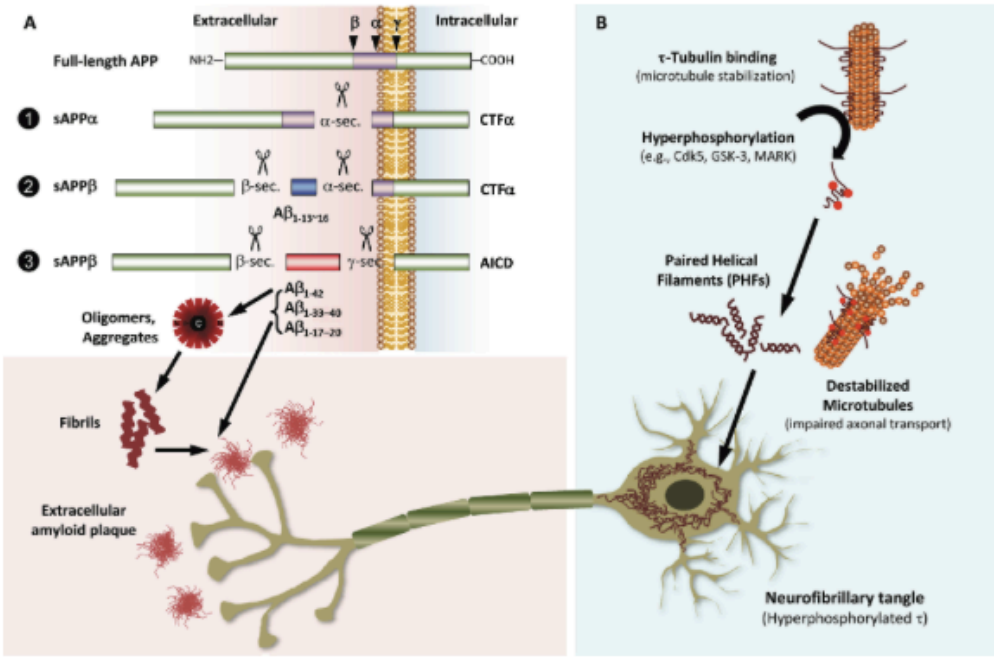

Figure 2. APP misprocessing together with tau hyperphosphorylation and other post translational modifications have been implicated in their aggregation and subsequent cell death, as seen in AD. Adapted from (Kang et al. 2013).

Diagnosis

At present, diagnosis of dementia is based on neuropsychological testing, brain imaging and the use of CSF biomarkers (Cummings et al. 2004). Currently AD diagnostic use MRI to assess changes in cortical thickness, hippocampal volume and vascular brain changes (Frisoni et al. 2010). In addition, PET scan which measures glucose uptake by neurons and indicates early synaptic changes is a valuable diagnostic tool for dementia (Perani et al. 2014). PET with Aβ ligands is relatively novel and with high accuracy, however it has mostly exclusionary value, as brain amyloidosis also occurs in healthy aged people (Marchant et al. 2012). As a result, Aβ imaging is costly and cannot alone provide a definite diagnosis.
CSF is in a constant exchange with the brain interstitial fluid, which is in a direct contact with the neurons. In this sense, characterization of CSF proteins may describe molecular events occurring in the live neurons, and could help our understanding of neurodegenerative diseases (Fig. 3). CSF biomarkers routinely used in AD diagnosis are amyloid-β (showing cortical amyloid deposition), total tau (intensity of neurodegeneration), and phosphorylated tau (correlated with neurofibrillary pathology) (Blennow et al. 2010a). They have high sensitivity and specificity (85-90%), and allow to differentiate AD from mild cognitive impairment stage in patients (Shaw et al. 2009). However, standardization of CSF analysis for routine laboratory use is still ongoing and there is significant measurements variability at present (Scheltens et al. 2016).
Finally, the combination of imaging and CSF markers has a good positive and good negative predictive value to differentiate AD from normal aging in patients with mild cognitive impairment.

Analysis sample	Biomarker	BIPED classification	Relationship with pathology
CSF	t-tau	B,D	Increased in AD, indicates the neuronal degeneration
	p-tau	B,D	Increased in AD, reflects the formation of tangles
	Aβ42	B,D	Reduced in the onset stage of AD, it remains unchanged after onset of AD
	Aβ oligomers	B,D	Increased in AD
	APPs-a	B,D	Soluble APPa is decreased in AD
	APPs-β	B,D	APPs-β is a product of APP cleavage by BACE-1; it cannot discriminate normal from AD
	APLIβ	B,D	Fragments generated by β- and r-secretase are increased in AD
	α-Synuclein	B,D	There is an inverse relationship between severity of disease and α-synuclein, it increases rapidly after neuron death in DLB
	BACE-1	B,D	Increased activity in MCI but not AD

Figure 3. Present CSF biomarkers for dementias. Adapted from (Wang et al. 2012).

Pathology

Alois Alzheimer first described the senile plaques and neurofibrillary tangles (NFTs) typical of the disease (Fig. 4) (Alzheimer et al. 1906). Today we know that the cerebral plaques consist of Aβ peptide, and neurofibrillary tangles are composed of tau protein (Hardy & Selkoe 2002). The pathology precedes and may parallel the observed neurodegeneration (i.e. neuronal cell loss and atrophy). However, the exact link between protein aggregation and toxicity is still unclear. Neuronal lesions primarily in the perirhinal and entorhinal cortex, the hippocampus and the cerebral cortex (Mouton et al. 1998), as well as synaptic and dendritic loss parallel the disease development (Terry et al. 1991). While the pathological lesions were considered main players in AD pathogenesis before, more and more evidences suggest the importance of pre-aggregation factors in Aβ and tau toxicity.

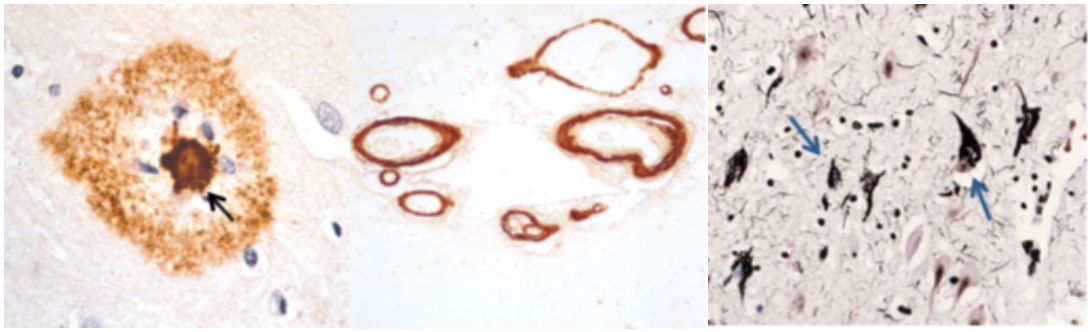

Figure 4. AD pathological hallmarks are senile plaques in the brain made out of Aβ protein (left image), Aβ deposition in the blood vessel walls (middle), and NFTs made of aggregated tau protein (right). Images adapted from Basler Neuropathology and (Castellani et al. 2004).

Amyloid-β

Aβ is the main component of senile plaques, extracellular deposits typical of AD that are surrounded by dystrophic neurites, activated microglia and reactive astrocytes (Masters et al. 1985; Selkoe et al. 1986, Probst et al. 1991). In addition to brain parenchyma, they may be also present in the walls of blood vessels and periarteriolar channels, a condition known as cerebral amyloid angiopathy (CAA) (Tagliavini et al. 1988). Aβ is a 4 kDa large protein made of 39-43 amino acids, which results from the proteolysis of the amyloid precursor

protein (APP) (Cappai & White 1999) (Fig. 5). APP is a transmembrane glycoprotein, which is proteolytically cleaved by the membrane associated enzymes alpha-, beta- and gamma-secretase. Cleavage of APP by beta-secretase followed by gamma-secretase (via the amyloidogenic pathway) results in the generation of a highly fibrillogenic Aβ peptide. This process requires the presence of proteins and enzymes such as BACE1, presenilin complex, nicastrin, and others.

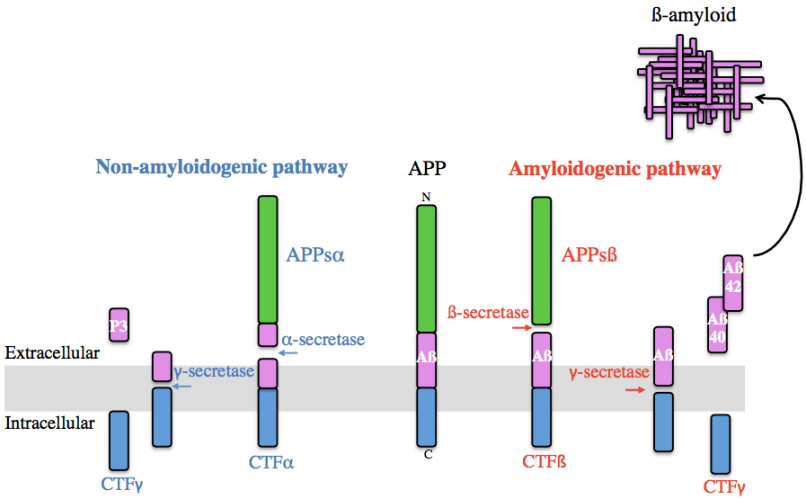

Figure 5. Schematic representation of APP processing and Aβ production**.** Adapted from (Kahle & De Strooper 2003)**.**

The aggregation of Aβ peptide is thought to be an early event that drives Alzheimer's disease pathogenesis and begins at least a decade before clinical symptoms are detected. The idea that the pathogenesis of AD is driven by the aggregation of Aβ fibrils, the so called "amyloid cascade" hypothesis, has been first suggested in 1991 (Chartier-Harlin et al. 1991). According to it, the progression of the disease, including formation of neurofibrillary lesions, microglia activation, synaptic dysfunction and neuronal loss, would be an outcome of an imbalance between Aβ production and clearance. However, abundant cortical Aβ deposits have been found in cognitively healthy elderly individuals, questioning the role of Aβ aggregation in memory loss and cell toxicity (Dickson et al. 1992). Several studies support a modification of the amyloid cascade hypothesis and suggest that Aβ assembly into neurotoxic oligomers, and not into amyloid plaques, is the major toxic effector in AD pathogenesis (Klein et al. 2001). Most probably fibrillar amyloid plaques serve as a container for the amyloid oligomers or constitute a pool of sequestered soluble and precipitated Aβ. They would, therefore, have a protective role or simply constitute the end stage of the Aβ cascade (Masters et al. 2006).

Amyloid-β transgenic mice

To better understand AD pathophysiology, different transgenic mice lines have been created. Animals overexpressing human APP are widely used to model aspects of AD *in vivo*, since they develop Aβ plaques progressively with the age. Some of the first APP transgenic

mice described are the APP23 line, carrying human *APP* gene with a known London mutation, located near the beta-secretase cleavage site (Sturchler-Pierrat et al. 1997). At 6 months of age, these mice start developing plaques, which cover up to 25% of their neocortex and hippocampus by 24 months of age. They also exhibit dystrophic neurites, activated microglia and reactive astrocytes in proximity to the plaques. NFTs are lacking, however they also develop CAA (Winkler et al. 2010), and show memory impairment at an early age, mirroring some aspects of AD (Kelly et al. 2003). APP transgenic mice are a useful model in acquiring basic understanding of Aβ pathology, but also in the development of diagnostic and therapeutic tools.

Tau

Another hallmark of AD pathology is the intracellular accumulation of hyperphosphorylated tau protein in NFTs or neuropil threads (NT). Tau is a soluble protein normally located in the axons, that promotes microtubules stability in neuronal cells. However, in pathological conditions, it becomes hyperphosphorylated, may localize in the dendrites and soma, where it may form intracellular aggregates. Tau's relationship with Aβ - whether parallel or downstream, is still a matter of debate (Small & Duff 2008). However, tau pathology can be present independently of Aβ in a variety of neurodegenerative disorders known as tauopathies, including progressive supranuclear palsy (PSP), corticobasal degeneration (CBD), and frontotemporal dementia (FTD) (Goedert et al. 2010; Mandelkow & Mandelkow 2011; Jucker & Walker 2013a). Indeed, mutation in the tau gene was first identified in cases of frontotemporal dementia caused by tau mutation (FTDP-17, Goedert et al. 2010). Tauopathies may exhibit different morphologies of tau aggregation, but they are all characterized by changes in personality and social conduct, and neuropathologically by the presence of NFTs and neuronal loss (Fig. 6).

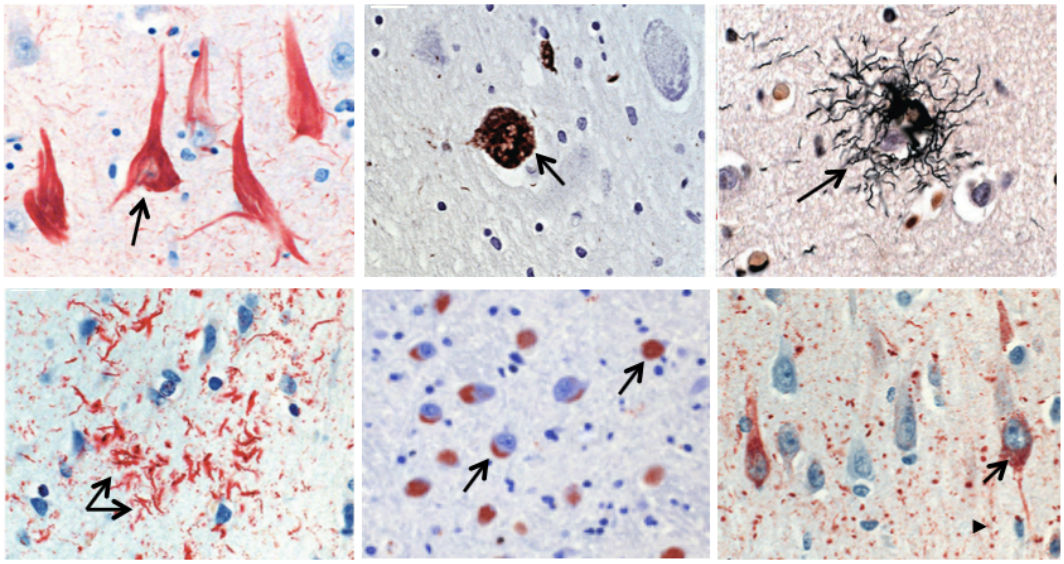

Figure 6. Variety of aggregated tau morphotypes in tauopathies. From upper left corner, clockwise: tau hyperphosphorylation as seen in AD; Gallyas positive globose tangle, AD; silver stained tufted actrocyte in PSP;

hyperphosphorylated tau in Argyrophilic grain disease; hyperphosphorylated tau forming pick bodies in Pick's diseas; hyperphosphorylated tau in astrocytic plaques in CBD. Images adapted from (Neumann et al. 2009).

The importance of tau for cellular functioning is reflected in its structural diversity. Tau is encoded by the *MAPT* gene, located on the chromosome 17, and exists in six different isoforms in the adult human brain, products of alternative splicing of exons 2, 3 and 10 (Goedert et al. 1989). The six isoforms differ by the presence or absence of either three (3R tau) or four (4R tau) microtubule-binding domains, and by the number of amino terminal (N- terminal) inserts. In parallel, the alternative splicing of exons 2 and 3 results in the absence (0N) or presence of one (1N) or two (2N) insert(s) of 29 amino acids in the half N-terminal part of tau. Thereby, alternative splicing allows for six different combinations corresponding to isoforms containing longest 441 aa tau (4R2N), 410 aa (3R2N), 412 aa (4R1N), 381 aa (3R1N), 393 aa (4R0N) and the shortest, 352 aa (3R0N) (Fig. 7).

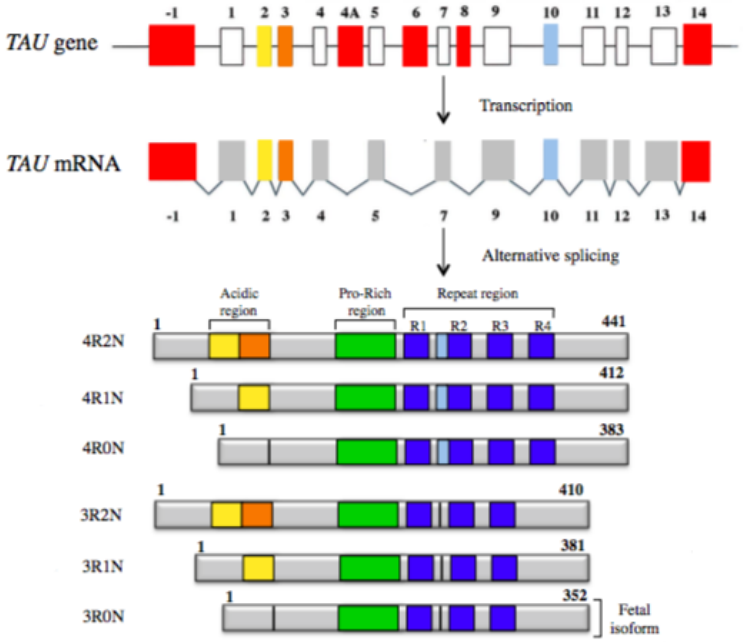

Figure 7. Schematic representation of the human *MAPT (TAU)* gene, mRNA, and all the 6 tau protein isoforms as a result of alternative splicing. Adapted from (Buée *et al*. 2000).

Tau is expressed in both central and peripheral nervous system and consists of an N-terminal acidic portion followed by a proline-rich region and a C-terminal tail, which is the basic part of the protein. Tau protein binds to the microtubules through the repeat regions (R1-R4), and is involved in tubulin polymerization and microtubules stabilization and maintenance of flexibility (Fig. 8). Thereby, tau is important for the maintenance of axonal transport and cell trafficking, and its function is regulated by different kinases and phosphatases (Weingarten et al. 1975; Bohm et al. 1990).

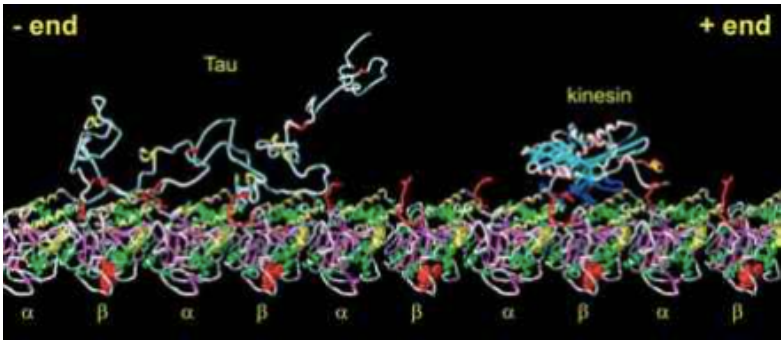

Figure 8. Model of microtubule profilament with attached Tau and kinesin. Tau is flexibly bound to tubulin, providing microtubules dynamic stability, while kinesin is involved in transport along the microtubules. Adapted from (Stamer et al. 2002)**.**

Tau is subjected to diverse post-translational modifications such as phosphorylation, glycosylation, ubiquitination or truncation. Their role in tau aggregation is still to be clarified.

Tau phosphorylation

Phosphorylation of tau is controlled by an equilibrium of a set of protein kinases and phosphatases. Dysfunction of this balance leads to the abnormal tau phosphorylation seen in AD. Two main domains have been distinguished, depending on whether the Ser/Thr phosphorylation site targeting by the kinase is followed by a proline residue or not. Proline-directed kinases include the tau protein kinase I (also called glycogen synthase kinase 3, GSK3), tau protein kinase II (cdk5), kinases of the MAPK (p38) or JNK families, as well as other stress kinases, such as cdc2. In parallel, the protein kinase A (PKA), protein kinase C (PKC), calmodulin (CaM) kinase II, microtubule-affinity regulating kinase (MARK) and casein kinase II (CKII), which modifies residues close to acidic residues mainly in protein region corresponding to exons 2 and 3, define the non-proline-directed kinases (Correas et al. 1992). It is thought that changes in the phosphorylation of tau play an important role in the regulation of tau function by modifying its affinity to microtubules, and tau hyperphosphorylation has been linked to pathogenesis (Götz et al. 1995).

Tau fragmentation

The relation between tau aggregation and toxicity is still unclear. Tau truncation may be associated with tau aggregation as truncated forms of tau have been detected in paired helical filaments (PHFs) in AD brains (Mena et al. 1996). Truncated tau has also been implicated in cognitive decline in patients (Rohn et al. 2002; Fasulo et al. 2000). It has been suggested that hyperphosphorylation of tau appears before its cleavage and that fragmentation occurs before NFT formation (Mondragón-Rodríguez et al. 2008). *In vitro* experiments have revealed that tau truncated at its C-terminal domain was more toxic than the full-length form of tau, most probably due to its faster and greater aggregation propensity (Abraha et al. 2000). Furthermore, truncation of tau in the N-terminal region has been previously reported and this truncation may promote tau aggregation, although its pathological significance remains to be proven (Horowitz et al. 2004). The progression of AD correlates with the extent of tau fragmentation and precedes NFT formation (García-

Sierra et al. 2012). Together, these data put emphasis on the pathophysiological importance of truncated tau in AD, which is of importance for the development of novel therapeutic tools.
Further analyses suggest that hyperphosphorylated tau or oligomeric tau is involved in synaptic loss, whereas granular tau is responsible for neuronal loss. Thus, different forms of tau may be involved in different pathological changes that occur in tauopathies (Takashima 2013).

Tau transgenic mice

In order to study tau pathology in AD and tauopathies in general, tau transgenic animals have been created. Transgenic mice carrying a FTDP-17 mutation in the *MAPT* gene, as seen in familial forms of frontotemporal dementia (P301S mice), develop a progressive motor deficit, which is related to the abundance of NFTs in the brainstem and spinal cord (Allen et al. 2002). These filaments contain hyperphosphorylated tau protein. While in FTDP-17 patients nerve and glial cells are affected (Bugiani et al. 1999), in P301S mice the accumulation of tau is restricted to nerve cells which is due to the selective neuronal expression of the tau transgene by the Thy 1.2 promoter. This mouse model highlights the role of tau in neurodegenerative diseases and is currently being used for the development of therapeutic and diagnostic strategies against tauopathies.

It is important to note that the formation of NFTs is not responsible *per se* for neurodegeneration or neuronal death. In rat models expressing fragmented human tau (3R or 4R), there was accumulated tau in the brainstem and cortex, and the animals developed muscle weakness and wasting (Zilka et al. 2006; Filipcik et al. 2009). These studies highlight the role of truncated tau in the development of pathologic condition possibly by increasing the propensity for tau accumulation. Better understanding of tau truncation and its role in tau toxicity and aggregation is needed in order to develop more efficient treatment strategies.

Prion like properties of amyloid-β and tau

Proteins are an essential block of the cellular architecture and preserving their correct structure enables proper cell functioning and survival. Hence, it is crucial for the cell to have an efficient quality control system of protein production, folding and elimination (Fig. 9). Prions are infectious agents consisting of misfolded prion proteins, that when misshapen, can trigger the aggregation of benign prion proteins in a chain-reaction, acting like corruptive templates (seeds). They can cause variety of diseases such as Creutzfeldt-Jakob disease, fatal familial insomnia, kuru, scrapie, etc., and can be of genetic, infectious or sporadic origin (Jucker & Walker 2013b). However, they all lead to neurodegeneration.

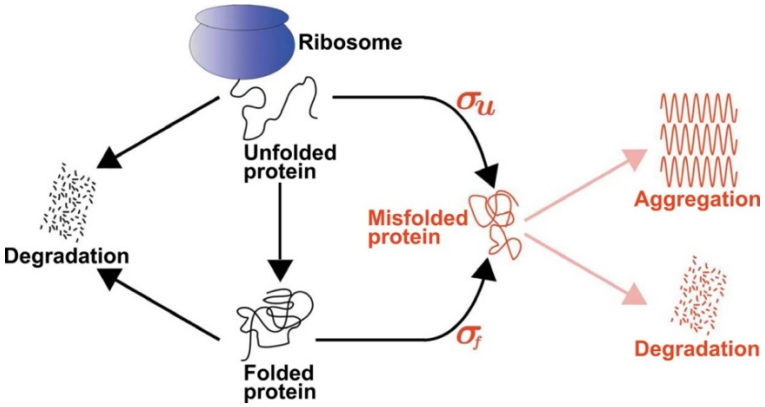

Figure 9. Protein metabolism in the cell in a normal and pathologic (red) condition. Adapted from (Ciryam et al. 2013)**.**

Amyloid-β and tau, together with alpha-synuclein, TDP-43 and other proteins implicated in neurodegenerative disorders, collectively termed amyloids due to their property to misfold, have been lately recognized as having prion-like behavior. This is due to the fact that they are β-sheet rich proteins that are thermodynamically stable, have the potential to aggregate and this has been linked to toxicity, and they also exhibit strain specificities. Most importantly, they can seed naive amyloidogenic protein molecules with β-sheet rich aggregates of a similar protein, similar to prions (Jucker & Walker 2013b). However, they substantially differ from prions due to the lack of an infectious agent and the presence of genetic factors implicated in AD (Lahiri 2012).
Amyloid formation in vitro starts with a slow nucleation phase that leads to the formation of the initial nucleus of an amyloid fibril (Harper & Lansbury 1997). After this slow nucleation phase amyloid formation occurs rapidly by recruiting more soluble molecules and inducing their abnormal conformation (Fig. 10). With increasing size, the amyloid fibril has a tendency to break and form new prion-like seeds. These in vitro observations of amyloid formation have recently been translated to *in vivo* models for both Aβ and tau.

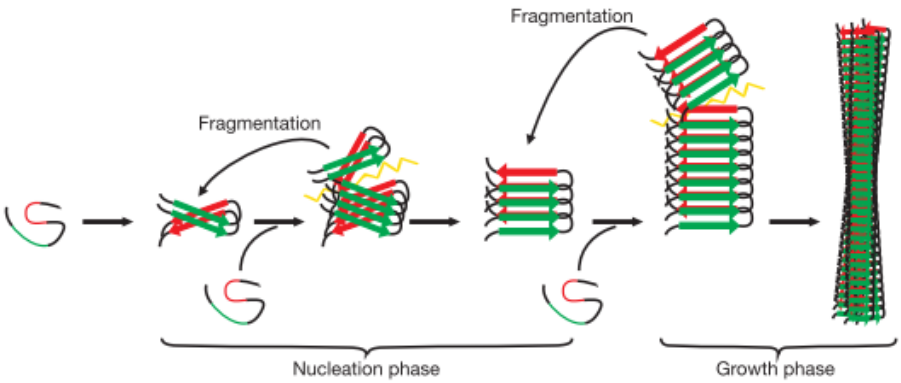

Figure 10. Amyloid formation starts with a nucleation phase (seed formation) by the addition of monomers and oligomers that are conformationally converted, until a more stable growth phase is reached, leading finally to fibrils formation. The growing fibril can break and then cause the nucleation of additional molecules, in a self-propagating manner (seeding). Adapted from (Jucker & Walker 2013b).

Amyloid-β seeding

Evidence for Aβ seeding derives from human and animal studies. Intracerebral or peripheral injection of brain extracts from AD patients or from aged APP transgenic mice induced amyloidosis prematurely in APP transgenic mice (Kane et al. 2000; Meyer-Luehmann et al. 2006; Eisele et al. 2010). Injection of Aβ brain extracts in one brain region caused amyloidosis in synaptically connected regions (Hamaguchi, 2012), indicating that Aβ deposition can spread throughout the brain. It has been suggested, that the induction of amyloid-β aggregation depends on both the seed concentration and the host expressing human Aβ (Meyer-luehmann et al. 2006).
In AD patients, Aβ pathology starts in the frontal cortex and slowly progresses towards the midbrain and brain stem (Fig. 11) (Braak & Braak 1991). Lately, it was reported that injections of human pituitary-derived growth hormone caused amyloid depositions in 4 out of 8 patients that died from iatrogenic Creutzfeld-Jakob disease (Jaunmuktane et al. 2015). However, it is unclear whether the injected material contained also Aβ seeds. In addition, seeding with sporadic or heritable AD derived brain homogenates resulted in a differential pathology, indicating the presence of distinct Aβ strains (Watts et al. 2014).
Taken together, these studies suggest that aggregation of Aβ can be seeded in susceptible hosts in a way similar to the molecular templating of prions.

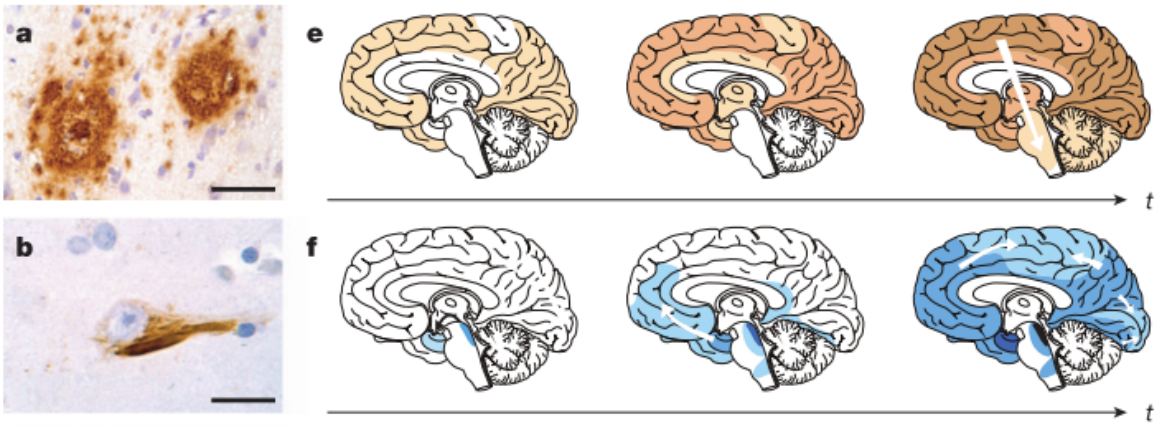

Figure 11. Propagation of Aβ plaques (a, e) or tau NFTs (b, f) as a function of age and disease progression, as based on autopsy studies of AD patient brains. Adapted from (Jucker & Walker 2013b).

Tau seeding

Similar to Aβ, tau aggregation can be experimentally induced and transmitted. Tau propagates from one brain region to another in a specific pattern in AD patients, and this correlates with their cognitive decline (Nelson et al. 2012). NFTs pathology starts from the perirhinal/entorhinal cortex (EC), followed by the hippocampus and finally the neocortex, following existing anatomical connections between regions (Fig. 10) (Braak & Braak 1997). In addition, propagation of tau pathology can be induced experimentally in animal models. Injection of brain extracts from human P301S tau transgenic mice into wild type tau transgenic mice, that normally do not develop NFTs, induced the aggregation of the wild type tau and tangles formation (Clavaguera et al. 2009). Also, injection of recombinant tau

fibrils or brain extracts containing aggregated tau caused formation of NFTs that propagated from the injection site to connected brain regions in a stereotypic and time dependent manner (Iba et al. 2013; Ahmed et al. 2014). This suggests that the pathological tau protein conformation can be transmitted and locally propagated in a way similar to prions (Frost & Diamond 2009). Tau seeds can be of different sizes, from full length to small soluble fragments (Iba et al. 2013; Lasagna-Reeves et al. 2012). In addition, injections of brain extracts from various tauopathies in mice can induce tau pathology similar to the one of the corresponding human disease, indicating the presence of various tau strains (Clavaguera et al. 2013).

Aβ and tau seeding is a hot topic of research and our understanding of their molecular behavior is slowly expanding. How could this be used in a clinical setting, e.g. for improving existing diagnostic methods?

Limitations of present AD biomarkers and research questions

Present biomarkers are based on decrease of neuronal integrity and loss of cognitive function, reflecting late stage of the disease. According to the hypothetical model of dynamic biomarkers in AD, amyloid and/or tau deposition precedes clinical symptoms by decades and occurs before biomarker detectable pathology and/or neurodegeneration occurs (Fig. 12) (Rosen et al. 2010). What is needed are biomarkers to reflect very early changes in neuronal integrity, that could also be used to efficiently measure efficacy of drugs tested against AD. Novel biomarkers of dementias should focus on detection of very early stages of the disease, which will allow treatment at an earlier time point and assist in the selection of patients at risk for progression (Wang et al. 2012).
Reliable early AD markers, that predict the disease occurrence, and not only its progression, are still missing (Blennow et al. 2010b; Blennow et al. 2014). In this sense, better understanding of Aβ and tau in the CSF and improving its diagnostic application is of a growing importance.

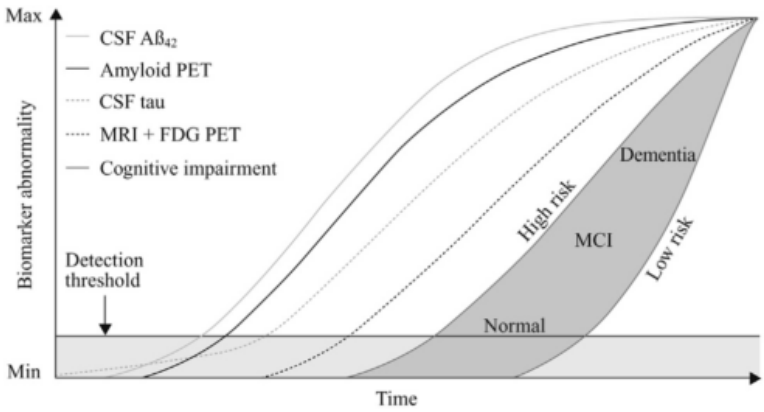

Figure 12. Hypothetical model for biomarkers in AD. Currently detection is possible at the beginning of cognitive impairment in patients, as earliest markers are a drop in CSF Aβ levels and abnormal PET scan. However, by this time pathological changes in the brain have already started. Adapted from (Blennow et al. 2014).

Amyloid-β in CSF

Reduced levels of Aβ42, as well as increased retention of amyloid-β binding agents (Pittsburgh compound B) in the brain during PET scan, are used in current clinical practice to identify AD patients (Brys et al. 2009; Blennow et al. 2012). In addition, level of Aβ42 in CSF obtained postmortem inversely correlate with cortical plaque load (Tapiola et al. 2009). Taken together, this suggests that decreased CSF concentration of Aβ reflects an already present amyloid deposition in the brain. Also, it has been sown that in APP23 transgenic mice levels of Aβ40 and Aβ42 in the CSF decrease significantly with age, in parallel to the appearance of senile plaques (Maia et al. 2013).

Could CSF Aβ act like a seed?

Aβ aggregation can be induced due to the prion-like properties of Aβ. In fact, the most potent Aβ seeds identified so far in brain extracts from APP23 mice are small and soluble Aβ assemblies (Langer et al. 2011). These findings suggest that soluble Aβ in the human brain are also potent seeds, and that such seeds may be found in bodily fluids such as CSF. In this case, they could serve as an early diagnostic biomarker for cerebral amyloidogenesis.

In order to test this hypothesis, our collaborators injected CSF from AD patients into APP23 transgenic mice. However, they did not observe any induction or acceleration of amyloidosis, indicating that human CSF Aβ is not seed-competent, in contrast to brain Aβ (Fritschi et al. 2014). In order to test this further, we injected susceptible mice with APP23 mice derived CSF, containing Aβ at higher amounts than the human CSF, and sacrificed the mice after longer seeding time. As a result, we did not see a seeding effect, confirming that CSF Aβ does not show prion-like properties *in vivo* (Skachokova et al. 2015).

Tau in CSF

In contrast to Aβ, tau levels in the CSF increase during AD progression (Blennow et al. 2014). It has been shown, that CSF phospho-tau correlates with the amount of cortical NFTs pathology in live patients (Tapiola et al. 2009). CSF total tau is thought to be a more dynamic marker, reflecting the intensity of neuronal damage, and higher CSF total tau has been associated with faster progression from MCI to AD in demented patients (Samgard et al. 2010). Higher CSF tau has been linked to AD and Creutzfeld-Jakob disease, presumably as a result of neuronal death. CSF phospho-tau possibly reflects the formation of tangles in the brain and the phosphorylation state of tau.
In symptomatic FTD patients carrying a *MAPT* mutation, CSF tau levels are slightly elevated but are significantly lower than in AD patients, indicating that tau release is modified by changes in the tau protein that are associated with tauopathies (Karch et al. 2012).
Evidences mostly based on *in vitro* studies suggest that tau can be actively secreted from the cells, even in the absence of disease or toxicity, and in addition it has been detected in the CSF and interstitial fluid (ISF) in humans and mice models (Yamada et al. 2011; Kang et

al. 2013). The exact mechanism of tau secretion is not clear yet, but tau has been detected in exosomes of healthy and AD patients (Saman et al. 2012; Pooler et al. 2013), implicating exosomal release as a possibility.

Because of the low amount of tau in CSF there are rather contradictory results derived from western blot, ELISA, chromatography and mass spectrometry studies, regarding tau structure. One study identified N-terminal and mid domain tau fragments in the CSF, however no fragments containing the C-terminal or the 4R MTBR region were present (Jr et al. 2013). At the same time, a recent mass spectrometry analysis revealed significantly more abundant mid-domain tau, compared to the C- and N-terminals (Barthélemy et al. 2016). Truncated tau may be present in the CSF of AD patient, however this is still a topic of research, and better understanding of tau fragmentation, seeding and aggregation is needed.

Could CSF tau act like a seed?

There are numerous experiments demonstrating that brain-derived tau can induce and accelerate the aggregation of the host tau. Soluble tau is physiologically present in the CSF, which is clinically more accessible than brain biopsies, however it is not known whether tau there is in an aggregated, seed like state, which could be of a diagnostic significance. To test this, we collected CSF from tangle-bearing P301S mice and injected it into young pretangle stage P301S mice. As a result, we observed significantly higher number of aggregated and hyperphosphorylated tau in the injected hippocampus, indicating that CSF tau has seed like properties (*see* Skachokova et al. 2016, *in preparation*). In a follow up study, we tested whether human AD CSF could induce tau aggregation using the same method, however our results are still inconclusive (*see* additional data).

Could fragmented tau increase the toxicity of full length tau?

The relevance of tau fragmentation for neurodegeneration and AD pathogenesis is not clear, and especially the relationship between truncated and full-length tau. To study this, we generated an inducible mouse line expressing truncated 3R tau, and crossed it with full-length tau carrying mice (3R mice, or 4R mice with and without a mutation). As a result, double transgenic mice exhibited severe neuronal loss and motor palsy, however recovered once the expression of fragmented tau was ceased, except for 3R expressing mice (Ozcelik et al. 2016). This shows the importance of fragmented tau for toxicity and points at new therapeutic targets.

Aim

Alzheimer's disease (AD) is a deleterious neurodegenerative disorder with an increasing prevalence. Currently, there are neither reliable early diagnostic markers nor available cure.

AD is characterized by the aggregation of Aβ and tau proteins. Based on previously demonstrated prion-like characteristics of brain derived Aβ and tau, here we tested 1) whether CSF Aβ from plaque bearing mice could exhibit seed-like properties *in vivo,* 2) whether P301S mice CSF tau or 3) human AD CSF tau could harbor seeding potential when injected into susceptible mice, and 4) the importance of tau fragmentation in disease toxicity.

These research results could serve for the development of early diagnostic bioassays and novel treatment options against AD.

Results

Amyloid-β in the cerebrospinal fluid of APP transgenic mice does not show prion-like properties

Current Alzheimer Research, 2015, *12*, 886-891

Send Orders for Reprints to reprints@benthamscience.ae

886 *Current Alzheimer Research*, 2015, *12*, 886-891

Amyloid-β in the Cerebrospinal Fluid of APP Transgenic Mice Does not Show Prion-like Properties

Zhiva Skachokova[1,2], Frederik Sprenger[1,2], Karin Breu[1,2], Dorothee Abramowski[3], Florence Clavaguera[1], Jürgen Hench[1], Matthias Staufenbiel[3,4], Markus Tolnay[1] and David T. Winkler[1,2,*]

[1]*Institute of Pathology, University Hospital Basel, Basel, Switzerland;* [2]*Department of Neurology, University Hospital Basel, Basel, Switzerland;* [3]*Institute of Biomedical Research, Novartis Pharma AG, Basel, Switzerland;* [4]*Department of Cellular Neurology, Hertie Institute for Clinical Brain Research, University of Tübingen, Tübingen, Germany*

Abstract: Early diagnosis of Alzheimer's disease (AD) is currently difficult and involves a complex approach including clinical assessment, neuroimaging, and measurement of amyloid-β (Aβ) and tau levels in cerebrospinal fluid (CSF). A better mechanistic understanding is needed to develop more accurate and even presymptomatic diagnostic tools. It has been shown that Aβ derived from amyloid-containing brain tissue has prion-like properties: it induces misfolding and aggregation of Aβ when injected into human amyloid precursor protein (APP) transgenic mice. In contrast, Aβ in the CSF has been less studied, and it is not clear whether it also exhibits prion-like characteristics, which might provide a sensitive diagnostic tool. Therefore, we collected CSF from APP transgenic mice carrying the Swedish mutation (APP23 mice), and injected it intracerebrally into young mice from the same transgenic line. We found that CSF derived Aβ did not induce increased β-amyloidosis, even after long incubation periods and additional concentration. This suggests that Aβ present in the CSF does not have the same prion-like properties as the Aβ species in the brain.

Keywords: Alzheimer's disease, amyloid-beta, Aβ, prion, cerebrospinal fluid, diagnostics, transgenic mouse models.

1. INTRODUCTION

Alzheimer's disease (AD) is the most common neurodegenerative disorder, and while its prevalence is increasing [1], curative treatment options are still lacking. In the course of AD, amyloid-β (Aβ) aggregates to form extracellular plaques, while hyperphosphorylated tau protein constitutes intracellular neurofibrillary tangles. The aggregation of Aβ is thought to be an early event that drives AD pathogenesis and begins at least a decade before clinical symptoms emerge [2-5].

In routine clinical practice, diagnosis of AD is often late and of limited accuracy [6]. At present, levels of Aβ and tau in the cerebrospinal fluid (CSF) are used as biomarkers of AD within a multimodal diagnostic approach [7, 8]. However, the validity of CSF biomarkers and their use for early or even presymptomatic diagnosis of AD is still a matter of debate. At the same time, an increasing number of experimental studies suggest that the aggregation of the proteins involved in AD pathogenesis occurs by a self-propagating process during which misfolded proteins act as templates, inducing misfolding and aggregation of native molecules [9-12]. As this self-propagating propensity is shared with prions, these proteins have been termed prion-like [13], even though they substantially differ from prions in their pathomechanisms [14, 15]. Aβ present in brain homogenates derived from AD patients or plaque-bearing amyloid precursor protein (APP) transgenic mice induces and/or accelerates Aβ deposition when injected into susceptible mouse models, in a prion-like manner [16-20]. This suggests that the pathological protein conformation can be transmitted and locally propagated a process we refer to here as 'seeding'.

Transgenic mice overexpressing human APP are widely used to model aspects of AD *in vivo*, since they develop Aβ plaques progressively with the age and have been established as a seeding model [16-18]. At the same time, little is known about the presence of pathological Aβ variants in their CSF. Such molecules could serve as sensitive early AD diagnostic markers. In a recent study, Fritschi *et al.* [21] demonstrated that CSF from both AD patients and APP transgenic mice lack *in vivo* seeding activity. Here we investigate this question further by injecting murine CSF into young APP mice and analyzing them after very long seeding times and inoculation of highly concentrated CSF. Even under these conditions, we didn't observe a significant increase in Aβ aggregation, neither at the injection site nor within the injected hippocampus, suggesting a low to absent prion-like activity of the Aβ forms present in the CSF.

*Address correspondence to this author at the Institute of Pathology, University Hospital Basel, Basel, Switzerland; Tel: 0041 61 265 25 25; Fax: 0041 61 265 41 00; E-mail: david.winkler@usb.ch

1875-5828/15 $58.00+.00

2. METHODS

2.1. Mice

We used heterozygous APP23 transgenic mice [22], expressing human APP (751-aa isoform) containing the Swedish mutation under the control of the Thy-1.2 promoter. All experiments were approved by the University of Basel Ethics and Animal Care and Use Committees. Initial qualitative data of a subset of the mice used for the present analysis has been included in a previous study [21]. An overview of all the mice included in the study is provided in Table **S1**.

2.2. Stereotaxic Injections

Three months old APP23 mice (n=20) and non-transgenic C57BL6 (n=10) control mice were anaesthetized with a mixture of ketamine (10 mg/kg) and xylazine (20 mg/kg) and placed on a heating pad to maintain body temperature during surgery. Mice were injected in the right hippocampus (A/P, −2.5 mm from bregma; L, − 2.0 mm; D/V, −1.8 mm) using a Hamilton syringe, as previously reported [23]. Each received a unilateral stereotaxic injection of 5 µl at a speed of 1.25 µl/min. Mice were monitored until recovery from anesthesia and checked regularly following surgery.

2.3. CSF Sampling

For CSF sampling we used 3, 18 and 24 months old APP23 and C57BL6 mice (n=45). CSF was collected by puncturing the cisterna magna after deeply anesthetizing the animals, as previously described [24]. Next it was spun down at 2500 rpm for 2 min and the supernatant was collected and immediately frozen. Visibly blood contaminated CSF was discarded. For injections, CSF from 3 mice at the same age was pooled. For concentration, pooled CSF from 5-7 mice was lyophilized and later resuspended with a reduced volume of sterile H_2O.

2.4. Immunohistochemistry

Following 11 to 21 months from the date of injection, mice were deeply anaesthetized with pentobarbital (100 mg/kg) and killed by transcardial perfusion with cold PBS, followed by 4% paraformaldehyde in PBS. The brains were dissected and post-fixed overnight. 4 µm coronal sections were prepared following paraffin embedding. For immunohistochemical analysis, sections were deparaffinized, pretreated with 100% formic acid for 5 min, blocked with 10% normal horse serum and incubated overnight with an anti-Aβ 82E1 antibody (human N-terminal specific, 1:1000, *Demeditec Diagnostics GmbH*). For detection we used the Vectastain ABC Peroxidase kit (*Vector Laboratories*). Slides were counterstained with hematoxylin and eosine, and pictures were taken using Olympus DP73 microscope.

2.5. Quantification and Statistical Analysis

For quantification, we used 8 to 10 82E1 stained brain sections, depending on the tissue quality. Sections were selected for each animal from the injected right (R) and lateral left (L) hemisphere at corresponding Bregma levels, spanning the hippocampus (starting anterior to the injection site at -1.8 mm and extending to -3.1 mm posterior), with at least 50 µm distance in between. The hippocampal Aβ-plaque burden (the area occupied by all plaques as percent of the total area) was estimated for each section using ImageJ software [25]. In order to analyze the effect of CSF inoculation on Aβ-plaque-burden, linear mixed-effects models were used. We thereby compared the injected to the non-injected hippocampal side. Aβ-plaque burden served as dependent variables, independent variables were hippocampal sides (injected vs. non-injected). Subject was treated as a random factor. Side was nested within time point and group. To achieve approximately normal distribution, Aβ-plaque burden values were log-transformed (zeros were replaced by half the smallest value). Results were expressed as geometric mean ratios (GMR) with corresponding 95% confidence intervals and p-values. A p-value <0.05 was considered as significant. All analyses were done using R version 3.0.1 (R Foundation for Statistical Computing, Vienna, Austria).

3. RESULTS

3.1. Prolonged Seeding with APP23 CSF Did not Induce Increased Aβ Pathology

To test the prion-like properties of CSF derived amyloid-β, we inoculated CSF from aged APP23 or C57BL6 mice into the hippocampus of young APP23 mice. APP23 mice show robust plaque development starting at the age of 8-9 months [22], and seeding studies are mostly terminated close to this stage. To allow longer inoculation periods, we analyzed the seeding effect of CSF from aged APP23 mice 14 or 21 months post inoculation. In order to control for the endogenous pathology present at this age, we compared Aβ plaque densities of the injected with the non-injected hippocampus for each mouse. However, we did not observe a significant difference in hippocampal Aβ pathology in mice injected with transgenic CSF (Fig. **1A, B**, Fig. **2A, B**), showing that additional inoculation time did not contribute to a possible local increase of the pathology. As expected, Aβ plaque burden was unchanged after inoculation of wild type CSF (Fig. **1C**, Fig. **2C**). Seeding with APP23 brain homogenates resulted in a significant enhancement of the endogenous Aβ pathology in the right hippocampus and visible focal aggregation around the injection site, similar to previous reports (Fig. **1D**, Fig. **2D**) [17, 18]. No Aβ pathology was induced up to 21 months post inoculation of APP23 CSF into C57BL6 host mice (Fig. **1E**, Table **S3**).

3.2. Seeding with Concentrated APP23 CSF Did not Induce Increased Aβ Pathology

In order to test the hypothesis that Aβ concentration in the CSF might be too low to induce a seeding effect, we injected APP23 mice with concentrated APP23 CSF comprising a 22 fold higher amount of $Aβ_{40}$ (Table **S2**). This highly concentrated CSF did not cause tissue necrosis at or in proximity to the injection site. Because of the high number of donor mice required for the collection of a sufficient amount of mouse CSF for concentration, we were able to inject only a very limited number of mice. A quantitative analysis of the Aβ plaque load, comparing the injected versus non-injected hippocampus did not show a significant seeding effect after 11 (Fig. **3A**, Table **S3**) or 20 months (Fig. **3B**, Table **S3**). No focal Aβ aggregation was visible at or close to the injection

site. In addition, inoculation of concentrated C57BL6 CSF did not result in any seeding effect after 11 months, as expected (Fig. **3C**, Table **S3**).

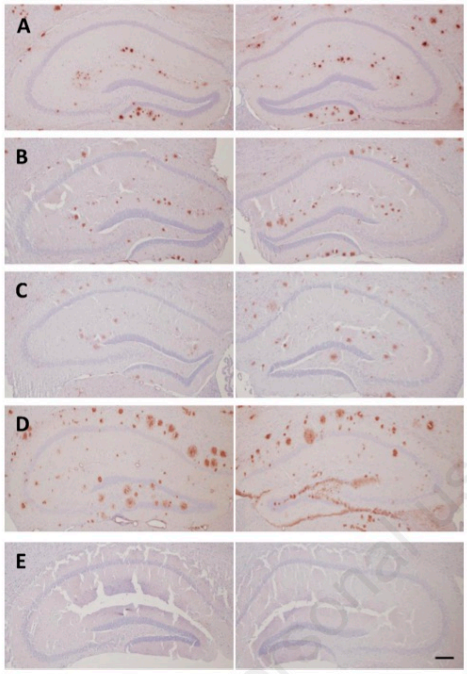

Fig. (1). Immunohistochemical anaylsis of injected mice using 82E1 antibody. APP23 mice analyzed 14 (**A**) or 21 months (**B**) after inoculation with CSF derived from aged APP23 mice (18 and 24 months old, respectively) did not show an increase in Aβ plaque burden in the injected hippocampus (right images), compared to the non-injected side (left images). Inoculation of wild-type mouse CSF did not provoke any seeding effect (**C**), while mice seeded with forebrain homogenate derived from aged APP23 mice exhibited enhanced Aβ deposition in the injected hippocampus (**D**). C57BL6 mice injected with APP23 CSF did not demonstrate any pathology (**E**). Scale bar equals 200 μm.

DISCUSSION/CONCLUSION

This study extends the findings recently reported on CSF Aβ seeding [21]. Our analysis includes mice injected with concentrated CSF for very long incubation time, and confirms the absence of relevant *in vivo* seeding effect of CSF derived Aβ.

In the present study, we used APP23 mice as a seeding model to test whether CSF Aβ exhibits prion-like properties. APP23 mice were inoculated unilaterally into the hippocampus with forebrain homogenate or CSF. This allowed an intra-individual comparison of the pathology between the injected and non-injected hippocampus. APP23 mice seeded with forebrain homogenate for 20 months exhibited a significantly higher Aβ plaque load and focal seeding effects in the injected hippocampus, confirming previous reports [16-20]. In contrast, APP23 mice injected with CSF derived from plaque-bearing APP23 mice for a period of up to 21 months did not show any increase in Aβ load at or close to the injection site. This suggests a lower seeding effect of the Aβ in the CSF, as compared to the one in the brain.

The lack of seeding activity of Aβ containing CSF could be attributed to different factors. Previously, it has been reported that seed-induced Aβ deposition increases significantly with time [16]. For this reason, we have extended our seeding time to the maximum possible with regard to the mouse life span. Our seeding periods by far exceed those reported previously (6-9 months) in studies using brain homogenates [16-20]. The time factor is thus not very likely to be responsible for the observed lack of seeding by CSF compared to brain extract.

Induction of Aβ seeding is furthermore dependent on the amount of Aβ present in the injected extract [17]. Indeed, the Aβ concentration is much lower in the CSF compared to that in standard diluted brain homogenates from plaque-bearing mice. However, only minimal amounts of brain-derived Aβ are required to induce seeding. Langer and co-workers have previously demonstrated that Aβ within the soluble fraction of ultracentrifugated brain homogenates harbors a very high seeding potential even at low concentrations [26]. In this light, concentrated AD patients` CSF was intra hippocampally injected into APP transgenic mice in a recent study, but also failed to demonstrate any Aβ seeding activity after 6-8 months [21]. In contrast, diluted brain extracts containing comparable amounts of Aβ did increase amyloid deposition [21]. We here used concentrated CSF comprising a much higher Aβ concentration than the one used in the aforementioned study (0.46 vs 0.008 ng/μl), and extended the seeding time up to 20 months. The absence of quantitative and qualitative seeding effects even under these conditions suggests that seeding competent Aβ species are absent in CSF, or their fraction is much smaller in the CSF than in the brain, and thus not detectable in a standard *in vivo* seeding model as the APP23 mice. As a limitation, we can not exclude a reduction of the seeding competence of the concentrated CSF due to freeze-thawing and/or lyophilization [27].

Small and soluble Aβ containing assemblies constitute the most potent Aβ seeds in brain extracts derived from APP23 transgenic mice [26]. Such small aggregates may be almost absent in the CSF, even if oligomeric Aβ forms have recently been detected in human CSF [28-31]. The lower level of Aβ seeds in CSF compared to brain tissue could be attributed to a reduced transport rate to the CSF compartment, possibly caused by their binding to cerebral amyloid-plaques, or an increased degradation within the CSF compartment. Additionally, the rapid turn-over of CSF might in parallel prevent a de novo assembly of prion-like Aβ strains within the CSF compartment. Aβ species present in brain homogenates or CSF may differ in their seeding potential due to structural varieties. As an example, N-truncated Aβ have been detected in the brain, but found largely absent in the CSF of AD patients [21]. Although it remains difficult to study the conformational state of Aβ *in vivo*, studies so far suggest the occurrence of conformationally distinct Aβ

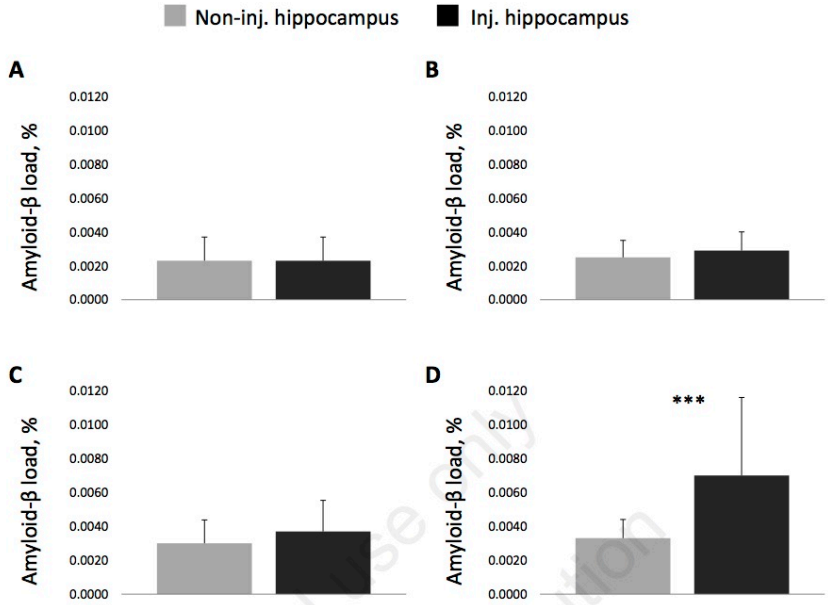

Fig. (2). Quantitative analysis of seeded mice. To assess a possible seeding effect we compared Aβ plaque burden between the non-injected (non-inj.) and injected (inj.) hippocampus in a mixed effect model for APP23 mice injected with transgenic CSF for 14 (**A**, n=4) or 21 months (**B**, n=5). In addition, we analysed APP23 mice seeded with wild type CSF (**C**, n=3) and with transgenic forebrain homogenates (**D**, n=2), as only in the last group there was a seeding effect present. Aβ plaque burden was calculated as a mean from all assessed hippocampal sections of mice in a group; error bars represent SD; *** indicates p<0.001. All p-values are listed in Table **S3**.

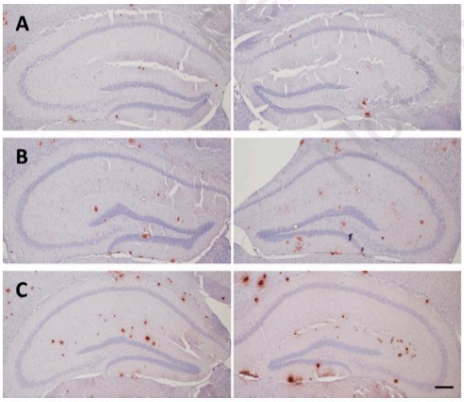

Fig. (3). Immunohistochemical analysis of mice injected with concentrated mouse CSF using 82E1 antibody. APP23 mice injected with concentrated APP23 CSF and analyzed 11 (**A**) or 20 (**B**) months later did not show an increased Aβ deposition in the inoculated hippocampus (right images), as compared to their non-injected sides (left images). The same was observed for littermates seeded with concentrated C57BL6 CSF (**C**). Scale bar equals 200 μm.

deposits in the brain [32, 33]. Different Aβ morphotypes may indicate that local factors may influence Aβ aggregation [34, 35]. Given its very low concentration in CSF, the structure of Aβ present there has still remained undescribed. This precludes us from drawing specific conclusions on the Aβ structure required for its seeding competence.

In addition, Aβ seeding may be dependent on brain components that are absent in the CSF compartment. For instance, the synaptic variant of acetylcholinesterase (AChE) has been shown to facilitate Aβ fibril formation [36]. In return, inhibitory cofactors may preferentially reach the CSF, such as the monomeric read through variant of AChE, which has been shown to delay aggregation [37].

Toxicity and seeding competence of Aβ may furthermore be influenced by RNA metabolism. miRNAs may be transmitted from one cell to another via exosomes, and RNA binding proteins have furthermore been shown to promote fibril formation [38-40]. This may contribute to the observed difference in seeding competence of brain-derived material versus CSF.

Further analysis of the potentially selective transport of particular Aβ species to the CSF and the possible co-factors involved might help to explain the apparent lack of *in vivo* active Aβ seeds in AD CSF. This knowledge could also help the development of sensitive early AD diagnostic tools.

CONFLICT OF INTEREST

The authors confirm that this article content has no conflict of interest.

ACKNOWLEDGEMENTS

We thank Andreas Schötzau (www.eudox.ch) for expert statistical advice. This work has been supported by the Swiss National Science Foundation (32323B_123812 to D.T.W.), the Mach-Gaensslen Foundation, the D&N Yde Foundation, the Velux Foundation, and the Synapsis Foundation, Switzerland.

DTW designed the study, KB, FC, JC, DA, and DTW developed the methodology, ZS, KB, FS and DTW collected the data and performed the analysis, and ZS, MS, MT, and DTW wrote the manuscript.

SUPPLEMENTARY MATERIAL

Supplementary materials are available on the publishers website along with the published article.

REFERENCES

[1] Thies W, Bleiler L. Alzheimer's disease facts and figures. Alzheimer's Dement 7: 208-244 (2011).

[2] Bateman RJ, Xiong C, Benzinger TLS, Fagan AM, Goate A, Fox NC, *et al.* Clinical and biomarker changes in dominantly inherited Alzheimer's disease. N Engl J Med 367(9): 795-804 (2012).

[3] Holtzman DM, Morris JC, Goate AM. Alzheimer's disease: the challenge of the second century. Sci Trans Med 3: 77sr1 (2011).

[4] Villemagne VL, Burnham S, Bourgeat P, Brown B, Ellis KA, Salvado O, *et al.* Amyloid β deposition, neurodegeneration, and cognitive decline in sporadic Alzheimer's disease: a prospective cohort study. Lancet Neurol 12: 357-367 (2013).

[5] Skoog I, Davidsson P, Aevarsson O, Vanderstichele H, Vanmechelen E, Blennow K. Cerebrospinal fluid beta-amyloid 42 is reduced before the onset of sporadic dementia: a population based study in 85-year-olds. Dement Geriatr Cogn Disord 15: 169-176 (2003).

[6] Blennow K, Dubois B, Fagan AM, Lewczuk P, de Leon MJ, Hampel H. Clinical utility of cerebrospinal fluid biomarkers in the diagnosis of early Alzheimer's disease. Alzheimers Dement 11(1): 58-69 (2015).

[7] Blennow K, Hampel H, Weiner M, Zetterberg H. Cerebrospinal fluid and plasma biomarkers in Alzheimer disease. Nat Rev Neurol 6: 131-144 (2010).

[8] Fagan AM, Holtzman DM. Cerebrospinal fluid biomarkers of Alzheimer's disease. Biomark Med 4: 51-63 (2010).

[9] Braak H, Braak E. Neuropathological stageing of Alzheimer-related changes. Acta Neuropathol 82: 239-259 (1991).

[10] Harper JD, Lansbury PT. Models of amyloid seeding in Alzheimer's disease and scrapie: mechanistic truths and physiological consequences of the time-dependent solubility of amyloid proteins. Annu Rev Biochem 66: 385-407 (1997).

[11] Jucker M, Walker LC. Self-propagation of pathogenic protein aggregates in neurodegenerative diseases. Nature 501: 45-51 (2013).

[12] Thal DR, Rüb U, Orantes M, Braak H. Phases of Aβ-deposition in the humanbrain and its relevance for the development of AD. Neurology 58: 1791-1800 (2002).

[13] Ashe KH, Aguzzi A. Prions, prionoids and pathogenic proteins in Alzheimer disease. Prion 7: 55-59 (2013).

[14] Lahiri DK, Maloney B, Zawia NH. The LEARn model: an epigenetic explanation for idiopathic neurobiological diseases. Mol Psychiatry 11: 992-1003 (2009).

[15] Lahiri DK. Prions: a piece of the puzzle? Science 337: 1172 (2012).

[16] Kane MD, Lipinski WJ, Callahan MJ, Bian F, Durham RA, Schwarz RD, *et al.* Evidence for seeding of beta-amyloid by intracerebral infusion of Alzheimer brain extracts in beta-amyloid precursor protein-transgenic mice. J Neurosci 20: 3606-3611 (2000).

[17] Meyer-Luehmann M, Coomaraswamy J, Bolmont T, Kaeser S, Schaefer C, Kilger E, *et al.* Exogenous induction of cerebral beta-amyloidogenesis is governed by agent and host. Science 313: 1781-1784 (2006).

[18] Eisele YS, Obermüller U, Heilbronner G, Baumann F, Kaeser SA, Wolburg H, *et al.* Peripherally applied Abeta-containing inoculates induce cerebral beta-amyloidosis. Science 330: 980-982 (2010).

[19] Morales R, Duran-Aniotz C, Castilla J, Estrada LD, Soto C. De novo induction of amyloid-β deposition *in vivo*. Mol Psychiatry 17: 1347-1353 (2012).

[20] Watts JC, Condello C, Stöhr J, Oehler A, Lee J, DeArmond SJ, *et al.* Serial propagation of distinct strains of Aβ prions from Alzheimer`s disease patients. Proc Natl Acad Sci USA 111: 10323-10328 (2014).

[21] Fritschi S, Langer F, Kaeser S, Maia L, Portelius E, Pinotsi D, *et al.* Highly potent soluble Aβ seeds in human Alzheimer brain but not cerebrospinal fluid. Brain 137: 2909-2915 (2014).

[22] Sturchler-Pierrat C, Abramowski D, Duke M, Wiederhold KH, Mistl C, Rothacher S, *et al.* Two amyloid precursor protein transgenic mouse models with Alzheimer disease-like pathology. Proc Natl Acad Sci USA 94: 13287-13292 (1997).

[23] Clavaguera F, Bolmont T, Crowther RA, Abramowski D, Frank S, Probst A, *et al.* Transmission and spreading of tauopathy in transgenic mouse brain. Nat Cell Biol 11: 909-913 (2009).

[24] Winkler DT, Abramowski D, Danner S, Zurini M, Paganetti P, Tolnay M, *et al.* Rapid cerebral amyloid binding by Aβ antibodies infused into β-amyloid precursor protein transgenic mice. Biol Psychiatry 68: 971-974 (2010).

[25] Griciuc A, Serrano-Pozo A, Parrado AR, Lesinski AN, Asselin CN, Mullin K, *et al.* Alzheimer's disease risk gene CD33 inhibits microglial uptake of amyloid beta. Neuron 78: 631-643 (2013).

[26] Langer F, Eisele YS, Fritschi SK, Staufenbiel M, Walker LC, Jucker M. Soluble Aβ seeds are potent inducers of cerebral β-amyloid deposition. J Neurosci 31: 14488-14495 (2011).

[27] Schoonenboom NS, Mulder C, Vanderstichele H, Van Elk EJ, Kok A, Van Kamp GJ, *et al.* Effects of processing and storage conditions on amyloid beta (1-42) and tau concentrations in cerebrospinal fluid: implications for use in clinical practice. Clin Chem 51: 189-95 (2005).

[28] Gao CM, Yam AY, Wang X, Magdangal E, Salisbury C, Peretz D, *et al.* Aβ40 oligomers identified as a potential biomarker for the diagnosis of Alzheimer's disease. PLoS One 5: e15725 (2010).

[29] Klyubin I, Betts V, Welzel AT, Blennow K, Zetterberg H, Wallin A, *et al.* Amyloid beta protein dimer-containing CSF disrupts synaptic plasticity: prevention by systemic passive immunization. J Neurosci 28: 4231-4237 (2008).

[30] Santos AN, Ewers M, Minthon L, Simm A, Silber RE, Blennow K, *et al.* Amyloid-β oligomers in cerebrospinal fluid are associated with cognitive decline in patients with Alzheimets disease. J Alzheimers Dis 29: 171-176 (2012).

[31] Salvadores N, Shahnawaz M, Scarpini E, Tagliavini F, Soto C. Detection of misfolded Aβ oligomers for sensitive biochemical diagnosis of Alzheimers disease. Cell Rep 10: 261-268 (2014).

[32] Nilsson KP, Aslund A, Berg I, Nyström S, Konradsson P, Herland A, *et al.* Imaging distinct conformational states of amyloid-beta fibrils in Alzheimer's disease using novel luminescent probes. ACS Chem Biol 2: 553-60 (2007).

[33] Meier BH, Böckmann A. The structure of fibrils from 'misfolded' proteins. Curr Opin Struct Biol 30C: 43-4 (2014).

[34] Jucker M, Walker LC. Self-propagation of pathogenic protein aggregates in neurodegenerative diseases. Nature 501: 45-51 (2013).

[35] Eisenberg D, Jucker M. The amyloid state of proteins in human diseases. Cell 148: 1188-203 (2012).

[36] Inestrosa NC, Alvarez A, Pérez CA, Moreno RD, Vicente M, Linker C, *et al.* Acetylcholinesterase accelerates assembly of amyloid-beta-peptides into Alzheimer's fibrils: possible role of the peripheral site of the enzyme. Neuron 16: 881-91 (1996).

[37] Berson A, Knobloch M, Hanan M, Diamant S, Sharoni M, Schuppli D, *et al.* Changes in readthrough acetylcholinesterase expression modulate amyloid-beta pathology. Brain 131: 109-19 (2008).

[38] Barbash S, Soreq H. Threshold-independent meta-analysis of Alzheimer's disease transcriptomes shows progressive changes in hippocampal functions, epigenetics and microRNA regulation. Curr Alzheimer Res 9: 425-35 (2012).

[39] Lau P, Bossers K, Janky R, Salta E, Frigerio CS, Barbash S, *et al.* Alteration of the microRNA network during the progression of Alzheimer's disease. EMBO Mol Med 5: 1613-34 (2013).

[40] Kim HJ, Kim NC, Wang YD, Scarborough EA, Moore J, Diaz Z, *et al.* Mutations in prion-like domains in hnRNPA2B1 and hnRNPA1 cause multisystem proteinopathy and ALS. Nature 495: 467-73 (2013).

Received: February 10, 2015 **Revised: April 13, 2015** **Accepted: June 17, 2015**

Supplementary materials

1.1. ELISA

Abeta 40 and sAPP levels were measured using Human 6E10 and APPalpha/sAPPbeta Kits respectively, both from Meso Scale Discovery, according to the manufacturer's instructions.

1.2. Mice

Genotype	**Seed**	**Seed donor age, *mo***	**Seeding time, *mo***
App23	tg CSF	18	14
App23	tg CSF	24	14
App23	tg CSF	24	14
App23	tg CSF	24	14
App23	tg CSF	18	21
App23	tg CSF	18	21
App23	tg CSF	24	21
App23	tg CSF	24	21
App23	tg CSF	24	21
App23	wt CSF	3	21
App23	wt CSF	24	21
App23	wt CSF	24	21
App23	FB	24	20
App23	FB	24	20
C57BL6	tg CSF	24	21
C57BL6	tg CSF	18	21
C57BL6	tg CSF	18	21
App23	conc. tg CSF	24	11
App23	conc. wt CSF	24	11
App23	conc. tg CSF	24	20

Table S1. Table of all mice used for quantitative analysis in the study. Abbreviations used: tg=transgenic, wt=wild type, FB=forebrain homogenate, conc.=concentrated.

Supplementary results

1.3. ELISA

Sample	**Aβ40**, *pg/µl CSF*	**sAPPα**, *pg/µl CSF*	**sAPPβ**, *pg/µl CSF*
APP23 CSF	4.2	92	121
Concentrated APP23 CSF	92.6	2594	3659

Table S2. ELISA table of results.

1.4. Quantification of Aβ pathology comparing injected vs non-injected hippocampus

Genotype	**Treatment group**	**Seeding time, mo**	**N**	**Lower ratio**	**GMR**	**Upper ratio**	**P value**
APP23	tg CSF	14	4	0.77	0.94	1.15	0.56
APP23	tg CSF	21	5	0.79	0.91	1.05	0.19
APP23	wt CSF	21	3	0.65	0.81	1.01	0.06
APP23	FB	20	2	0.41	0.54	0.70	0.00***
C57BL6	tg CSF	21	3	0.00	0.00	0.00	NA
APP23	conc. tg CSF	11	1	0.59	0.88	1.30	0.52
APP23	conc. wt CSF	11	1	0.72	1.10	1.67	0.66
APP23	conc. tg CSF	20	1	0.61	0.92	1.40	0.70

Table S3. Geometric mean ratios (GMR) of amyloid-β ratios comparing non-injected vs injected hippocampus. N indicates the number of mice used; tg=transgenic, wt=wild type, FB=forebrain homogenate, conc.=concentrated; *** indicates $p<0.001$.

Prion like properties of tau in P301S mice cerebrospinal fluid

Manuscript in preparation

Prion like properties of tau in P301S mice cerebrospinal fluid

Zhiva Skachokova[1,2], Frederik Sprenger[1,2], Marc Sollberger[,2], Florence Clavaguera[1], Jürgen Hench[1], Jens Kuhle[2], Axel Regeniter[4], Reto W Kressig[3], Andreas Monsch[3], Michel Goedert[5], Markus Tolnay[1], David T. Winkler[1, 2]

[1]*Institute of Pathology, University Hospital Basel, Schönbeinstrasse 40, CH-4003 Basel, Switzerland*
[2]*Department of Neurology, University Hospital Basel, Petersgraben 4, CH-4031 Basel, Switzerland*
[3]*Memory Clinic, Geriatric University Clinic, Felix-Platter-Hospital, CH-4003 Basel, Switzerland*
[4]*Laboratory Medicine, University Hospital Basel, Petersgraben 4, CH-4031 Basel, Switzerland*
[5]*MRC, Laboratory of Molecular Biology, Francis Crick Avenue, Cambridge CB2 0GH, UK*

Abstract

Tau is a microtubule stabilizing protein that forms aggregates in many neurodegenerative diseases named tauopathies, including Alzheimer's disease (AD). It was shown that tau derived from tauopathy patient brains could induce local protein aggregation in a prion-like manner when injected into susceptible mice models. At the same time, increase of tau levels in the cerebrospinal fluid (CSF) of AD patients correlates with severity of the disease. However, a reliable presymptomatic marker in AD is currently unavailable. A potential prion like property of tau in the CSF could have a possible diagnostic application.
Here we investigated the seed-like potential of tau present in the CSF of mice carrying a tau mutation (P301S). We collected CSF from aged, tangle bearing P301S mice and injected it into young, pretangle staged P301S mice. As a result, we observed significantly higher number of pathologically hyperphosphorylated, AT8 positive NFTs in mice treated with CSF from P301S mice. Increased tau pathology was noted anterior and posterior to the inoculation site, as well as in the contralateral hippocampus. This suggests that CSF tau can exhibit seed like properties *in vivo*, and can induce tau hyperphosphorylation and fibrillization that is transmitted along existing anatomical networks. This knowledge could be useful in the development of future diagnostic tools.

Introduction

Tau is a natively unfolded protein that promotes microtubules stability in neuronal cells. However, in pathological conditions, it becomes hyperphosphorylated, it oligomerizes, fibrillates and eventually forms intracellular aggregates. This is characteristic of Alzheimer's disease (AD), but also other neurodegenerative disorders known as tauopathies, including progressive supranuclear palsy (PSP), corticobasal degeneration (CBD), and frontotemporal dementia (FTD) (Goedert et al. 2010; Mandelkow & Mandelkow 2011; Jucker & Walker 2013a). In AD patients tau propagates from one brain region to another in a specific pattern during the course of the disease (Braak & Braak 1997). Moreover, the injection of brain extracts from human P301S tau transgenic mice into wild type human tau transgenic mice induces aggregation of the wild type human tau (Clavaguera et al. 2009), suggesting that tau aggregation can be transmitted in a prion-like manner. In a number of subsequent studies, injection of recombinant tau fibrils or patients' derived brain extracts containing aggregated tau caused formation of neuro fibrillary tangles (NFTs) that propagated from the injection site to connected brain regions in a stereotypic and time dependent manner (Liu et al. 2012; de Calignon et al. 2012; Clavaguera et al. 2013; Iba et al. 2013; Ahmed et al. 2014). This suggests that a pathological conformation or aggregation state of tau can be locally induced by an inoculated seed, followed by transneuronal spreading in a way similar to prions (Frost & Diamond 2009; Jucker & Walker 2011; Clavaguera et al. 2014). In this light, it has been shown that tau aggregates can transfer between cells and might be present in the extracellular space (Frost & Diamond 2009; Yanamandra et al. 2013; Pooler et al. 2014).

Tau is physiologically present in the cerebrospinal fluid (CSF). However, it has remained unexplored whether tau in the CSF is soluble, forms oligomers, and/or fibrillizes. CSF concentrations of tau and phosphorylated tau are being used for clinical diagnosis of AD, in conjunction with CSF amyloid-β levels, cognitive tests, and various forms of brain imaging. Increased tau levels in CSF correlate best with cognitive decline in AD patients (Blennow et al. 1995; Wallin et al. 2006; Blennow et al. 2015). However, most of those markers are associated with disease onset, and reliable early, presymptomatic markers, that might predict the conversion of mild cognitive impairment to AD, are still missing (Blennow et al.

2010b; Blennow et al. 2014). Detection of pathologically conformed tau species in CSF might thus be serving as an early diagnostic marker in AD and other tauopathies.

In order to study the presence of seeding competent tau species in CSF, we here inoculated CSF derived from tau transgenic mice into susceptible host mice. CSF was collected from P301S mice that carry a tau mutation typical of a familial form of FTD (Allen et al. 2002), and injected intrahippocampally into young mice of the same strain. P301S develop NFTs progressively with age while their level of CSF tau increases (Yamada et al. 2011). Unilateral injection of CSF collected from aged, tangle bearing P301S mice into pre-tangle staged P301S mice increased the number of NFTs in both the injected and non-injected hippocampus, as compared to littermates inoculated with non-transgenic murine CSF. This data suggests that seeding competent tau species with prion-like potential reach the CSF compartment in P301S mice. Given the easy accessibility of CSF in human patients, the detection of prionoid tau species in the CSF compartment could have a potential future diagnostic application.

Materials and Methods

Mice

We used homozygous tau transgenic mice expressing the shortest human four-repeat tau isoform containing the P301S mutation under the thy1.2 promoter (P301S mice) (Allen et al. 2002), and aged matched, non-transgenic C57BL/6 control mice. Animal experiments were performed in compliance with protocols approved by the official local Committee for Animal Care and Animal Use of the Canton of Basel.

Murine CSF collection

CSF was collected by puncturing the cisterna magna after deeply anesthetizing the animals, as previously described (Skachokova et al. 2015). Next, it was spun down at 2500 rpm for 2 min and the supernatant was collected and immediately frozen. Visibly blood contaminated CSF was discarded.

CSF processing

Freshly collected human CSF was spun down at 3000 rpm for 2 min to separate cell debris. The supernatant was collected and frozen at −80° C. Next it was pooled and concentrated by lyophilization (−80° C, 0.01 mbar vacuum pressure, for 24 hours) and reconstituted in sterile H_2O. The final concentration was measured by ELISA (see Fig. S6).

Stereotaxic surgery

Three months-old P301S mice and non-transgenic C57BL/6 control mice were anaesthetized with a mixture of ketamine (10 mg/kg) and xylazine (20 mg/kg) and placed on a heating pad to maintain body temperature during surgery. Mice were injected in the right (R) hippocampus (A/P, −2.5 mm from bregma; L, − 2.0 mm; D/V, −1.8 mm) using a Hamilton syringe, as previously reported (Clavaguera et al. 2009). Each received a unilateral stereotaxic injection of 5 µl concentrated CSF, at a speed of 1.25 µl/min. Following the injection, the needle was kept in place for additional 3 minutes before withdrawal. The surgical area was cleaned with sterile saline and the incision sutured. Mice were monitored until recovery from anaesthesia and checked regularly following surgery. For number of mice used and injected material see Table S1.

Immunohistochemical analysis

Following 4 months seeding time, mice were deeply anaesthetized with pentobarbital (100 mg/kg) and killed by transcardial perfusion with 20 ml cold PBS, followed by 20 ml 4% paraformaldehyde in PBS. The brains were dissected and post-fixed overnight. Following paraffin embedding, 5 µm coronal sections were prepared. Sections were silver-impregnated following the method of Gallyas-Braak to visualize filamentous tau pathology (Gallyas 1971; Braak et al. 1988). Haematoxylin and eosin staining was performed for morphological analysis. For immunohistochemistry, the following anti-tau antibodies were used: AT8 and AT100 (both 1:1000, Thermo Scientific), with secondary antibodies from Vector Laboratories, Burlingame, CA (Vectastain ABC kit), as previously described (Ozcelik et al. 2013; Ozcelik et al. 2016).

Quantification and statistical analysis

For quantification, on average 7-9 sections per mouse (sections with bad quality were discarded) were analyzed at levels comprising the injection site (from -2 to -3 um from Bregma), and sections form the injected and non-injected hippocampal side were selected at corresponding levels. The number of silver stained tangles and AT8 and AT100 positive aggregates was counted using the Cell counter plugin in ImageJ. Then average score per group was made. For the AT8 heat map average tau pathology per Bregma level per group was calculated and manually color graded. The amounts of granular tau pathology in 3 hippocampal regions (CA1, CA3, dentate gyrus) at varying Bregma levels were qualitatively assessed by two independent researchers and an average score was obtained. Brain images that were used and modified are from the Mouse Brain Atlas (Franklin and Paxinos, Elsevier 2007). All group scores were compared using unpaired Student t-test. P values are reported when significant.

Results

Parallel to age increase, P301S mice develop hyperphosphorylated tau, later assembled into PHFs and NFTs, that is AT8, AT100 and Gallyas positive (Allen et al. 2002) (Fig. S2). In seeded mice, we quantified any change in their endogenous pathology based on those markers (Fig. 1). Injections of CSF from tangle bearing P301S into young, pretangle P301S mice resulted into increased number of hyperphosphorylated tau, as compared to wild type CSF seeded mice (Fig.2 A, B). Moreover, this effect was present throughout the hippocampus and also bilaterally, in the non-injected hippocampal side (Fig.2 E). Also, when we looked at sections anterior/around the injection side, we found significant differences between the P301S CSF and BL6 CSF injected hippocampi, and also between same groups non-injected sides (Fig.2 A, B; $p<0.05$). This indicates that hyperphosphorylated tau pathology can be transmitted and induced via CSF derived from mutated tau expressing mice.

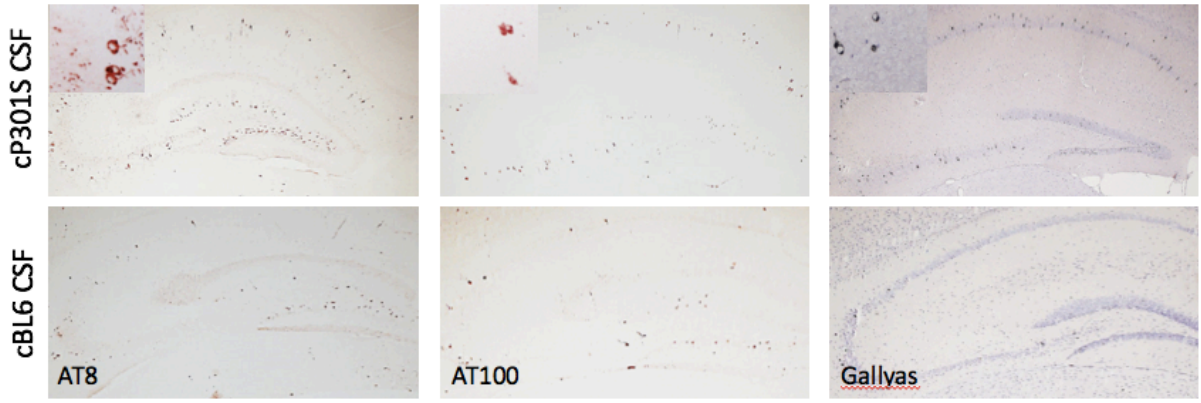

Figure 1. P301S mice normally develop hyperphosphorylated tau positive for AT8 and AT100 antibodies, and Gallyas silver stained NFTs in both hippocampi. The magnified immunohistochemical images show cells of the CA3 region in the right hippocampus.

Injection of P301S brainstem homogenate (BS) resulted in a higher number of AT8 positive neurons in both hippocampal sides, as compared to BL6 BS injections, that was significant in the left hippocampus and showed a trend in the right (Fig.2 F). When we focused on sections anterior/close to the injection site, we found significant increase in the number of hyperphosphorylated tau in both injected and non-injected P301S BS seeding hippocampi, as compared to BL6 BS seeded (Fig. 2 C, D, $p<0.05$ for R and $p<0.001$ for L). Finally, injection with P301S CSF resulted in an effect similar to the P310S brain stem homogenate, even

though total tau/ phospho-tau concentrations in the first one are more than a thousand times lower (Table S2, Fig. S5).

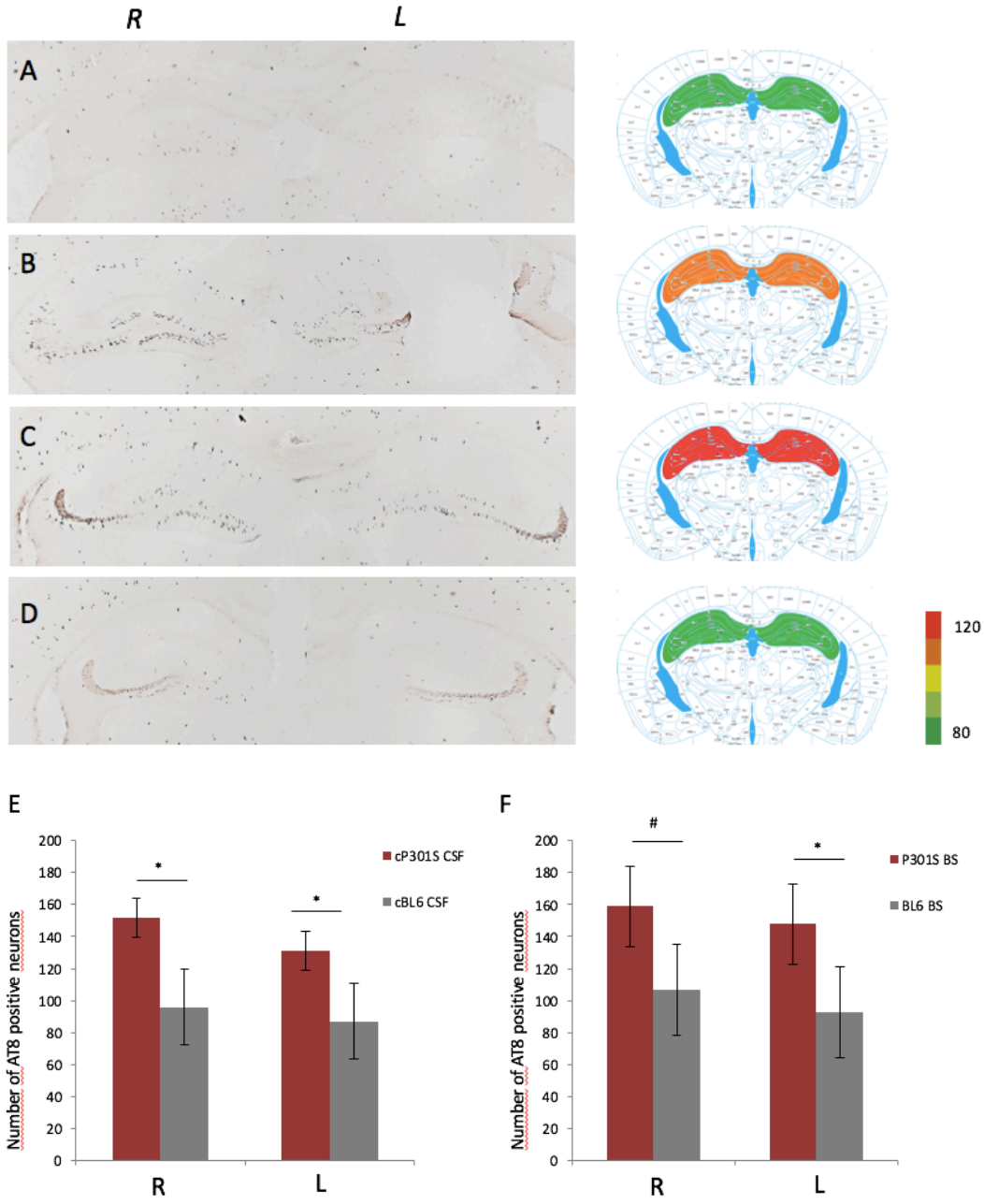

Figure 2. Assessment of AT8 positive tau in mice seeded mice with BL6 CSF (A, n=5), P301S CSF (B, n=5), P301S BS (C, n=6) and BL6 BS (D, n=5). Hippocampal pathology between groups and between injected (R) and non-injected (L) sides was assessed for sections anterior/in proximity to the injection site (A-D), or for the whole hippocampus in CSF (E) and brain stem (F) seeded mice. Color scale indicates the number of NFTs. * = $p<0.05$, #=$p=0.07$, as based on unpaired t-test. Error bars represent SEMs.

Next, we analyzed the AT8 pathology in the CSF seeded mice on different anatomical levels and hippocampal subregions. We found a significant effect anterior and in proximity to the injection site, specifically in the CA1 and DG regions between the injected hippocampus of P301S and BL6 CSF seeded mice (Fig. 3 A, B). Furthermore, in P301S CSF seeded mice we found a tendency for higher amount of hyperphosphorilated tau in the injected hippocampus CA3 region, versus the contralateral one. When analyzing AT8 load posterior to the injection site, we saw significant increase of AT8 positive hyperphosphorylated tau in both the CA1 and DG of the injected and non-injected hippocampus in P301S seeded mice (Fig. 3 A, C). This shows that injection of mutated tau containing CSF induced a local seeding effect after 4 months time that was spread throughout the hippocampus based on existing anatomical connections.

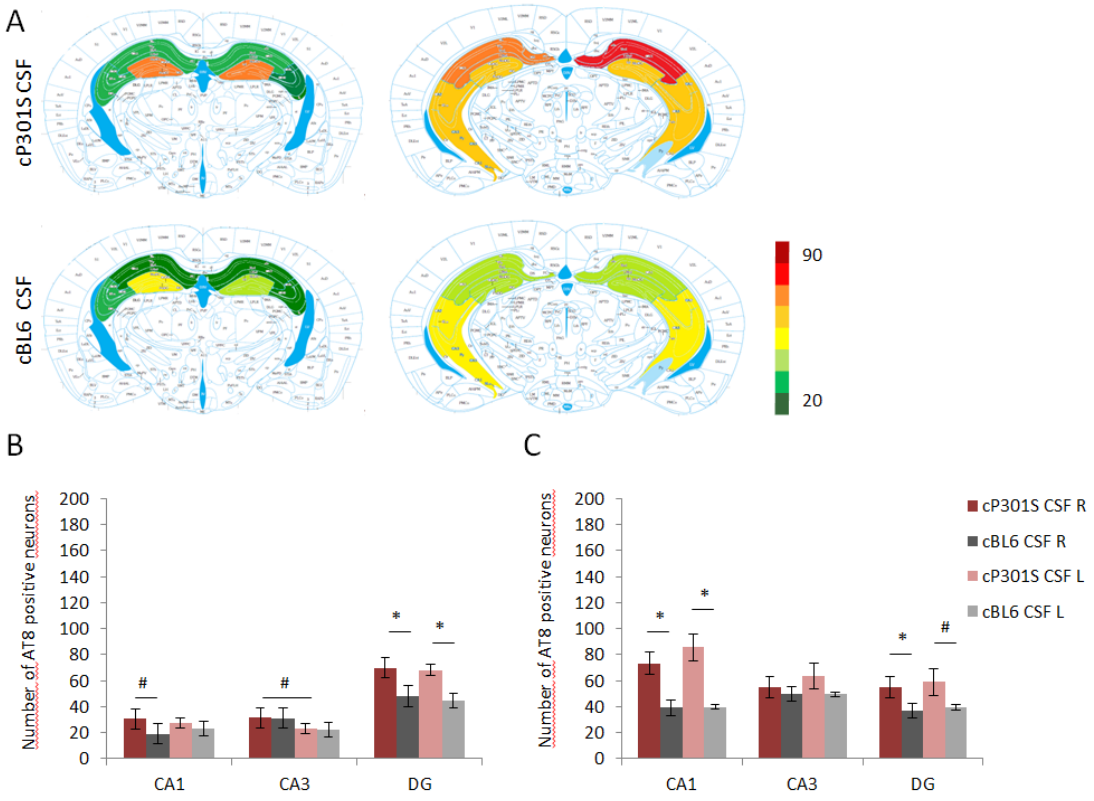

Figure 3. Quantification of hyperphosphorylated tau pathology in murine CSF seeded mice in different subhippocampal regions. Number of AT8 positive neurons in the CA1, CA3 (incl. CA2) and DG in P301S CSF (n=5) and BL6 CSF (n=5) seeded mice is presented as a heat map anterior (comprising sections at -2 to -2.5 from Bregma) and posterior (-2.6 to -3 from Bregma) to the injection site (A). Scale bar depicts AT8 load. Number of AT8 positive tau is presented as an average value from all sections anterior (B) and posterior to the injection site (C). *=p<0.05, #=p=0.07. Error bars represent SEMs.

Quantification of AT100 pathology, a later marker of tau hyperphosphorylation (Augustinack et al. 2002), also resulted in a significant increase as a result of P301S CSF seeding, as compared to BL6 CSF treatment, as seen in the injected hippocampus (Fig.3 A). At the same time, there was no significant difference in the amount of Gallyas positive tangles in the right hippocampus between P301S and BL6 CSF seeded mice (Fig.3 B), or for BS seeded mice (Fig.3 C). Thus, our injections induced an increase of endogenous tau hyperphosphorylation and formation of prefibrillar tau, but not of late stage Gallyas positive NFTs, in P301S host mice. This may be due to the limited seeding time, restricted by the life span of homozygous P301S mice due to their progressive motor symptoms (Allen et al. 2002).

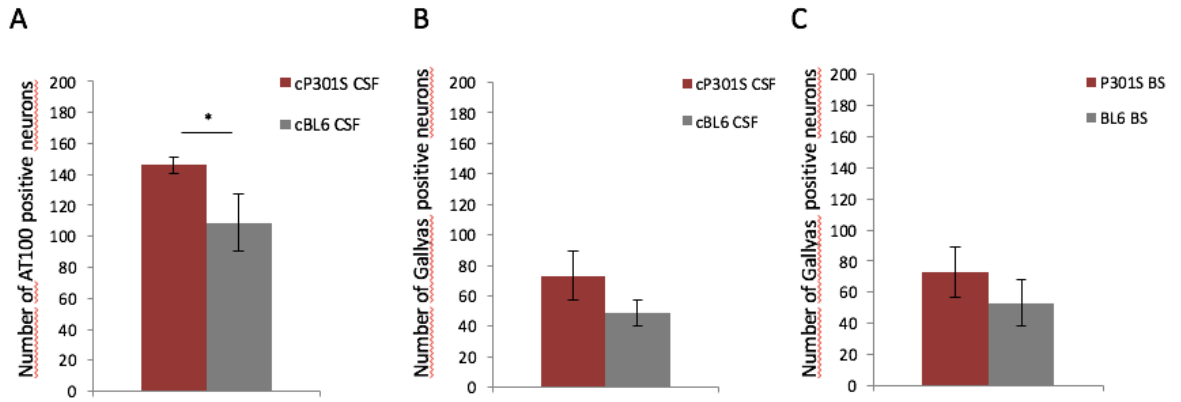

Figure 4. Quantification of tau pathology in the injected right hippocampus between conc. P301S CSF (n=5) and conc. BL6 CSF (n=5) seeded mice as based on AT100 antibody (A), or Gallyas silver staining (B). The number of Gallyas positive NFTs in brain stem seeded mice (P301S BS n=6, BL6 BS n=5) was also analyzed (C). * indicates $p<0.05$, as based on unpaired t-test. Error bars represent SEMs.

Discussion

We recently showed that CSF derived amyloid-beta lacks prion-like potential (Skachokova et al. 2015; Fritschi et al. 2014). In the present study, we investigated the prion-like potential of tau protein present in the CSF of tau transgenic mice and compared it to that in wild type-mice CSF.

Induction of tau propagation along synaptically connected regions using brain homogenates has been previously reported in P301S mice (Ahmed et al. 2014; Boluda et al. 2014). In order to see whether also CSF harbors seeding competent tau species, we here collected CSF from aged, tangle bearing P301S mice and injected it into young, pre-tangle staged P301S mice. Tau pathology was assessed and compared to littermate mice inoculated with non-transgenic mouse CSF. As a result, we observed significantly higher hyperphosphorylated, AT8 positive tau, a marker of prefibrilar tau pathology, throughout the hippocampus in mice treated with CSF from aged P301S mice. In addition, the observed pathology was present bilaterally in the contralateral hippocampus, and also in anterior and posterior directions, and not only localized to the injection site. This suggests that mouse CSF tau can exhibit seed like properties *in vivo*, and tau hyperphosphorylation could be induced and transmitted based on synaptic connections. These are the first evidences that CSF tau could exhibit prion-like characteristics.

As a result of CSF seeding we observed increased AT8 and AT100 positive structures as indicators of pathological, hyperphosphorylated tau (Allen et al. 2002), but no increase in the number of late, Gallyas positive NFTs. Tau hyperphosphorylation is an early marker of AD, characteristic of the preclinical phase, and precedes tau aggregation by decades in human sporadic AD cases (Braak & Del Tredici 2015). It may be the case that because of the limited seeding time, an increase in Gallyas positive NFTs was not apparent in our P30S mice, or simply CSF tau causes the hyperphoshorylation, but not aggregation of endogenous tau. In addition, seeding of AD brain in P301S mice for 3 months increased AT8 signal in the CA3 region of the injected hippocampus, versus the non-injected one, and tau propagation happened in a timely and connectivity based manner (Boluda et al. 2014). These findings are similar to our P301S CSF seeding results, however, we also note an increase in other hippocamapal subregions as the CA1 and DG that may be due to the variation in the injection site and/or extended seeding time. In another study, injection of tau seeds into P301S hetero

mice for 6 months induced AT8 hyperphosphorylation in interconnected to the injection site regions, resulting in network dysfunction and memory impairment. Importantly, this was correlated with the presence of tau oligomers and tau hyperphosphorylation, rather than with fully mature NFTs (Stancu et al. 2015), implicating early pathological forms of tau as culprits of neuronal dysfunction. Furthermore, hyperphosphorylated tau in the CSF is best correlated with cognitive decline, as opposed to total tau (Braak et al. 2013). All this suggests that increase in AT8 positive tau per se, as seen in our model and previous studies, can be an indicator of both toxicity and seeding effect.

Currently, it is not known how seeding competent tau reaches the CSF. Previously, it has been shown that tau propagates via synaptically connected regions, however the exact mechanisms are still unknown (Pooler et al. 2014; Clavaguera et al. 2015). Using an *in vitro* cell model it was demonstrated that phosphorylated tau is actively secreted via exosomal release, and also found in vesicles in AD patients CSF (Saman et al. 2012), as well as in exosomes isolated from P301S mouse brains (Asai et al. 2015). Furthermore, infusion of tau antibodies into tau transgenic mice lateral ventricles reduced tau seeding activity by reducing tau hyperphosphorylation and aggregation, implicating extacellular tau in AD pathology as seed responsible (Yanamandra et al. 2013). Based on these evidences and our results, it is possible that seeding prone tau is released by the neurons and reaches the CSF. In addition, we injected our mice with a mixture of P301S CSF and AT8 and AT100 antibodies to see whether this would inhibit the observed seeding effect (data pending).

In conclusion, our results suggest the presence of prion-like tau in the CSF of P301S mice. This provides the basis for future studies using human patients CSF, and possibly opens a perspective for novel diagnostic approaches.

References

Ahmed, Z. et al., 2014. A novel in vivo model of tau propagation with rapid and progressive neurofibrillary tangle pathology: the pattern of spread is determined by connectivity, not proximity. *Acta neuropathologica*, 127(5), pp.667–83.

Allen, B. et al., 2002. Abundant Tau Filaments and Nonapoptotic Neurodegeneration in Transgenic Mice Expressing Human P301S Tau Protein. , 22(21), pp.9340–9351.

Asai, H. et al., 2015. Depletion of microglia and inhibition of exosome synthesis halt tau propagation. *Nature Neuroscience*, (October). Available at: http://www.nature.com/doifinder/10.1038/nn.4132.

Augustinack, J.C. et al., 2002. Specific tau phosphorylation sites correlate with severity of neuronal cytopathology in Alzheimer's disease. *Acta Neuropathologica*, 103(1), pp.26–35.

Blennow, K. et al., 2010. Cerebrospinal fluid and plasma biomarkers in Alzheimer disease. *Nature Publishing Group*, 6(3), pp.131–144.

Blennow, K. et al., 2014. Clinical utility of cerebrospinal fluid biomarkers in the diagnosis of early Alzheimer's disease. *Alzheimer's & dementia : the journal of the Alzheimer's Association*, pp.1–12.

Blennow, K. et al., 1995. Tau protein in cerebrospinal fluid: a biochemical marker for axonal degeneration in Alzheimer disease? *Molecular and chemical neuropathology / sponsored by the International Society for Neurochemistry and the World Federation of Neurology and research groups on neurochemistry and cerebrospinal fluid*, 26(3), pp.231–245.

Blennow, K., Zetterberg, H. & Fagan, A.M., 2015. Fluid Biomarkers in Alzheimer Disease.

Boluda, S. et al., 2014. Differential induction and spread of tau pathology in young PS19 tau transgenic mice following intracerebral injections of pathological tau from Alzheimer's disease or corticobasal degeneration brains. *Acta Neuropathologica*, 129, pp.221–237.

Braak, H. et al., 2013. Intraneuronal tau aggregation precedes diffuse plaque deposition, but amyloid-beta changes occur before increases of tau in cerebrospinal fluid. *Acta Neuropathologica*, 126(5), pp.631–641.

Braak, H. et al., 1988. Silver impregnation of Alzheimer's neurofibrillary changes counterstained for basophilic material and lipofuscin pigment. *Stain technology*, 63(4), pp.197–200.

Braak, H. & Braak, E., 1997. Diagnostic criteria for neuropathologic assessment of Alzheimer's disease. *Neurobiology of aging*, 18(4 Suppl), pp.S85–8.

Braak, H. & Del Tredici, K., 2015. The preclinical phase of the pathological process underlying sporadic Alzheimer's disease. *Brain : a journal of neurology*, 138(Pt 10), pp.2814–2833.

de Calignon, A. et al., 2012. Propagation of tau pathology in a model of early Alzheimer's disease. *Neuron*, 73(4), pp.685–97.

Clavaguera, F. et al., 2013. Brain homogenates from human tauopathies induce tau inclusions in mouse brain. *Proceedings of the National Academy of Sciences of the United States of America*, 110(23), pp.9535–40.

Clavaguera, F. et al., 2015. Invited review : Prion-like transmission and spreading of tau pathology. , *Acta Neuropathologica* pp.47–58.

Clavaguera, F. et al., 2009. Transmission and spreading of tauopathy in transgenic mouse brain. , *Nature Cell Biology* 11, pp.909 - 913

Clavaguera, F., Grueninger, F. & Tolnay, M., 2014. Intercellular transfer of tau aggregates and spreading of tau pathology: Implications for therapeutic strategies. *Neuropharmacology*, 76 Pt A,

pp.9–15.

Fritschi, S.K. et al., 2014. Highly potent soluble amyloid-?? seeds in human Alzheimer brain but not cerebrospinal fluid. *Brain*, 137(11), pp.2909–2915.

Frost, B. & Diamond, M.I., 2009. Prion-like mechanisms in neurodegenerative diseases. Available at: http://dx.doi.org/10.1038/nrn2786.

Gallyas, F., 1971. Silver staining of Alzheimer's neurofibrillary changes by means of physical development. *Acta morphologica Academiae Scientiarum Hungaricae*, 19(1), pp.1–8.

Goedert, M., Clavaguera, F. & Tolnay, M., 2010. The propagation of prion-like protein inclusions in neurodegenerative diseases. *Trends in neurosciences*, 33(7), pp.317–25.

Iba, M. et al., 2013. Synthetic tau fibrils mediate transmission of neurofibrillary tangles in a transgenic mouse model of Alzheimer's-like tauopathy. *The Journal of neuroscience : the official journal of the Society for Neuroscience*, 33(3), pp.1024–37.

Jucker, M. & Walker, L.C., 2011. Pathogenic protein seeding in Alzheimer disease and other neurodegenerative disorders. *Annals of neurology*, 70(4), pp.532–40.

Jucker, M. & Walker, L.C., 2013. Self-propagation of pathogenic protein aggregates in neurodegenerative diseases. *Nature*, 501(7465), pp.45–51.

Liu, L. et al., 2012. Trans-synaptic spread of tau pathology in vivo. *PloS one*, 7(2), p.e31302.

Mandelkow, E.M. & Mandelkow, E., 2011. Biochemistry and cell biology of Tau protein in neurofibrillary degeneration. *Cold Spring Harbor Perspectives in Biology*, 3(10), pp.1–25.

Ozcelik, S. et al., 2016. Co-expression of truncated and full-length tau induces severe neurotoxicity. *Mol Psychiatry*.

Ozcelik, S. et al., 2013. Rapamycin Attenuates the Progression of Tau Pathology in P301S Tau Transgenic Mice. *PLoS ONE*, 8(5), p.e62459.

Pooler, A.M., Noble, W. & Hanger, D.P., 2014. A role for tau at the synapse in Alzheimer's disease pathogenesis. *Neuropharmacology*, 76(PART A), pp.1–8.

Saman, S. et al., 2012. Exosome-associated tau is secreted in tauopathy models and is selectively phosphorylated in cerebrospinal fluid in early Alzheimer disease. *Journal of Biological Chemistry*, 287(6), pp.3842–3849.

Skachokova, Z. et al., 2015. Amyloid-beta in the Cerebrospinal Fluid of APP Transgenic Mice Does not Show Prion-like Properties. *Current Alzheimer research*, 12(9), pp.886–891.

Stancu, I.-C. et al., 2015. Templated misfolding of Tau by prion-like seeding along neuronal connections impairs neuronal network function and associated behavioral outcomes in Tau transgenic mice. *Acta Neuropathologica*.

Wallin, a K. et al., 2006. CSF biomarkers for Alzheimer's Disease: levels of beta-amyloid, tau, phosphorylated tau relate to clinical symptoms and survival. *Dementia and geriatric cognitive disorders*, 21(3), pp.131–8.

Yamada, K. et al., 2011. In vivo microdialysis reveals age-dependent decrease of brain interstitial fluid tau levels in P301S human tau transgenic mice. *The Journal of neuroscience : the official journal of the Society for Neuroscience*, 31(37), pp.13110–7.

Yanamandra, K. et al., 2013. Anti-tau antibodies that block tau aggregate seeding invitro markedly decrease pathology and improve cognition in vivo. *Neuron*, 80(2), pp.402–414.

Prion like properties of tau in P301S mice cerebrospinal fluid

Supplementary Materials and Results

Injected mice

Genotype	Seed	Seeding time, mo	N
P301S	P301S CSF	4	5
P301S	BL6 CSF	4	5
P301S	P301S BS	4	6
P301S	BL6 BS	4	5
P301S	-	-	4

Table S1. Mice used in the study were injected with murine CSF, or murine brain stem (BS) homogenate at 3 months of age, and sacrificed 4 months after (seeding time). Some non-injected control mice were used as well.

P301S mice tau pathology

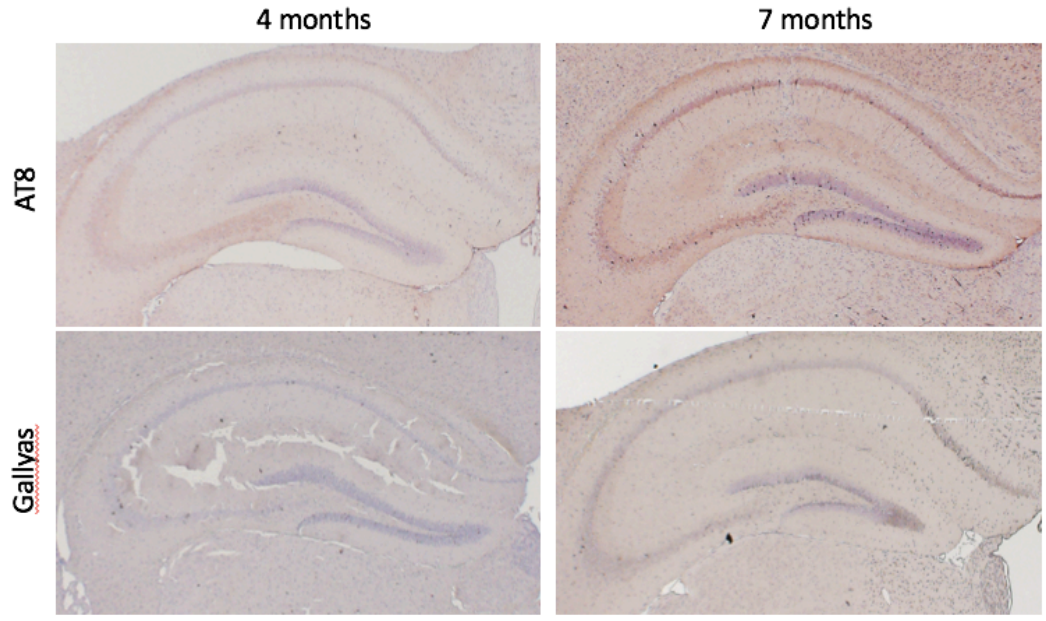

Figure S2. Endogenous tau pathology as analyzed by AT8 immunohistochemistry and Gallyas silver staining in 4 and 7 months old P301S mice.

Seeding with P301S CSF and brain stem homogenates

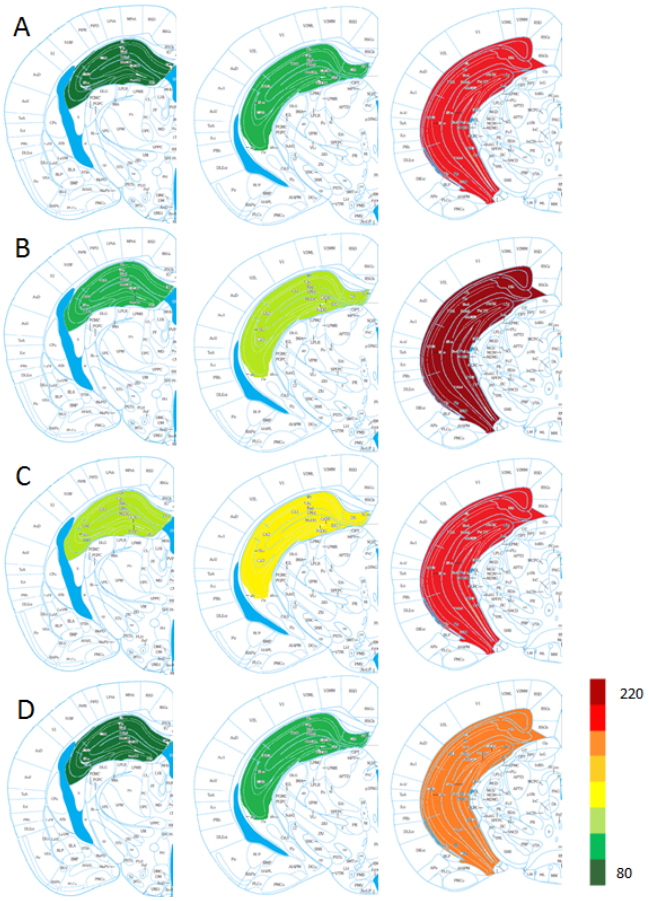

Figure S3. Qualitative assessment of AT8 positive tau pathology at different Bregma levels. P301S mice seeded with Bl6 CSF (A), P301S CSF (B), P301S BS (C), or BL6 BS (D), were evaluated at -2, -2.5 and -2.9 mm from Bregma, corresponding to the left, central and right columns. Scores were made as based on average AT8 values per anatomical level per group. Scale bar depicts number of AT8 positive neurons in the injected hippocampus. Student`s T-test between A and B and C and D did not show any significant differences for any anatomical level, but at -2 from Bregma the T-test between Bl6 CSF and P301S CSF seeded mice resulted in a p=0.07.

Non-seeded P301S mice endogenous tau pathology

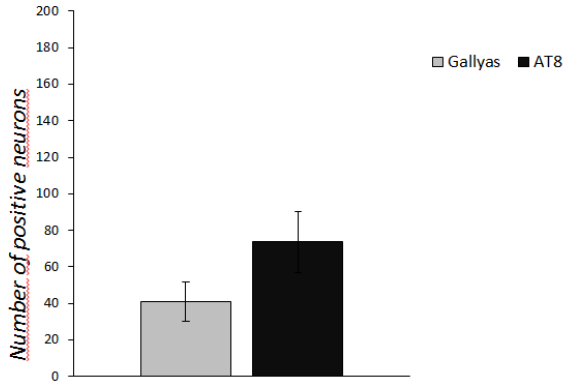

Figure S4. Number of silver positive tangles (Gallyas) and hyperphosphorylated tau (AT8) containing neurons in the right hippocampus of 7 months old, non-treated P301S mice (n=4).

Mouse brain stem / CSF Tau concentrations

Seed	Tau, ng/ml	P-Tau, ng/ml
P301S BS homogenate	180 553	308 575
P301S CSF	29	27
Conc. P301S CSF	80	100

Table S2. Tau and phospho-tau (P-Tau, T231) concentration of P301S brain stem homogenates (n=1), CSF (n=3),a nd concentrated CSF (n=1), as measured by ELISA.

Western blot

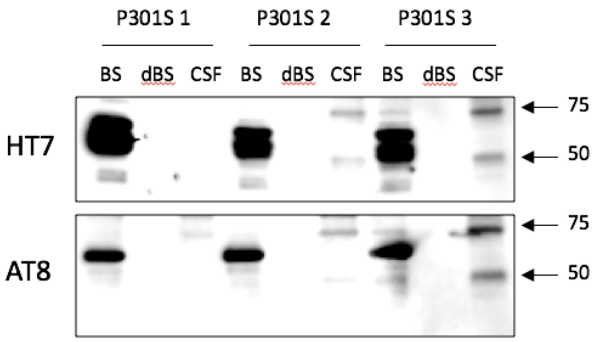

Figure S5. Western blot with HT7 (against total tau) and AT8 (hyperphosphorylated tau) antibodies of non-diluted 10% brain stem homogenate (BS), 1000 times diluted 10% BS (dBS), and non-concentrated CSF from 6 months aged P301S mice (n=3).

Co-expression of truncated and full-length tau induces severe neurotoxicity

Molecular Psychiatry, 2016, 1-9

The author of the present thesis performed some of the behavioral tests (grid test, object recognition test), immunofluorescence (Thioflavine-S, MG160, COX) and immunohistochemistry (VAMP2, Synaptophysin) experiments, all this including data collection and analysis, and contributed to the manuscript writing.

OPEN

Molecular Psychiatry (2016), 1–9

www.nature.com/mp

ORIGINAL ARTICLE

Co-expression of truncated and full-length tau induces severe neurotoxicity

S Ozcelik[1,2,5], F Sprenger[1,2,5], Z Skachokova[1,2], G Fraser[3], D Abramowski[4], F Clavaguera[1], A Probst[1], S Frank[1], M Müller[4], M Staufenbiel[4], M Goedert[3], M Tolnay[1] and DT Winkler[1,2]

Abundant tau inclusions are a defining hallmark of several human neurodegenerative diseases, including Alzheimer's disease. Protein fragmentation is a widely observed event in neurodegenerative proteinopathies. The relevance of tau fragmentation for the neurodegenerative process in tauopathies has yet remained unclear. Here we found that co-expression of truncated and full-length human tau in mice provoked the formation of soluble high-molecular-weight tau, the failure of axonal transport, clumping of mitochondria, disruption of the Golgi apparatus and missorting of synaptic proteins. This was associated with extensive nerve cell dysfunction and severe paralysis by the age of 3 weeks. When the expression of truncated tau was halted, most mice recovered behaviorally and functionally. In contrast, co-expression of full-length tau isoforms did not result in paralysis. Truncated tau thus induces extensive but reversible neurotoxicity in the presence of full-length tau through the formation of nonfilamentous high-molecular-weight tau aggregates, in the absence of tau filaments. Targeting tau fragmentation may provide a novel approach for the treatment of human tauopathies.

Molecular Psychiatry advance online publication, 2 February 2016; doi:10.1038/mp.2015.228

INTRODUCTION

Tau pathology is a defining characteristic of a number of human neurodegenerative diseases, including Alzheimer's disease, progressive supranuclear palsy, corticobasal degeneration, argyrophilic grain disease, chronic traumatic encephalopathy and some cases of frontotemporal dementia.[1,2] Physiologically, tau promotes microtubule assembly and stability. In tauopathies, soluble tau assembles into insoluble filaments, resulting in neurodegeneration.[2–4] It remains to be determined which tau species are the most toxic and how toxicity is mediated.

Abnormal protein aggregation underlies the vast majority of human neurodegenerative diseases.[5] In some diseases, the aggregates are made of cleavage products of larger proteins, such as Aβ in Alzheimer's disease[6] and amyloid-Bri in familial British dementia.[7] In other diseases, full-length and truncated proteins co-exist in the aggregates, as is the case of α-synuclein in Parkinson's disease and dementia with Lewy bodies[8,9] and TDP-43 in cases of frontotemporal dementia and amyotrophic lateral sclerosis.[10,11] Truncated proteins are often more aggregation prone than their full-length counterparts.[12,13]

It is being increasingly debated whether tau fragmentation may play a role in the pathogenesis of Alzheimer's disease. Cleaved tau has been detected in patient brains and in mouse models.[14–20] In Alzheimer's disease, tau fragmentation has been described as an early event. Caspases and calpains have been implicated, with the caspase 3 cleavage after D421 being the most studied.[21] More recently, asparagine endopeptidase has also been shown to cleave tau and promote pathology.[22] However, the general relevance of tau fragmentation for neurodegeneration has been questioned. Thus, in mouse lines transgenic for human mutant P301S[23] or P301L[24] tau, cleavage after D421 was a late event and only small amounts of caspase-cleaved tau were detected. Moreover, earlier studies found tau fragmentation to be primarily associated with degradation of the fuzzy filament coat.[25,26] Full-length tau is the major component of the paired helical and straight filaments of Alzheimer's disease.[27] On the other hand, truncation of tau increases its propensity to aggregate and it has been suggested that cleaved tau may seed the aggregation of the full-length protein.[28–30] Taken together, it is therefore possible that truncation of a small amount of tau can lead to its aggregation and the seeding of full-length tau.

Here we studied the interaction of truncated and full-length human tau. We generated an inducible mouse line (TAU62) overexpressing human 3R $tau_{151–421}$ (Δtau). This 239 amino acid tau protein extends from the proline-rich region to the caspase cleavage site. We co-expressed it with either wild-type full-length 3R tau or 4R tau,[31] or with mutant full-length 4R P301S tau.[32] In all double transgenic lines, high-molecular-weight tau, severe nerve cell damage and motor palsy were observed in young mice. Following cessation of truncated tau expression, functional and structural recovery was observed in mice expressing full-length 4R tau. In contrast, young mice double transgenic for full-length 3R and 4R tau were unaffected.

MATERIALS AND METHODS

Production of transgenic mouse lines and doxycycline treatment

An overview of the mouse lines used in this study is provided in Supplementary Table 1. For the neuron-specific, inducible expression of 3R $tau_{151–421}$ (Δtau), TAU62 transgenic mice were generated by coinjection of

[1]Institute of Pathology, University Hospital Basel, Basel, Switzerland; [2]Department of Neurology, University Hospital Basel, Basel, Switzerland; [3]MRC, Laboratory of Molecular Biology, Cambridge, UK and [4]Institute of Biomedical Research, Novartis Pharma AG, Basel, Switzerland. Correspondence: Dr DT Winkler, Institute of Pathology and Department of Neurology, University Hospital Basel, Petersgraben 4, CH-4031 Basel, Switzerland.
E-mail: winklerd@uhbs.ch
[5]These two authors contributed equally to this work.
Received 1 September 2015; revised 3 December 2015; accepted 15 December 2015

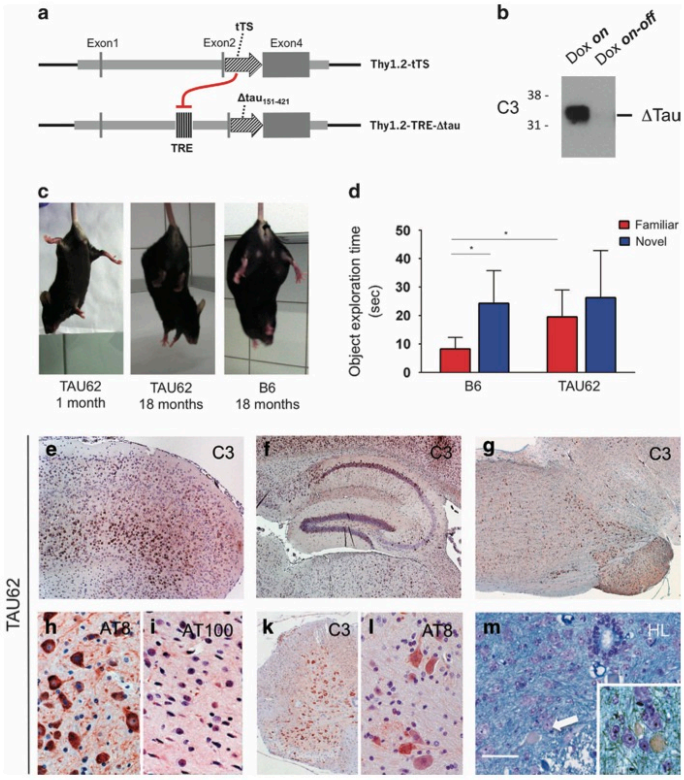

Figure 1. TAU62 mice express Δtau, develop a mild motor phenotype, memory deficits and pretangle pathology. (**a**) Expression constructs. In the presence of doxycycline, 3R $tau_{151-421}$ (Δtau) is expressed. In the absence of doxycycline, tTS (tetracycline-controlled transcriptional silencer) binds to TRE (tetracycline-responsive element), preventing the expression of Δtau. (**b**) Western blot of brain using anti-tau antibody C3 of a 1-month-old TAU62 mouse under doxycycline (Dox *on*) and 3 days after doxycycline withdrawal (Dox *on-off*). (**c**) Tail suspension test on young TAU62 mouse (1 month), aged B6 mouse (18 months) and aged TAU62 mouse (18 months). (**d**) Object recognition test. Object exploration time of adult TAU62 mice (aged 6 months) and their C57Bl6 littermates. (**e–m**) Histology of TAU62 mice aged 12 months (**e–g**) and 18 months (**h–m**). Immunohistochemistry with C3 of somatomotor cortex and orbital area (**e**), hippocampus (**f**), brainstem with tegmental reticular nucleus (**g**) and spinal cord (**k**). Immunohistochemistry of brainstem with AT8 (**h**) and AT100 (**i**); immunohistochemistry of spinal cord with AT8 (**l**). Holmes–Luxol (HL) staining shows the presence of spheroids in spinal cord (arrow; inset) (**m**). The scale bar in (**m**) corresponds to 60 μm in (**h**, **l** and **m**), 80 μm in (**i**), 200 μm in (**e**) and 400 μm in (**f**, **g** and **k**). $^*P < 0.05$.

robustly expressed in spinal cord neurons (Figure 1k) where AT8-positive tau accumulated in motor neurons (Figure 1l). Occasional axonal spheroids were seen by Holmes–Luxol staining (Figure 1m). These findings are comparable to those obtained in aged ALZ17 mice.[31]

Co-expression of Δtau and full-length four-repeat human mutant P301S tau causes early, but reversible, nerve cell dysfunction

We crossed TAU62 mice with tau inclusion-developing four-repeat P301S tau mice (383 amino acid tau isoform with P301S mutation).[32] Surprisingly, P301SxTAU62^{on} mice showed a drastic motor phenotype at 3 weeks of age (Supplementary Video S1). In contrast, homozygous P301S tau mice developed immobilizing limb paralysis at ~5 to 7 months (Supplementary Video S2), whereas heterozygous mice remained ambulatory until up to 16 months of age. In P301SxTAU62^{on} mice, motor impairment started with gait ataxia at 9 days and had evolved to a severe palsy by 3 weeks of age. Paralysis was reversible when Δtau expression was halted at 3 weeks of age. P301SxTAU62$^{on\text{-}off}$ mice recovered from severe palsy, and their gait normalized within 2–3 weeks (Figures 2a and b, Supplementary Video S3).

Paralysis of P301SxTAU62 mice is associated with the presence of high-molecular-weight tau

In P301S tau mice, paralysis evolves in parallel to tau tangle formation.[32] It was therefore surprising that paralyzed P301SxTAU62^{on} mice showed only mild pretangle pathology, in the absence of tau filaments (Figures 2c–f, for positive controls see Supplementary Figure 2a). However, the presence of soluble high-molecular-weight tau paralleled the motor impairment (Figure 2g and Supplementary Figure 2b). These tau species comprised Δtau as detected by antibody RD3 (Supplementary Figure 2c). There were

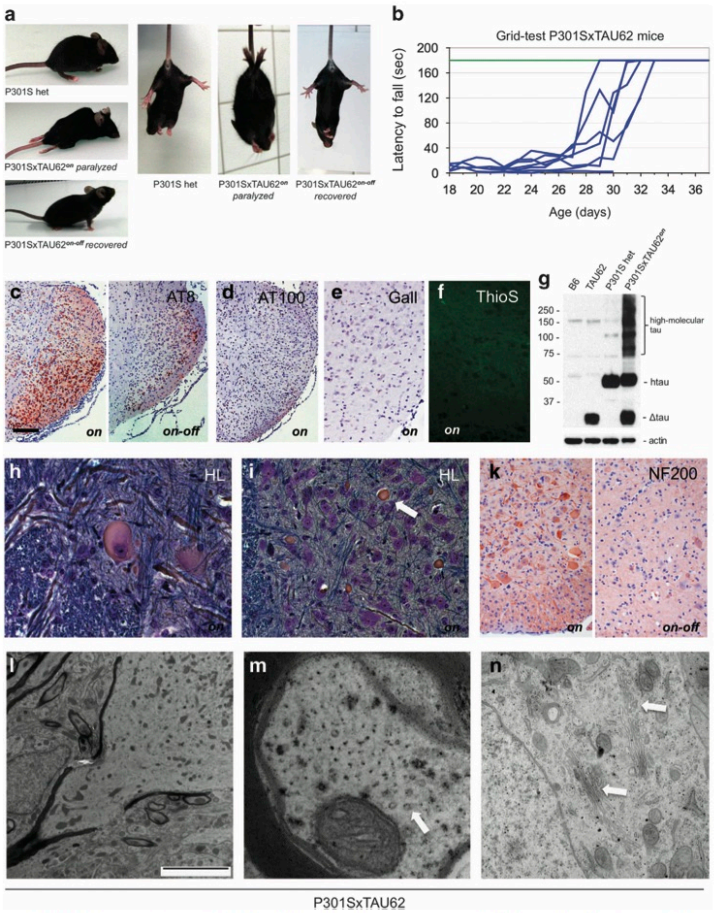

Figure 2. Co-expression of 4R P301S tau and Δtau (P301SxTAU62 mice) causes nerve cell dysfunction that is reversible upon cessation of Δtau expression. Paralysis is associated with the presence of soluble high-molecular-weight tau in the absence of sarkosyl-insoluble tau and tau filaments. Paralyzed mice exhibit axonal accumulations of neurofilaments and mitochondria. (**a**) Heterozygous P301S mouse (aged 3 weeks); paralyzed (aged 3 weeks) and recovered (3 weeks after cessation of Δtau expression) P301SxTAU62 mice (see also Supplementary Videos S1 and S3). (**b**) Recovery of motor function was assessed by a grid test of P301SxTAU62 mice following the removal of doxycycline at 21 days of age (blue lines). Motor function of heterozygous P301S tau littermates (green line, $n = 8$). (**c**) Immunohistochemistry with AT8 of the tegmental reticular nucleus of the brainstem of paralyzed ('*on*') and recovered ('*on-off*') P301SxTAU62 mice; immunohistochemistry with AT100 (**d**), Gallyas–Braak silver (**e**) and Thioflavin S staining (**f**) of the reticular nucleus of paralyzed mice. (**g**) Western blot with human-specific anti-tau antibody HT7 of brainstem tissue from nontransgenic (B6), TAU62, P301S and P301SxTAU62 mice. (**h** and **i**) Holmes–Luxol (HL) staining of spinal cord of paralyzed 3-week-old P301SxTAU62 mice. The arrow in (**i**) points to a spheroid; (**k**) immunohistochemistry of paralyzed ('*on*') and recovered ('*on-off*') mice using antibodies against the 200 kDa subunit of neurofilaments (NF200). The scale bar in (**c**) corresponds to 26 μm in (**h**), 40 μm in (**f** and **i**), 80 μm in (**k**), 100 μm in (**e**) and 200 μm in (**c** and **d**). (**l–n**) Electron microscopy of the spinal cord of paralyzed mice. Only a few isolated microtubules are present in axons (**m**, arrow). Fragmented Golgi material is seen in nerve cell bodies (**n**, arrows). The scale bar in (**l**) corresponds to 5 nm in (**l**), 220 nm in (**m**) and 1.4 nm in (**n**).

no tau bands in the sarkosyl-insoluble fraction (Supplementary Figure 2d). Although high-molecular-weight tau forms were absent in young heterozygous P301S tau mice, similar species were observed in aged homozygous mice (Supplementary Figure 2b). After the expression of Δtau had ceased and P301SxTAU62$^{on\text{-}off}$ mice were moving normally, high-molecular-weight tau was no longer detectable (Supplementary Figure 2b).

Reversible axonal damage

The Δtau was widely expressed in the spinal cord of P301SxTAU62^{on} mice, resulting in a reversible pretangle pathology (Supplementary Figures 2e–g). Spinal cord neurons of paralyzed mice showed signs of severe dysfunction with pathological swelling, chromatolysis (Figure 2h) and axonal damage, with extensive accumulation of neurofilaments, partly in the form of

axonal spheroids (Figures 2i and k). Neurofilament accumulation normalized upon cessation of Δtau expression (Figure 2k).

By electron microscopy, spheroids comprised massed, poorly oriented neurofilaments intermixed with multiple small, congested mitochondria (Figure 2l), compatible with axonal transport disruption. Spinal cord axons of paralyzed P301SxTAU62^{on} mice contained only sparse microtubules, whereas neurofilaments were abundant (Figure 2m). Widespread fragmentation of the Golgi network was also seen (Figure 2n).

Reversible disruption of the Golgi network, dysregulation of synaptic proteins and mitochondrial mislocalization

When aged 3 weeks, P301SxTAU62^{on} mice exhibited a fragmented and swollen Golgi network in CA1 pyramidal cells (Supplementary Figures 3a, b, d and e). After Δtau expression was halted, the Golgi structure normalized (Supplementary Figures 3c and f). Synaptophysin immunoreactivity accumulated within the soma of pyramidal cells (Supplementary Figures 3g–i), indicative of transport dysfunction. VAMP2 was lost from CA1 dendrites when Δtau was co-expressed with full-length mutant tau (Supplementary Figures 3k–m). Mitochondria reversibly accumulated within the soma of pyramidal cells, as well as in axons (Supplementary Figures 3n–p).

Reversible neuropathy and myopathy

In paralyzed mice, nerve cell damage was accompanied by an axonal neuropathy (Figures 3a–i and Supplementary Figures 4a–c). The sciatic nerve fibers exhibited vacuolated (Figure 3b) as well as collapsed myelin sheets (Figure 3e), indicating Wallerian degeneration. Neurofilament staining revealed thinned nerve fibers and spotty areas of fiber loss in paralyzed mice (Figure 3h, arrow). Upon motor recovery, myelin debris was no longer detectable and intact nerve fibers of slightly reduced diameter were seen (Figures 3c, f and i). Hindlimb paralysis was associated with muscle wasting (Figure 3k) and marked muscle fiber atrophy (Figure 3n), whereas muscle fibers of heterozygous P301S and TAU62 mice were of normal size (Figures 3k–m and Supplementary Figures 4d and e). Atrophic muscle fibers of paralyzed mice (Figure 3n) were significantly smaller compared with nonparalyzed controls (Figure 3p, $P < 0.001$). Both type 1 and 2 fibers were affected and groups of angulated atrophic fibers present, consistent with neurogenic muscle atrophy (Supplementary Figures 4d–g). In parallel with motor improvement, the muscles largely recovered macroscopically (Figure 3k). Recovered mice exhibited partly hypertrophic muscle fibers, with grouping of type 2 fibers, again indicative of neurogenic muscular atrophy (Figure 3o and Supplementary Figure 4g). Upon motor recovery, the percentage of muscle fibers with centralized nuclei was significantly increased in P301SxTAU62$^{on\text{-}off}$ mice (Figure 3q).

Co-expression of Δtau and full-length four-repeat human wild-type tau causes early, but reversible, nerve cell dysfunction

In Alzheimer's disease, tau pathology develops in the absence of *MAPT* mutations. We therefore crossed TAU62 mice with ALZ17 transgenic mice[31] that express wild-type full-length human four-repeat tau (441 amino acid isoform). ALZ17xTAU62^{on} mice showed a similar phenotype to that of P301SxTAU62^{on} mice. They developed severe motor palsy within 3 weeks (Figures 4a and b and Supplementary Video S4), and soluble high-molecular-weight tau was present (Figure 4c). Pretangle pathology was accompanied by the accumulation of neurofilaments and the formation of axonal spheroids (Figures 4d–g). Peripheral nerves showed evidence of Wallerian degeneration with ovoid-shaped myelin debris (Figure 4h) with consecutive neurogenic muscle atrophy (Figure 4k). Structural and functional changes were reversible, following the cessation of Δtau expression (Figures 4b, i and l and Supplementary Video S5).

Co-expression of Δtau and full-length three-repeat human wild-type tau causes early and largely irreversible nerve cell dysfunction

We crossed TAU62 mice with ALZ31 transgenic mice that express wild-type full-length three-repeat human tau (352 amino acid tau isoform). ALZ31xTAU62^{on} mice showed severe and early paralysis (Supplementary Figures 5a and b and Supplementary Video S6), developed soluble high-molecular-weight tau (Supplementary Figure 5c) and pre-tangle pathology, as well as neuronal and muscular damage occurred (Supplementary Figures 5d–i). However, unlike what we observed before, most mice failed to recover when Δtau expression was halted.

Co-expression of two full-length human tau isoforms causes only late nerve cell dysfunction

Slowly progressive, initially mild, motor impairment occurred in mice co-expressing two full-length human tau isoforms (Figures 5a and b). P301SxALZ31 tau mice were still ambulatory at the age of 12 months (Figure 5a and Supplementary Video S7). Similarly, ALZ17xALZ31 tau mice confirmed the absence of severe nerve cell dysfunction (Figure 5b and Supplementary Video S8). Mice from both lines showed robust tau expression, whereas no high molecular tau was detected (Figure 5c and Supplementary Figure 6). They developed only mild motor impairment at the age of 4 months and showed pretangle pathology with extensive AT8 staining (Figures 5d–l).

DISCUSSION

Here we demonstrate the detrimental interplay between truncated and full-length human tau *in vivo*. Co-expression of truncated tau and full-length wild-type or mutant tau resulted in the formation of soluble, high-molecular-weight tau, severe nerve cell dysfunction, paralysis and marked histopathological changes. Full-length tau and tau truncated at D421 were present in the high-molecular-weight aggregates, consistent with the need for an interaction between the two species. Sarkosyl-insoluble tau or filaments were not present, indicating that nonfilamentous, sarkosyl-soluble, aggregated tau can cause extensive neurotoxicity.

These findings are in agreement with the postulated importance of oligomeric, sarkosyl-soluble tau for the pathogenesis of human tauopathies.[40–42] Tau oligomers have been detected in the brains of patients with Alzheimer's disease and progressive supranuclear palsy.[43–45] In transgenic mouse models of tauopathies, nerve cell loss and memory deficits can precede detectable filamentous tau pathology.[46–48] Moreover, nerve cell loss has been reported in the absence of filaments in tau-overexpressing *Drosophila*,[49] suggesting that the events that lead from tau accumulation to neurodegeneration may not involve filament formation. Reducing tau overexpression in mice transgenic for human mutant P301L tau has been reported to decrease nerve cell loss, despite the continued formation of tau filaments.[50]

Of the mouse lines transgenic for full-length tau, only that expressing human mutant P301S tau develops sarkosyl-insoluble tau inclusions, neurodegeneration and paralysis. However, these inclusions form only when animals heterozygous for the transgene are more than 12 months old.[51] When crossed with line TAU62, heterozygous P301S tau mice were paralyzed by the age of 3 weeks, in the absence of sarkosyl-insoluble tau. The same was true of mice transgenic for wild-type 4R tau when crossed with the TAU62 line; wild-type 4R tau-expressing mice do not develop tau inclusions or neurodegeneration.[31] Whereas soluble oligomeric tau can cause neurotoxicity, it has been reported that either

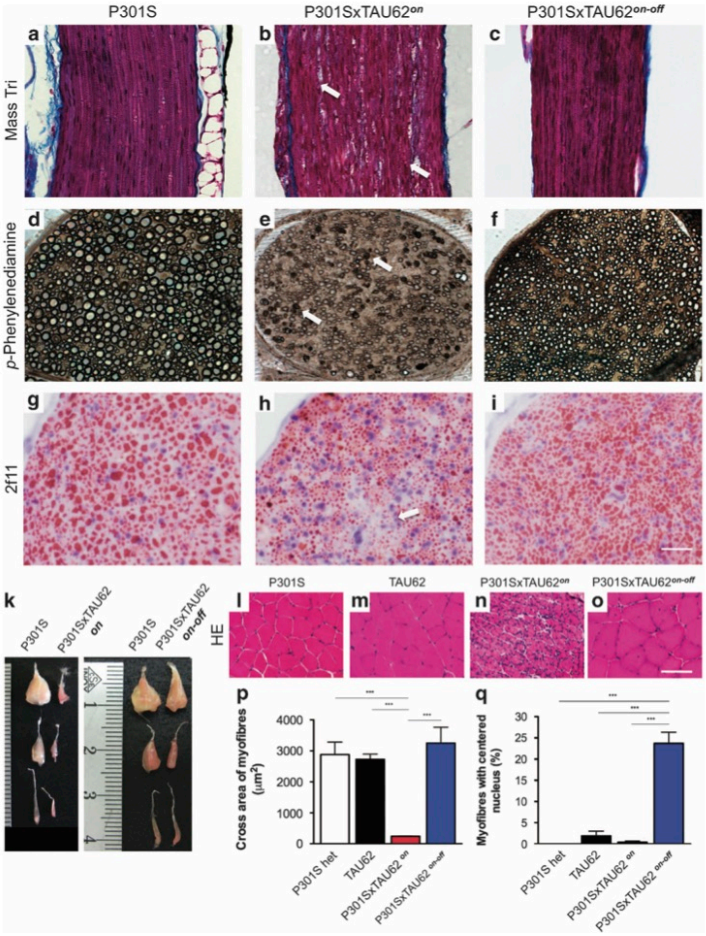

Figure 3. Co-expression of 4R P301S tau and Δtau (P301SxTAU62 mice) causes neuropathy and neurogenic muscle atrophy that are reversible upon cessation of Δtau expression. (**a–i**) Sciatic nerves stained using Masson's trichrom stain (**a–c**), *para*-phenylenediamine (**d–f**) and 2f11 immunohistochemistry (**g–i**). The scale bar in (**i**) corresponds to 50 µm in (**a–c**), 32 µm in (**d-f**) and 25 µm in (**g–i**). (**k**) Macroscopic view of hindlimb muscles. From the top: M. gastrocnemius and M. soleus; M. tibialis anterior; M. extensor digitorum longus. (**l–o**) M. gastrocnemius stained with hematoxylin and eosin (HE). The scale bar in (**o**) corresponds to 100 µm (for **l–o**). Quantification of myofiber area (**p**) and myofibers with internalized nucleus (**q**). P301S: heterozygous mice transgenic for human mutant P301S tau, aged 3 weeks; TAU62: heterozygous mice expressing 3R $tau_{151-421}$, aged 3 weeks; P301SxTAU62^{on}: paralyzed mice, aged 3 weeks; P301SxTAU62^{on-off}: recovered mice, 6 weeks after cessation of the expression of Δtau. ***$P < 0.001$.

soluble[52] or insoluble aggregated tau is required for the prion-like propagation of tau assemblies.[53] It will be interesting to see whether the soluble high-molecular-weight tau described here can seed tau assembly.

Similar to Alzheimer's disease,[54] axonal spheroids filled with small congested mitochondria and neurofilaments accumulated in the bigenic mouse lines, suggestive of axonal transport deficits. Microtubules were sparse in spinal cord axons, where neurofilaments accumulated, reminiscent of what has been described in Alzheimer's disease[55] and transgenic mouse models of human tauopathies.[56,57] Axonal transport defects have been reported in a broad spectrum of neurodegenerative diseases, including Alzheimer's disease, and the term 'dysferopathies' has been introduced for this group of disorders.[58,59] Paralyzed P301SxTAU62 mice exhibited dislocated and clustered mitochondria, similar to Alzheimer's disease and tauopathy models, where perinuclear mitochondrial clumping correlated with the accumulation of soluble tau species.[60] Dispersed and swollen Golgi networks, associated with the somatic accumulation of synaptophysin, suggested disrupted cellular transport mechanisms, similar to previous findings in mice transgenic for human mutant P301L tau.[61] In Alzheimer's disease, Golgi fragmentation has been

two Thy 1.2 minigene-based[33] constructs into C57BL/6J oocytes. The Thy1.2-tTS construct was obtained by inserting a tetracycline-controlled transcriptional silencer element (tTS) complementary DNA into the *Xho*I site of the murine Thy 1.2 minigene. The Thy1.2-TRE-Δtau construct contained a tetracycline-responsive element (TRE) in the *Spe*I site of the Thy1.2 cassette ~860 bp upstream of human wild-type Δtau complementary DNA encoding amino acids 151 to 421 of a 3-repeat domain spanning human wild-type tau fragment (0N3R $tau_{151-421}$) cloned in the *Xho*I site. Six transgenic founder TAU62 mice (C57BL/6J-TgN(TRE-Thy1$tau_{151-421}$ xThy1tTS)62) were identified and the inducible expression of human Δtau was assessed by western blotting and immunohistochemistry. Lines 62/2 and 62/48 expressed similar levels of Δtau (*'on'*) and stopped expression following the removal of doxycycline (*'on-off'*). Most experiments were performed using the TAU62/48 line, abbreviated TAU62. TAU62/2 mice were used to rule out an insertion site effect. The production of P301S mutant 0N4R tau transgenic mice (C57BL/6J-TgN(Thy1-hTau_{P301S}))[32] and full-length wild-type 2N4R tau transgenic ALZ17 mice (C57BL/6J-TgN (Thy1hTau)17) has been previously described.[31] For the generation of ALZ31 wild-type human 0N3R tau transgenic mice (C57BL/6J-TgN (Thy1hTau)31), 0N3R human tau complementary DNA was cloned into the Thy 1.2 minigene and injected into C57BL/6J oocytes. P301SxTAU62, ALZ17xTAU62 and ALZ31xTAU62 double transgenic mice were obtained by crossbreeding of the respective single transgenic lines using TAU62/48 mice if not indicated otherwise. All transgenic mice, including P301SxALZ31 and ALZ17xALZ31 mice, were heterozygous for the transgenes of interest, unless specifically mentioned otherwise. Food containing 500 mg kg^{-1} doxycycline was provided *ad libitum* also during breeding to induce Δtau expression. The number of mice used was minimized according to the Swiss regulation on Animal Experimentation. All animal experiments were approved by the local ethics and animal care and use committees.

Histology and immunohistochemistry

Mice were anesthetized with a mixture of ketamine (100 mg kg^{-1}) and xylazine (10 mg kg^{-1}) intraperitoneally and after deep sleeping, mice were injected by sodium pentobarbital (100 mg kg^{-1}) and transcardially perfused with cold phosphate-buffered saline (PBS). Spinal cord, sciatic nerve and the brain were quickly removed. Brain and spinal cord tissue was immersion fixed in 4% paraformaldehyde and embedded in paraffin. Sagittal and transverse serial sections (4–20 μm) were cut. Muscles were removed and snap frozen in liquid nitrogen cooled isopentane. Coronal sections (10 μm) were cut. Myofibers with or without internalized nuclei and fiber cross-sectional areas were quantified[34,35] in tissue derived from five mice per group, using ImageJ software v1.43 (NIH, Bethesda, MD, USA). Sciatic nerves were dissected and fixed for at least 2 h in 2.5% of glutaraldehyde, followed by washing of the tissues in 10 mM PBS overnight. The tissues were reduced in 1% osmium tetroxide and following dehydration, embedded in Durcupan. Semithin sections were cut. Hematoxylin–eosin, Holmes–Luxol, Thioflavin S,[36] as well as ATPase (pH 4.2), Masson's trichrom and *para*-phenylenediamine staining were performed according to standard protocols.[37] Fibrillar tau pathology was assessed by Gallyas silver staining. Antibodies used for immunohistochemistry are listed under Supplementary Experimental Procedures.

Electron microscopy

Mice were anesthetized with a mixture of ketamine (100 mg kg^{-1}) and xylazine (10 mg kg^{-1}) intraperitoneally, injected with sodium pentobarbital (100 mg kg^{-1}) and transcardially perfused with PBS, followed by perfusion with 2% paraformaldehyde and 2% glutaraldehyde. Brains and spinal cords were removed and postfixed for 1 h, followed by rinsing of the tissues in 10 mM PBS. The tissues were reduced in 1% osmium tetroxide and 1.5% potassium ferrocyanide and, following dehydration, embedded in Epon. Ultrathin sections from selected areas were cut with a microtome (Ultracut E; Leica Microsystems GmbH, Wetzlar, Germany), collected on single-slot grids and stained in 6% uranyl acetate. Sections were examined and photographed with a Morgagni FEI 80kV electron microscope (FEI Company, Eindhoven, The Netherlands).

Sarkosyl extraction and western blotting

Following PBS perfusion, one half of the mouse brain was dissected into forebrain and brainstem and frozen in liquid nitrogen. Brain tissue was homogenized 1:10 (w/v) in Tris-buffered saline Complete buffer (20 mM Tris, pH 7.5, 137 mM NaCl, 1 tablet of complete mini protease inhibitor cocktail tablets) and the samples were aliquoted. Sarkosyl extraction was performed as previously described.[23] Briefly, the brain tissue was homogenized in A68 buffer (0.5 ml of 800 mM NaCl, 10% sucrose, 10 mM Tris-HCl, pH 7.4, 1 mM EGTA) using a Kinetica polytron. Samples were centrifuged at 5000 *g* for 15 min. The supernatant was collected and sarkosyl added to 1%, followed by shaking for 1 h. The samples were then centrifuged at 80 000 *g* for 30 min and the pellet resuspended in 150 μl g^{-1} of 50 mM Tris-HCl, pH 7.4. Western blots were performed under nonreducing conditions by using samples composed of an appropriate amount of protein, 5 μl NuPAGE LDS sample buffer and deionized water. Additional application of 2 μl NuPAGE reducing agent was used to obtain reducing conditions. Antibodies used for western blotting are listed under Supplementary Experimental Procedures.

Behavioral assessment

Motor behavior, including gait ataxia, tremor and hindlimb reflexes, was assessed. Quantitative motor testing was performed by the grid test in which mice were placed on a vertical mesh grid and the latency to fall off from the grid was recorded for 3 min.

For object recognition test, mice were placed in a squared open field box (48 × 48 × 40 cm) under dim light conditions. Mice were let freely to explore the box during 3 consecutive days for 15 min, until no signs of stress were present (habituation phase). During the following 2 days, two identical objects were introduced at diagonal corners of the field for training sessions of 10 min duration (training phase). Training was halted when the mice had closely explored the objects for 20 s.[38] Next day, the animals' short-term memory was tested (test phase) by replacing one of the familiar objects with a novel one, and the time spent exploring each object during a period of 6 min was video recorded. Video scoring was done by a researcher blind to the genotype, and as exploration criteria nose sniffing/touching of the object at 2 cm or less distance[38] were used. For both training and test phases, 10 cm high objects composed of the same material were used, and the position of the novel and familiar objects were randomized across groups.

Statistics

Statistical analysis was performed using one-way analysis of variance followed by Bonferroni's multiple comparison test and Student's *t*-tests with Graphpad Prism software Version 5.0a (GraphPad Software, La Jolla, CA, USA). *P*-values are reported and outlined as follows: $*P < 0.05$, $**P < 0.01$ and $***P < 0.001$. The mean and s.d. are indicated.

RESULTS

Inducible expression of Δtau results in mild motor palsy, memory dysfunction and pretangle pathology

To study the interplay of truncated and full-length human tau *in vivo*, we first generated an inducible transgenic mouse model (line TAU62) overexpressing wild-type 3R $tau_{151-421}$ (Δtau). A tetracycline-controlled, neuron-specific Thy1.2 promoter element (Figure 1a) was used to drive expression that ceased completely upon the removal of doxycycline (Figure 1b).

The Δtau expression resulted in a mild motor phenotype starting at 3–6 months of age. At higher ages, tremor and gait ataxia were followed by mild hindlimb paralysis, and TAU62 mice showed an abnormal limb flexion reflex (Figure 1c and Supplementary Figure 1). Indicative of short-term memory deficits, adult TAU62 mice explored a familiar object significantly longer ($P = 0.04$) than their C57Bl6 littermates. The latter accurately discriminated familiar from novel objects ($P = 0.02$, Figure 1d).

The Δtau was expressed throughout the central nervous system, including cerebral cortex (Figure 1e), hippocampus (Figure 1f) and brainstem (Figure 1g), comparable to the expression patterns in other transgenic lines using the Thy1.2 promoter.[32]

Pretangle pathology, defined as tau hyperphosphorylation at the AT8 epitope, persisted in aged TAU62 mice (Figure 1h). In contrast to rat models overexpressing truncated tau,[39] TAU62 mice did not develop tau tangles and showed no hyperphosphorylation of late epitopes, such as AT100, consistent with the absence of tau filaments (Figure 1i). In addition, Δtau was

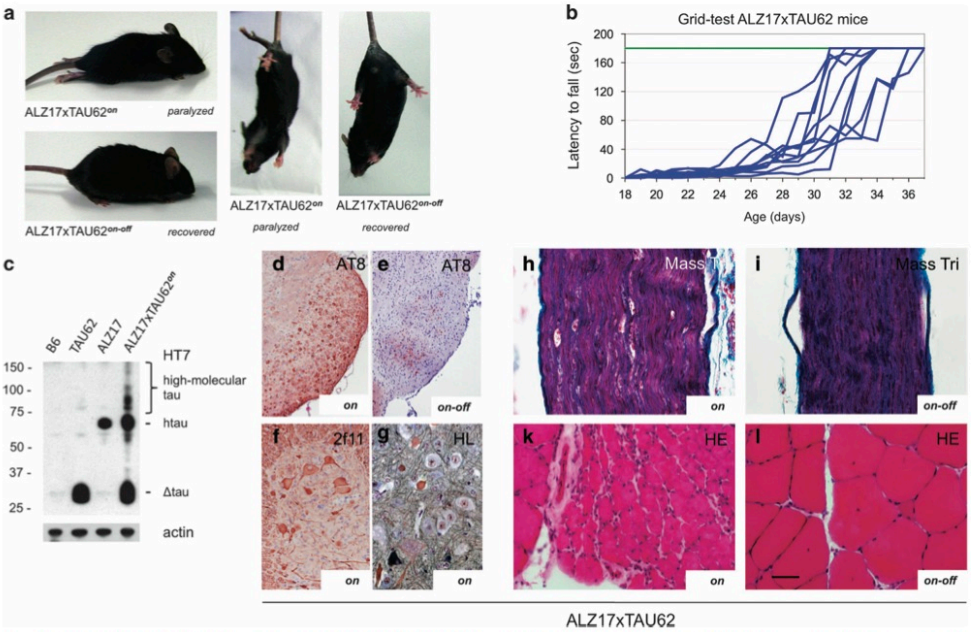

Figure 4. Co-expression of 4R wild-type tau and Δtau (ALZ17xTAU62) causes paralysis and neuropathy that are reversible upon cessation of Δtau expression. (**a**) Paralyzed (aged 3 weeks) and recovered (3 weeks after cessation of Δtau expression) ALZ17xTAU62 mice (see also Supplementary Videos S4 and S5). (**b**) Recovery of motor function as assessed by a grid test of ALZ17xTAU62 mice following the removal of doxycycline between 16 and 20 days of age (blue lines). Motor function of heterozygous ALZ17 littermates (green line) ($n=6$). (**c**) Western blot with HT7 of brainstem tissue from nontransgenic (B6), TAU62, ALZ17 and ALZ17xTAU62 mice. Actin staining was used as the loading control. (**d–l**) Histological analysis of paralyzed ('*on*'; **d**, **f**, **g**, **h** and **k**) and recovered ('*on-off*'; **e**, **i** and **l**) ALZ17xTAU62 mice using anti-tau antibody AT8 (**d** and **e**), anti-neurofilament antibody 2f11 (**f**), Masson's trichrome (**h** and **i**), Holmes–Luxol (HL) (**g**) and hematoxylin–eosin (HE) (**k** and **l**). The scale bar in (**l**) corresponds to 50 μm in (**h**, **i**, **g**, **k** and **l**), 100 μm in (**f**) and 200 μm in (**d** and **e**).

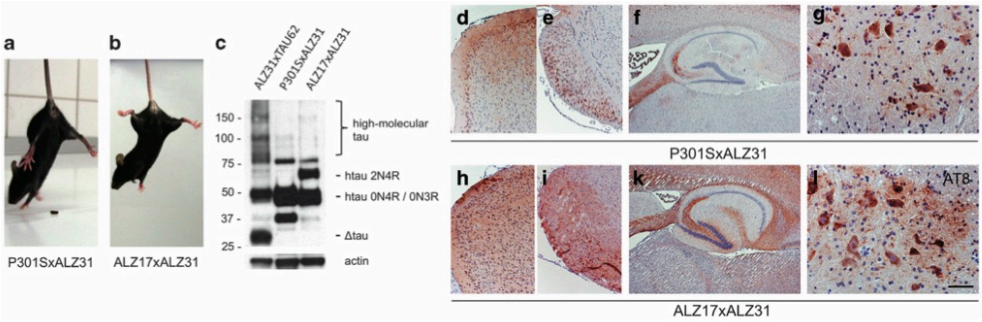

Figure 5. Co-expression of 4R mutant or wild-type tau and 3R wild-type (P301SxALZ31 or ALZ17xALZ31 mice) does not cause paralysis and results in pretangle pathology. (**a** and **b**) Unimpaired P301SxALZ31 and ALZ17xALZ31 mice aged 3 weeks (see also Supplementary Videos S7 and S8). (**c**) Western blot with HT7 of brainstem tissue from paralyzed ALZ31xTAU62 mice aged 3 weeks, unimpaired P301SxALZ31 aged 3 weeks and unimpaired ALZ17xALZ31 mice aged 4 months. Actin staining was used as the loading control. (**d–l**) Immunohistochemistry of 9-month-old P301SxALZ31 mouse and 4-month-old ALZ17xALZ31 mouse with AT8 ((**d** and **h**) cortex, (**e** and **i**) brainstem, (**f** and **k**) hippocampus and (**g** and **l**) spinal cord). The scale bar in (**l**) corresponds to 200 μm in (**d**, **e**, **h** and **i**), 500 μm in (**f** and **k**) and 50 μm in (**g** and **l**).

described in nontangle-bearing neurons,[62] consistent with the present findings. The neuronal dysfunction present in the absence of tau filaments in our bigenic mouse models may mirror an early stage of tauopathy in Alzheimer's disease.[63]

Although we observed partial nerve fiber loss in paralyzed mice, reflecting toxicity of the oligomeric tau species, the palsy appears mainly attributable to functional neuronal impairment. When Δtau expression was halted, the severe limb paralysis largely improved,

despite the continued expression of full-length wild-type 4R or mutant P301S 4R tau. After a lag phase of a few days, paralyzed mice rapidly regained full motor control within 2 days, pointing to a reversible impairment of axonal transport. Rapidly regained nerve fiber function then enables remodeling of atrophic muscle. Only when Δtau had been expressed together with full-length wild-type 3R tau, was paralysis not reversible following the cessation of the expression of truncated tau. Functional recovery thus appears to depend on the presence of mixed 3R/4R tau oligomers. Following cessation of Δtau expression and functional recovery, the high-molecular-weight tau bands disappeared. Co-expression of full-length and Δtau was required, because co-expression of full-length 3R and 4R tau did not cause paralysis.

While the C-terminal end of Δtau constitutes a main tau cleavage site in Alzheimer's disease, its N-terminal end has been set at the structural transition of the proline-rich region to the acidic N-terminal projection domain of tau. This limitation of our model has been unavoidable, as N-terminal tau cleavage sites are yet poorly characterized, and only few N-terminal cleavage sites, located at the beginning of the acidic region of tau, have been confirmed *in situ*.[18,64,65]

In conclusion, we show here that an interaction between full-length and Δtau can lead to the formation of neurotoxic tau species that interfere with axonal transport. The reversibility of paralysis upon cessation of truncated tau expression augurs well for the development of new therapies for Alzheimer's disease and other tauopathies.

CONFLICT OF INTEREST

The authors declare no conflict of interest.

ACKNOWLEDGMENTS

We thank Nicholas Gonatas, University of Pennsylvania Medical Center, Philadelphia, PA, for the MG160 antibody, the Microscopy Center of the University of Basel (M Dürrenberger and U Sauder) for experimental help and Professor Ludwig Kappos, University Hospital Basel, for helpful discussions and support of this work. MT and DTW are supported by the Swiss National Science Foundation (310030_135214 to MT and 32323B_123812 to DTW), the Velux Foundation, the Mach-Gaensslen Foundation, the Synapsis Foundation and the D&N Yde Foundation, Switzerland. GF and MG are supported by the UK Medical Research Council (U105184291).

REFERENCES

1 Spillantini MG, Goedert M. Tau pathology and neurodegeneration. *Lancet Neurol* 2013; **12**: 609–622.
2 Spires-Jones TL, Hyman BT. The intersection of amyloid beta and tau at synapses in Alzheimer's disease. *Neuron* 2014; **82**: 756–771.
3 Frost B, Hemberg M, Lewis J, Feany MB. Tau promotes neurodegeneration through global chromatin relaxation. *Nat Neurosci* 2014; **17**: 357–366.
4 Rosenmann H. Asparagine endopeptidase cleaves tau and promotes neurodegeneration. *Nat Med* 2014; **20**: 1236–1238.
5 Eisenberg D, Jucker M. The amyloid state of proteins in human diseases. *Cell* 2012; **148**: 1188–1203.
6 Masters CL, Selkoe DJ. Biochemistry of amyloid beta-protein and amyloid deposits in Alzheimer disease. *Cold Spring Harb Perspect Med* 2012; **2**: a006262.
7 Vidal R, Frangione B, Rostagno A, Mead S, Revesz T, Plant G *et al.* A stop-codon mutation in the BRI gene associated with familial British dementia. *Nature* 1999; **399**: 776–781.
8 Baba M, Nakajo S, Tu PH, Tomita T, Nakaya K, Lee VM *et al.* Aggregation of alpha-synuclein in Lewy bodies of sporadic Parkinson's disease and dementia with Lewy bodies. *Am J Pathol* 1998; **152**: 879–884.
9 Goedert M, Spillantini MG, Del Tredici K, Braak H. 100 years of Lewy pathology. *Nat Rev Neurol* 2013; **9**: 13–24.
10 Neumann M, Sampathu DM, Kwong LK, Truax AC, Micsenyi MC, Chou TT *et al.* Ubiquitinated TDP-43 in frontotemporal lobar degeneration and amyotrophic lateral sclerosis. *Science* 2006; **314**: 130–133.
11 Arai T, Hasegawa M, Akiyama H, Ikeda K, Nonaka T, Mori H *et al.* TDP-43 is a component of ubiquitin-positive tau-negative inclusions in frontotemporal lobar degeneration and amyotrophic lateral sclerosis. *Biochem Biophys Res Commun* 2006; **351**: 602–611.
12 Nonaka T, Kametani F, Arai T, Akiyama H, Hasegawa M. Truncation and pathogenic mutations facilitate the formation of intracellular aggregates of TDP-43. *Hum Mol Genet* 2009; **18**: 3353–3364.
13 Brower CS, Piatkov KI, Varshavsky A. Neurodegeneration-associated protein fragments as short-lived substrates of the N-end rule pathway. *Mol Cell* 2013; **50**: 161–171.
14 Gamblin TC, Chen F, Zambrano A, Abraha A, Lagalwar S, Guillozet AL *et al.* Caspase cleavage of tau: linking amyloid and neurofibrillary tangles in Alzheimer's disease. *Proc Natl Acad Sci USA* 2003; **100**: 10032–10037.
15 Rissman RA, Poon WW, Blurton-Jones M, Oddo S, Torp R, Vitek MP *et al.* Caspase-cleavage of tau is an early event in Alzheimer disease tangle pathology. *J Clin Invest* 2004; **114**: 121–130.
16 de Calignon A, Fox LM, Pitstick R, Carlson GA, Bacskai BJ, Spires-Jones TL *et al.* Caspase activation precedes and leads to tangles. *Nature* 2010; **464**: 1201–1204.
17 Khurana V, Elson-Schwab I, Fulga TA, Sharp KA, Loewen CA, Mulkearns E *et al.* Lysosomal dysfunction promotes cleavage and neurotoxicity of tau in vivo. *PLoS Genet* 2010; **6**: e1001026.
18 Horowitz PM, Patterson KR, Guillozet-Bongaarts AL, Reynolds MR, Carroll CA, Weintraub ST *et al.* Early N-terminal changes and caspase-6 cleavage of tau in Alzheimer's disease. *J Neurosci* 2004; **24**: 7895–7902.
19 Matsumoto SE, Motoi Y, Ishiguro K, Tabira T, Kametani F, Hasegawa M *et al.* The twenty-four KDa C-terminal tau fragment increases with aging in tauopathy mice: implications of prion-like properties. *Hum Mol Genet* 2015; **24**: 6403–6416.
20 Henriksen K, Wang Y, Sorensen MG, Barascuk N, Suhy J, Pedersen JT *et al.* An enzyme-generated fragment of tau measured in serum shows an inverse correlation to cognitive function. *PLoS One* 2013; **8**: e64990.
21 Avila J. Alzheimer disease: caspases first. *Nat Rev Neurol* 2010; **6**: 587–588.
22 Zhang Z, Song M, Liu X, Kang SS, Kwon IS, Duong DM *et al.* Cleavage of tau by asparagine endopeptidase mediates the neurofibrillary pathology in Alzheimer's disease. *Nat Med* 2014; **20**: 1254–1262.
23 Delobel P, Lavenir I, Fraser G, Ingram E, Holzer M, Ghetti B *et al.* Analysis of tau phosphorylation and truncation in a mouse model of human tauopathy. *Am J Pathol* 2008; **172**: 123–131.
24 Lin WL, Dickson DW, Sahara N. Immunoelectron microscopic and biochemical studies of caspase-cleaved tau in a mouse model of tauopathy. *J Neuropathol Exp Neurol* 2011; **70**: 779–787.
25 Goedert M, Wischik CM, Crowther RA, Walker JE, Klug A. Cloning and sequencing of the cDNA encoding a core protein of the paired helical filament of Alzheimer disease: identification as the microtubule-associated protein tau. *Proc Natl Acad Sci USA* 1988; **85**: 4051–4055.
26 Wischik CM, Novak M, Thogersen HC, Edwards PC, Runswick MJ, Jakes R *et al.* Isolation of a fragment of tau derived from the core of the paired helical filament of Alzheimer disease. *Proc Natl Acad Sci USA* 1988; **85**: 4506–4510.
27 Goedert M, Spillantini MG, Cairns NJ, Crowther RA. Tau proteins of Alzheimer paired helical filaments: abnormal phosphorylation of all six brain isoforms. *Neuron* 1992; **8**: 159–168.
28 Abraha A, Ghoshal N, Gamblin TC, Cryns V, Berry RW, Kuret J *et al.* C-terminal inhibition of tau assembly in vitro and in Alzheimer's disease. *J Cell Sci* 2000; **113**: 3737–3745.
29 Spires-Jones TL, Kopeikina KJ, Koffie RM, de Calignon A, Hyman BT. Are tangles as toxic as they look? *J Mol Neurosci* 2011; **45**: 438–444.
30 Wang YP, Biernat J, Pickhardt M, Mandelkow E, Mandelkow EM. Stepwise proteolysis liberates tau fragments that nucleate the Alzheimer-like aggregation of full-length tau in a neuronal cell model. *Proc Natl Acad Sci USA* 2007; **104**: 10252–10257.
31 Probst A, Gotz J, Wiederhold KH, Tolnay M, Mistl C, Jaton AL *et al.* Axonopathy and amyotrophy in mice transgenic for human four-repeat tau protein. *Acta Neuropathol* 2000; **99**: 469–481.
32 Allen B, Ingram E, Takao M, Smith MJ, Jakes R, Virdee K *et al.* Abundant tau filaments and nonapoptotic neurodegeneration in transgenic mice expressing human P301S tau protein. *J Neurosci* 2002; **22**: 9340–9351.
33 Luthi A, Putten H, Botteri FM, Mansuy IM, Meins M, Frey U *et al.* Endogenous serine protease inhibitor modulates epileptic activity and hippocampal long-term potentiation. *J Neurosci* 1997; **17**: 4688–4699.
34 Huang C, Tong J, Bi F, Zhou H, Xia XG. Mutant TDP-43 in motor neurons promotes the onset and progression of ALS in rats. *J Clin Invest* 2012; **122**: 107–118.
35 Demonbreun AR, Fahrenbach JP, Deveaux K, Earley JU, Pytel P, McNally EM. Impaired muscle growth and response to insulin-like growth factor 1 in dysferlin-mediated muscular dystrophy. *Hum Mol Genet* 2011; **20**: 779–789.
36 Winkler DT, Biedermann L, Tolnay M, Allegrini PR, Staufenbiel M, Wiessner C *et al.* Thrombolysis induces cerebral hemorrhage in a mouse model of cerebral amyloid angiopathy. *Ann Neurol* 2002; **51**: 790–793.

37 Romeis B. *Mikroskopische Technik*. Urban u. Schwarzenberg: München, Wien, Baltimore, 1989.
38 Leger M, Quiedeville A, Bouet V, Haelewyn B, Boulouard M, Schumann-Bard P *et al.* Object recognition test in mice. *Nat Protoc* 2013; **8**: 2531–2537.
39 Filipcik P, Zilka N, Bugos O, Kucerak J, Koson P, Novak P *et al.* First transgenic rat model developing progressive cortical neurofibrillary tangles. *Neurobiol Aging* 2012; **33**: 1448–1456.
40 Lasagna-Reeves CA, Castillo-Carranza DL, Sengupta U, Sarmiento J, Troncoso J, Jackson GR *et al.* Identification of oligomers at early stages of tau aggregation in Alzheimer's disease. *FASEB J* 2012; **26**: 1946–1959.
41 Blair LJ, Nordhues BA, Hill SE, Scaglione KM, O'Leary JC 3rd, Fontaine SN *et al.* Accelerated neurodegeneration through chaperone-mediated oligomerization of tau. *J Clin Invest* 2013; **123**: 4158–4169.
42 Gerson JE, Kayed R. Formation and propagation of tau oligomeric seeds. *Front Neurol* 2013; **4**: 93.
43 Maeda S, Sahara N, Saito Y, Murayama S, Ikai A, Takashima A. Increased levels of granular tau oligomers: an early sign of brain aging and Alzheimer's disease. *Neurosci Res* 2006; **54**: 197–201.
44 Patterson KR, Remmers C, Fu Y, Brooker S, Kanaan NM, Vana L *et al.* Characterization of prefibrillar Tau oligomers in vitro and in Alzheimer disease. *J Biol Chem* 2011; **286**: 23063–23076.
45 Gerson JE, Sengupta U, Lasagna-Reeves CA, Guerrero-Munoz MJ, Troncoso J, Kayed R. Characterization of tau oligomeric seeds in progressive supranuclear palsy. *Acta Neuropathol Commun* 2014; **2**: 73.
46 Oddo S, Caccamo A, Shepherd JD, Murphy MP, Golde TE, Kayed R *et al.* Triple-transgenic model of Alzheimer's disease with plaques and tangles: intracellular Abeta and synaptic dysfunction. *Neuron* 2003; **39**: 409–421.
47 Spires TL, Orne JD, SantaCruz K, Pitstick R, Carlson GA, Ashe KH *et al.* Region-specific dissociation of neuronal loss and neurofibrillary pathology in a mouse model of tauopathy. *Am J Pathol* 2006; **168**: 1598–1607.
48 Berger Z, Roder H, Hanna A, Carlson A, Rangachari V, Yue M *et al.* Accumulation of pathological tau species and memory loss in a conditional model of tauopathy. *J Neurosci* 2007; **27**: 3650–3662.
49 Wittmann CW, Wszolek MF, Shulman JM, Salvaterra PM, Lewis J, Hutton M *et al.* Tauopathy in Drosophila: neurodegeneration without neurofibrillary tangles. *Science* 2001; **293**: 711–714.
50 Santacruz K, Lewis J, Spires T, Paulson J, Kotilinek L, Ingelsson M *et al.* Tau suppression in a neurodegenerative mouse model improves memory function. *Science* 2005; **309**: 476–481.
51 Clavaguera F, Hench J, Lavenir I, Schweighauser G, Frank S, Goedert M *et al.* Peripheral administration of tau aggregates triggers intracerebral tauopathy in transgenic mice. *Acta Neuropathol* 2014; **127**: 299–301.
52 Lasagna-Reeves CA, Castillo-Carranza DL, Sengupta U, Guerrero-Munoz MJ, Kiritoshi T, Neugebauer V *et al.* Alzheimer brain-derived tau oligomers propagate pathology from endogenous tau. *Sci Rep* 2012; **2**: 700.
53 Clavaguera F, Bolmont T, Crowther RA, Abramowski D, Frank S, Probst A *et al.* Transmission and spreading of tauopathy in transgenic mouse brain. *Nat Cell Biol* 2009; **11**: 909–913.
54 Schmidt ML, Lee VM, Trojanowski JQ. Relative abundance of tau and neurofilament epitopes in hippocampal neurofibrillary tangles. *Am J Pathol* 1990; **136**: 1069–1075.
55 Cash AD, Aliev G, Siedlak SL, Nunomura A, Fujioka H, Zhu X *et al.* Microtubule reduction in Alzheimer's disease and aging is independent of tau filament formation. *Am J Pathol* 2003; **162**: 1623–1627.
56 Yoshiyama Y, Zhang B, Bruce J, Trojanowski JQ, Lee VM. Reduction of detyrosinated microtubules and Golgi fragmentation are linked to tau-induced degeneration in astrocytes. *J Neurosci* 2003; **23**: 10662–10671.
57 Zhang B, Carroll J, Trojanowski JQ, Yao Y, Iba M, Potuzak JS *et al.* The microtubule-stabilizing agent, epothilone D, reduces axonal dysfunction, neurotoxicity, cognitive deficits, and Alzheimer-like pathology in an interventional study with aged tau transgenic mice. *J Neurosci* 2012; **32**: 3601–3611.
58 Morfini GA, Burns M, Binder LI, Kanaan NM, LaPointe N, Bosco DA *et al.* Axonal transport defects in neurodegenerative diseases. *J Neurosci* 2009; **29**: 12776–12786.
59 Vossel KA, Zhang K, Brodbeck J, Daub AC, Sharma P, Finkbeiner S *et al.* Tau reduction prevents Abeta-induced defects in axonal transport. *Science* 2010; **330**: 198.
60 Kopeikina KJ, Carlson GA, Pitstick R, Ludvigson AE, Peters A, Luebke JI *et al.* Tau accumulation causes mitochondrial distribution deficits in neurons in a mouse model of tauopathy and in human Alzheimer's disease brain. *Am J Pathol* 2011; **179**: 2071–2082.
61 Liazoghli D, Perreault S, Micheva KD, Desjardins M, Leclerc N. Fragmentation of the Golgi apparatus induced by the overexpression of wild-type and mutant human tau forms in neurons. *Am J Pathol* 2005; **166**: 1499–1514.
62 Stieber A, Mourelatos Z, Gonatas NK. In Alzheimer's disease the Golgi apparatus of a population of neurons without neurofibrillary tangles is fragmented and atrophic. *Am J Pathol* 1996; **148**: 415–426.
63 Khan UA, Liu L, Provenzano FA, Berman DE, Profaci CP, Sloan R *et al.* Molecular drivers and cortical spread of lateral entorhinal cortex dysfunction in preclinical Alzheimer's disease. *Nat Neurosci* 2013; **17**: 304–311.
64 Derisbourg M, Leghay C, Chiappetta G, Fernandez-Gomez FJ, Laurent C, Demeyer D *et al.* Role of the Tau N-terminal region in microtubule stabilization revealed by new endogenous truncated forms. *Sci Rep* 2015; **5**: 9659.
65 Rohn TT, Rissman RA, Davis MC, Kim YE, Cotman CW, Head E. Caspase-9 activation and caspase cleavage of tau in the Alzheimer's disease brain. *Neurobiol Dis* 2002; **11**: 341–354.

Supplementary Information accompanies the paper on the Molecular Psychiatry website (http://www.nature.com/mp)

Supplemental Information

Table S1

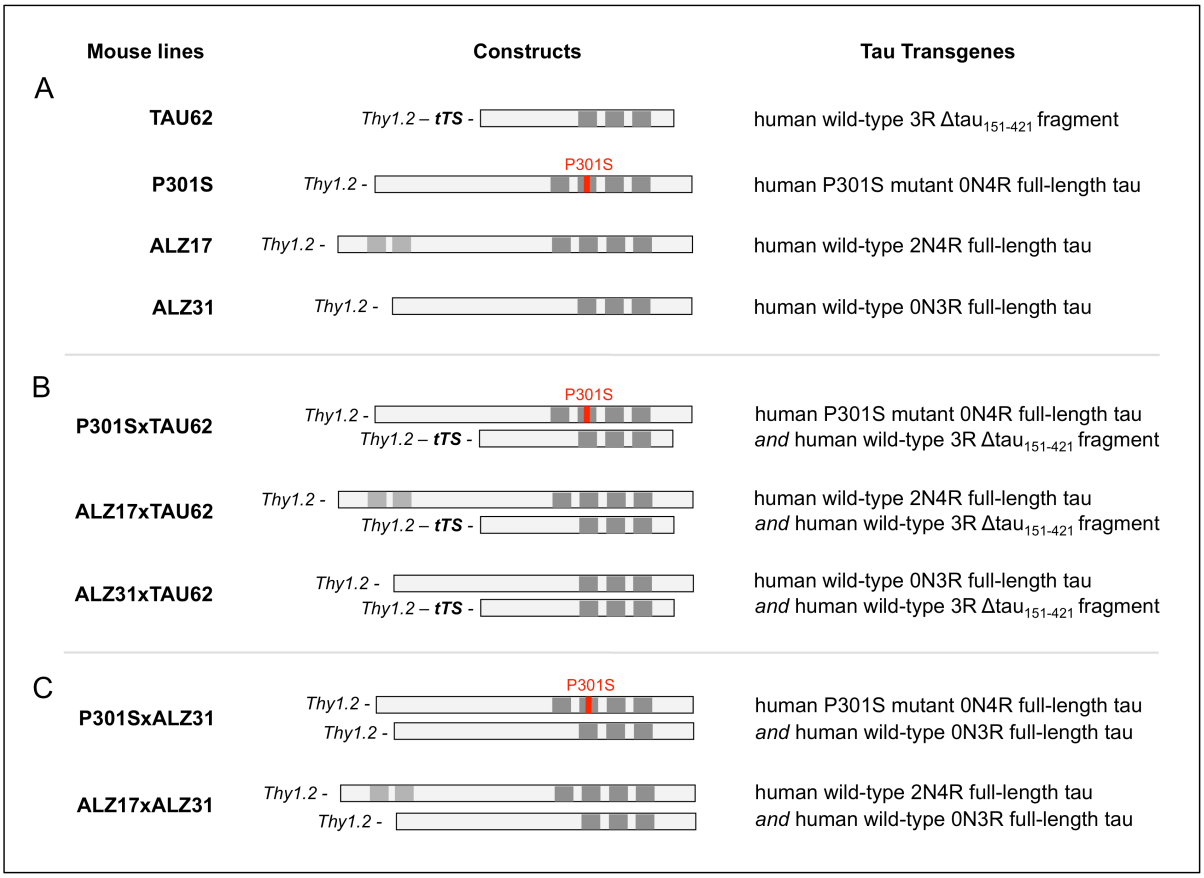

(**a-c**) Overview on the transgenic and co-transgenic mouse lines used for the present studies. Tau isoforms expressed are shown. Dark grey boxes indicate the tau repeat domains (3R or 4R isoforms), and light grey boxes N-terminal inserts (e.g. ALZ17 ≙ 2N4R).

The tau cDNA constructs are either driven by a standard Thy1.2 minigene (Thy1.2) or by a modified Thy1.2 minigene that contains a tetracycline controlled transcriptional silencer element (Thy1.2-tTS) in case of the TAU62 mouse. (**a**) shows the tau isoforms expressed in single-transgenic lines. (**b**) shows the tau forms of 3 mouse lines co-expressing full-length tau with Δtau. (**c**) depicts 2 mouse lines co-expressing different full-length tau isoforms.

Figure S1

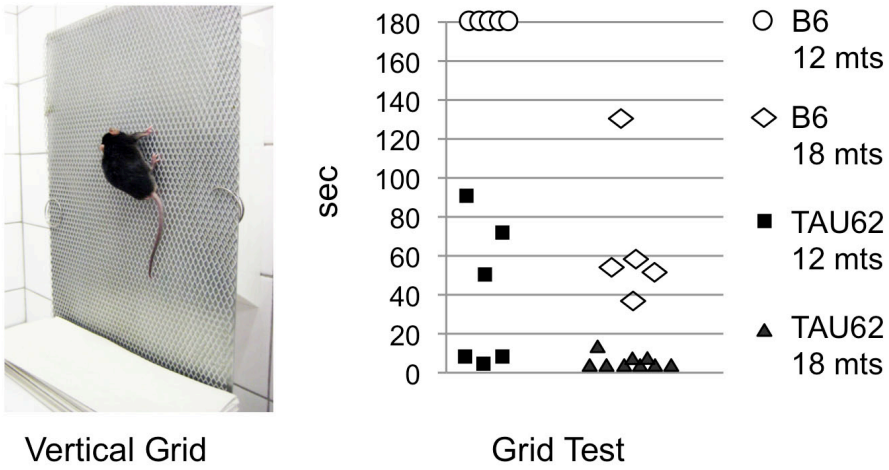

TAU62 mice develop a slowly progressive motor phenotype.
Motor fitness was assessed on a vertical mesh grid. Time spent on the grid progressively declined in TAU62 mice, while B6 controls were unimpaired at 12 months and showed a mild decline at 18 months of age.

Figure S2

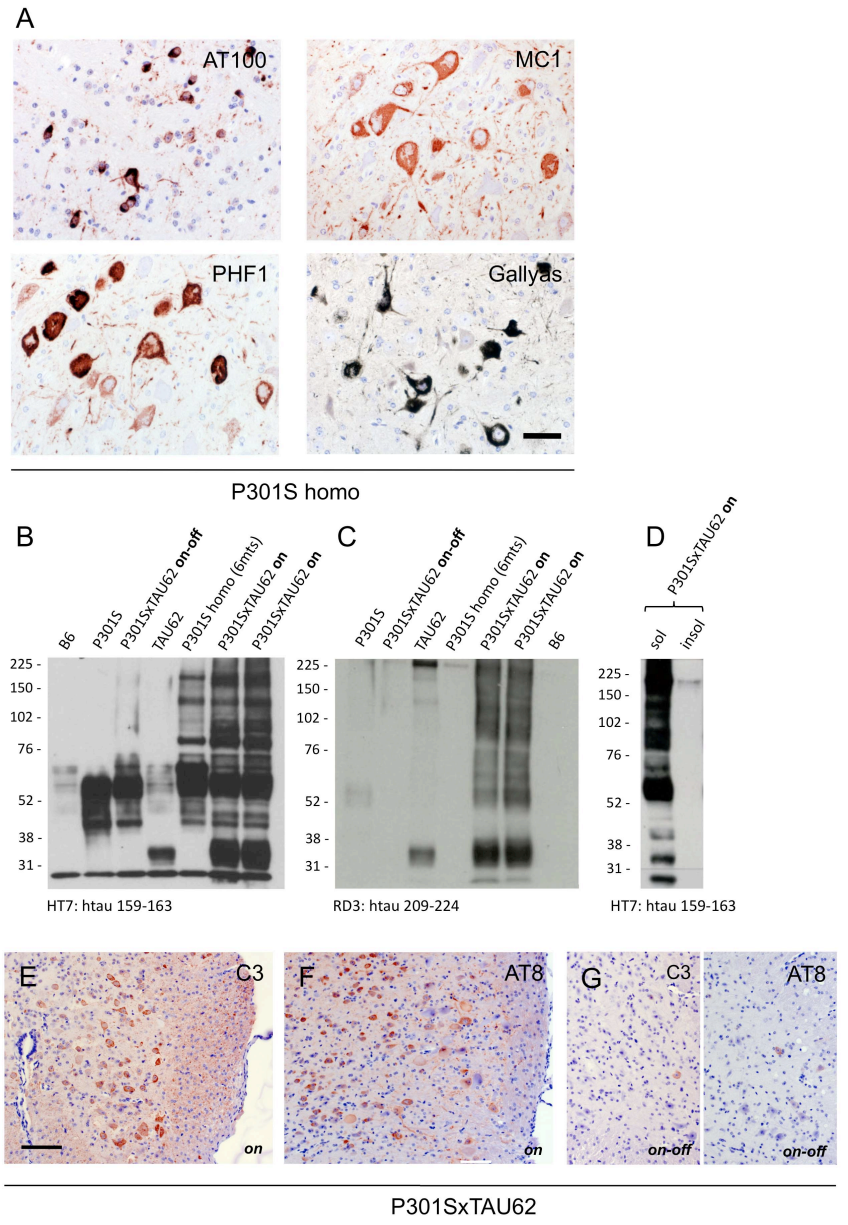

(**a**) Extensive hyperphosphorylation of tau was seen in the brainstem of old homozygous P301S mice by staining with antibodies targeting late phospho-epitopes. Multiple tau tangles and granular aggregates were detectable in these mice by Gallyas silver stain. The scale bar in **a** corresponds to 50 μm. (**b**) Western blotting under non-reducing conditions revealed high-molecular tau species in paralyzed P301SxTAU62^{on} mice (lanes 6&7); similar tau species were seen in aged tangle bearing homozygous P301S mice (lane 5). When tau expression was halted, no more high-molecular tau forms were detectable in P301SxTAU62$^{on\text{-}off}$ mice (lane 3; Western blot performed with anti-tau antibody HT7). (**c**) Staining with the RD3 antibody targeting Asp421 shows the presence of Δtau in the high molecular weight tau species. (**d**) Sarkosyl-extraction detects only soluble tau species in paralyzed P301SxTAU62^{on} mice ("sol": sarkosyl-soluble tau; "insol": sarkosyl-insoluble fraction).
(**e-g**) Δtau was widely expressed in the spinal cord of P301SxTAU62^{on} mice (**e**) and phosphorylated at the AT8 epitope **(f)**. Upon cessation of Δtau expression, Δtau- and AT8-positive tau was no longer detectable **(g)**. The scale bar in **e** corresponds to 100 μm in **e-g**.

Figure S3

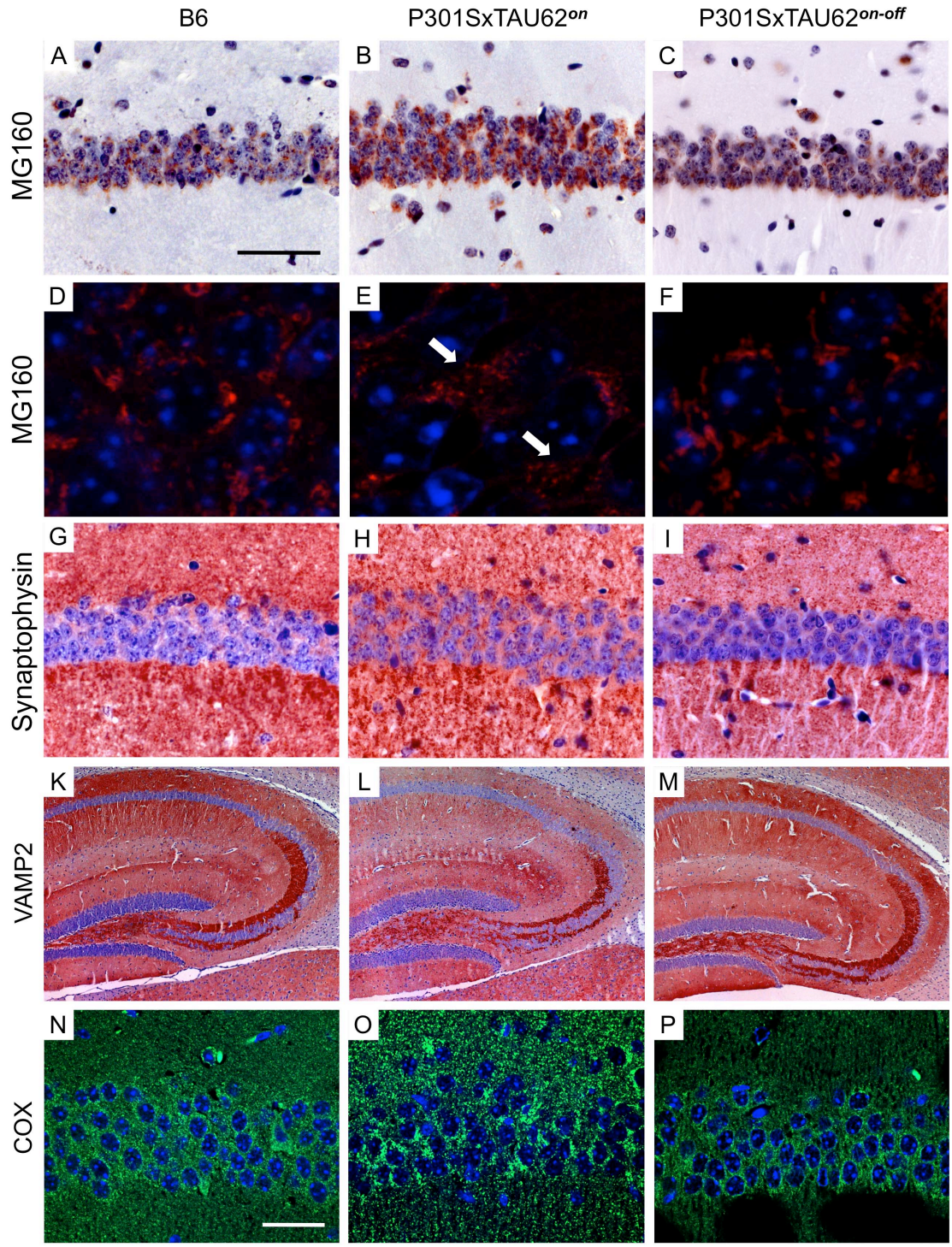

(**a-m**) P301SxTAU62 mice exhibit signs of Golgi disruption, protein missorting and mitochondrial clustering. These signs are reversible upon cessation of Δtau expression. Immunohistochemistry using antibodies against MG160 (**a-f**), synaptophysin (**g-i**), VAMP2 (**k-m**), and cytochrome C oxidase (COX) (**n-p**), in the hippocampus of non-transgenic mice (B6)**,** 3-week-old paralyzed mice (P301SxTAU62^{on}) and recovered mice 6 weeks after cessation of Δtau expression (P301SxTAU62^{on-off}). The scale bar in **a** corresponds to 19 μm in **d-f**, 63 μm in **a-c** and **g-i,** and 400 μm in **k-m**. The scale bar in **n** corresponds to 30 μm for **n-p**. Arrows in (**e**) indicate fragmented Golgi structures.

Figure S4

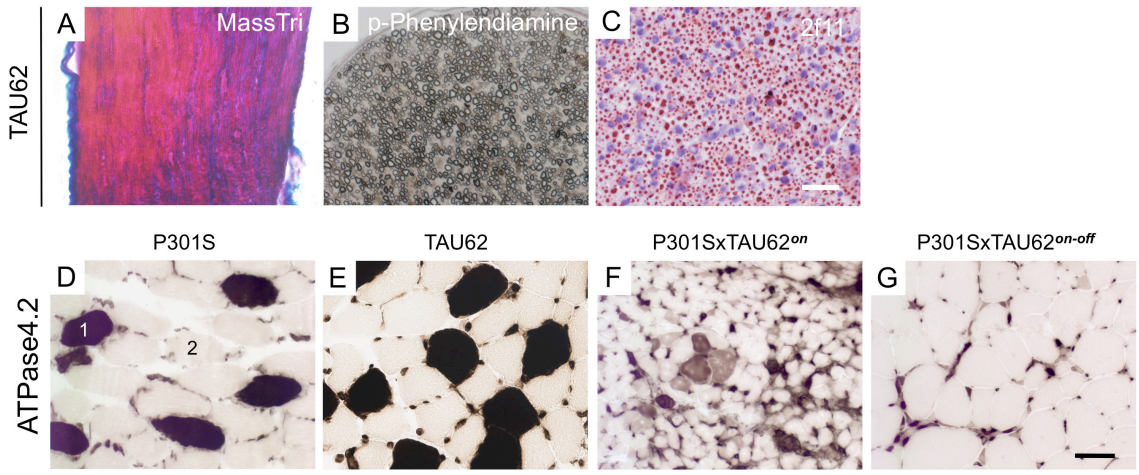

(**a-c**) Young TAU62 mice exhibit normal sciatic nerves (Masson's trichrom stain (**a**); para-Phenylenediamine (**b**); immunohistochemistry using 2f11 antibody (**c**)). The scale bar in **c** corresponds to 30 μm in **a-c.**
(**d-g**) M. gastrocnemius stained for ATPase (pH 4.2). Dark type 1 fibres (1) and light type 2 fibres (2). The scale bar in **g** corresponds to 50 μm (for **d-g**). P301S: heterozygous mice transgenic for human mutant P301S tau, aged 3 weeks; TAU62: heterozygous mice expressing 3R $tau_{151-421}$, aged 3 weeks; P301SxTAU62^{on}: paralyzed mice, aged 3 weeks; P301SxTAU62^{on-off}: recovered mice, 6 weeks after cessation of the expression of Δtau.

Figure S5

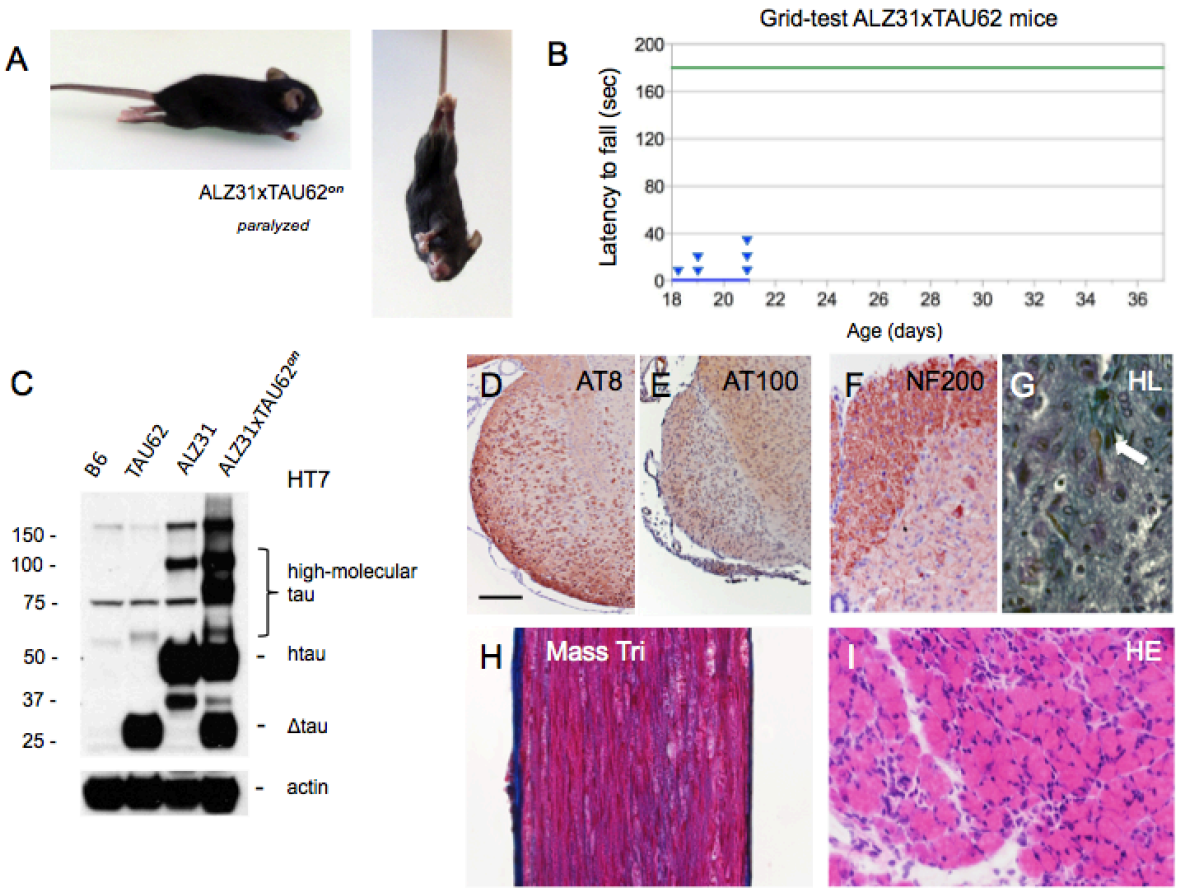

(a-i) Co-expression of 3R wild-type tau and Δtau (ALZ31xTAU62 mice) causes paralysis and neuropathy, which are not reversed upon cessation of Δtau expression. (**a**) Paralyzed (aged 3 weeks) and non-recovered (3 weeks after cessation of Δtau expression) ALZ31xTAU62 mice (see also video S6). (**b**) Absence of recovery of motor function as assessed by a grid-test of ALZ31xTAU62 mice following the removal of doxycycline between 14 and 16 days (blue line; triangles indicate the times of euthanasia, n=6). Motor function of heterozygous ALZ31 mice (green line, n=7). (**c**) Western blot with HT7 of brainstem tissue from non-transgenic mice (B6), TAU62 mice, ALZ31 mice and ALZ31xTAU62 mice. Actin staining was used as the loading control. (**d-i**) Histological analysis of paralyzed ALZ31xTAU62 mice aged 3 weeks, using AT8 (**d**), AT100 (**e**), NF200 (**f**), Holmes-Luxol (HL) (**g**), Masson's trichrome (**h**), and Hematoxylin-eosin (HE) stainings (**i**). The arrow in (**g**) points to a spheroid. The scale bar in **d** corresponds to 200 μm in **d** and **e**; 100 μm in **f**; 33 μm in **g**; 50 μm in **h, i**.

Figure S6

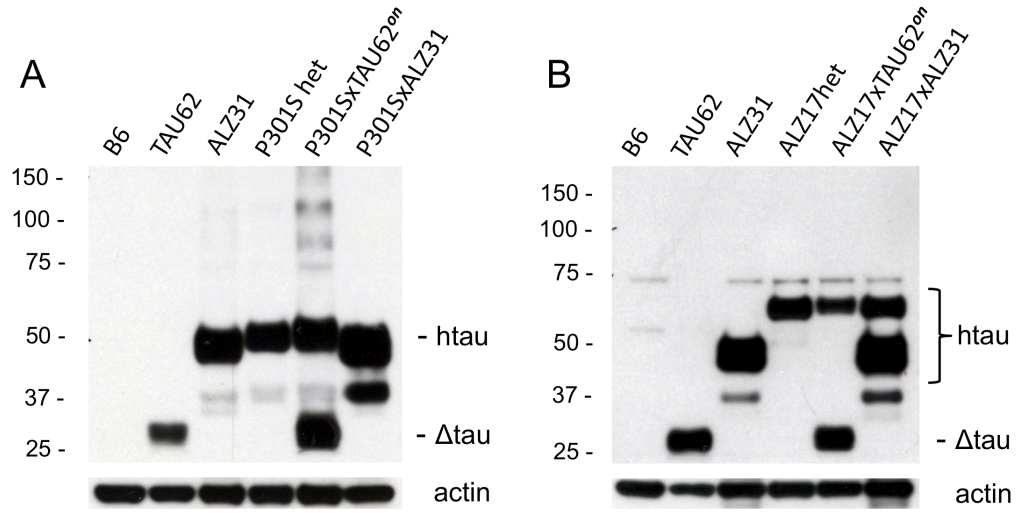

(**a,b**) Robust expression of the two full-length tau isoforms in P301SxALZ31 (**a**) and ALZ17xALZ31 (**b**) co-transgenic mice. For comparison, expression of mice co-transgenic for Δtau with full-length tau, as well as the respective single transgenic mice is shown. Western blots run under reducing conditions using HT7 antibody.

Supplemental Experimental Procedures

Antibodies used for immunohistochemistry (IHC) and Western blotting (WB)
(species is mouse, unless indicated otherwise):

Antibody	Target	Dilution	Source
HT7	human tau aa 159-163	WB 1:4000 IHC 1:800	Pierce, Rockford, IL #MN1000
BR134	human tau	WB 1:1000	(1)
Tau-C3	Tau cleaved at residue Asp421	WB 1:1000 IHC 1:1000	Santa Cruz Biotechnology, Inc, Dallas, TX #sc-32240
AT8	Tau pSer202/Thr205	WB 1:1000 IHC 1:800	Pierce, Rockford, IL #MN1020
AT100	Tau pThr212/Ser214	WB 1:1000 IHC 1:500	Pierce, Rockford, IL #MN1060
PHF-1	Tau pSer396/404	WB 1:2000 IHC 1:1000	Peter Davies, Albert Einstein College of Medecine, Bronx, NY
MC1	Tau aa 5-15, 312-322	IHC 1:100	Peter Davies, Albert Einstein College of Medecine, Bronx, NY
2F11	neurofilament (NF) NF-L, NF-H (70kD)	IHC 1:800	Dako, Glostrup, DK #M0762
NF200	neurofilament (200kD)	IHC 1:100	(2)
GFAP	glial fibrillary acidic protein	IHC 1:500	Thermo Fisher Scientific Inc., Kalamazoo, MI #MS-1407-R7
Synaptophysin	synaptophysin	IHC 1:1000	Millipore Corporation, Billerica, MA #MAB5258
MG160 (rabbit)	Golgi apparatus	IHC 1:1000	Nicholas Gonatas, Pathology and Laboratory Medicine, University of Pennsylvania, PA
VAMP2/Synaptobrevin 2 (rabbit)	transport vesicles	IHC 1:1000	Synaptic system, Goettingen, Germany # 104 202
GAPDH (6C5)	GAPDH	WB 1:1000	Santa Cruz Biotechnology, Santa Cruz, CA, #32233
ß-actin	actin	WB 1:5000	Sigma-Aldrich, Saint Louis, MO #A5316
Cox subunit 1a	mitochondrial staining	IHC 1:200	Abcam plc, Cambridge, UK #ab14705

Supplemental References:

1. Goedert M, Spillantini MG, Jakes R, Rutherford D, & Crowther RA (1989) Multiple isoforms of human microtubule-associated protein tau: sequences and localization in neurofibrillary tangles of Alzheimer's disease. *Neuron* 3(4):519-526.
2. Probst A*, et al.* (2000) Axonopathy and amyotrophy in mice transgenic for human four-repeat tau protein. *Acta Neuropathol* 99(5):469-481.

Potential prion-like properties of human CSF

Preliminary results

Potential prion-like properties of human CSF

Summary

We collected CSF from AD and age matched control patients, and injected it into young, pretangle stage P301S mice. As a result, we observed a local increase in hyperphosphorylated tau pathology in both AD and control CSF treated mice, indicating that human CSF tau could exhibit prion-like characteristics. However, more patient samples will be needed in order to discriminate between AD and non-AD cases, so that this method could serve a future diagnostic use.

Results

We collected CSF from AD and age matched control patients and developed a protocol in order to concentrate it around 100 times and so to be able to inject it intracerebrally into the mice (Fig. 1). We did not see a significant difference in levels of tau between AD and Control patients CSF after the concentration procedure as measured by ELISA (Fig. 2).

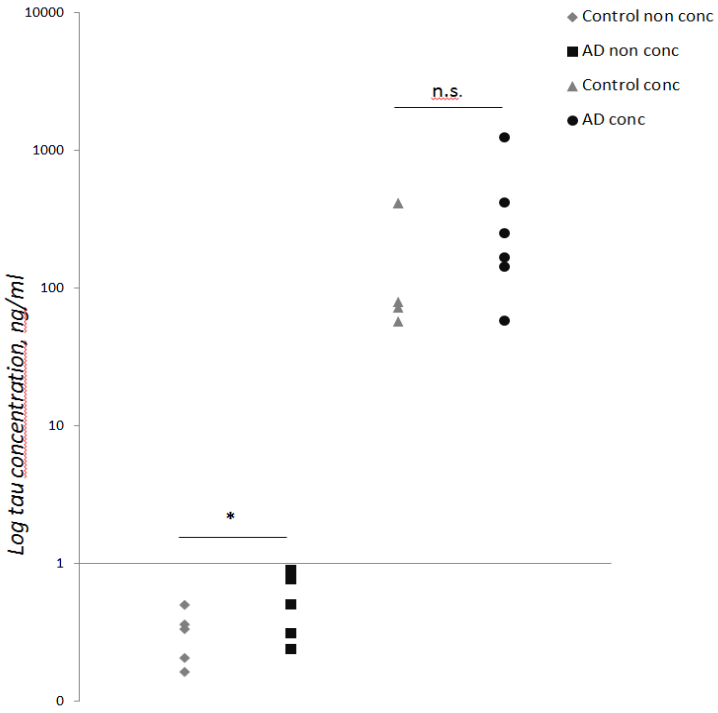

Figure 2. Levels of Total tau in concentrated and non-concentrated human Control (n=4) and AD (n=5) patients CSF, as measured by ELISA. * indicates *p*=0.04, however no significant difference was found between the concentrated CSF samples, as based on unpaired Student t-test.

Next, we evaluated the effect of human CSF injections into young, pretangle bearing P301S mice. Initial, preliminatry quantification of tau pathology in the whole hippocampus comprising the injection site (-2 to -3 mm from Bregma) did not show any significant difference between the injected or contralateral hippocampus in mice treated with AD or control CSF, as based on AT8 and Gallyas staining (Fig. 3, A-D).

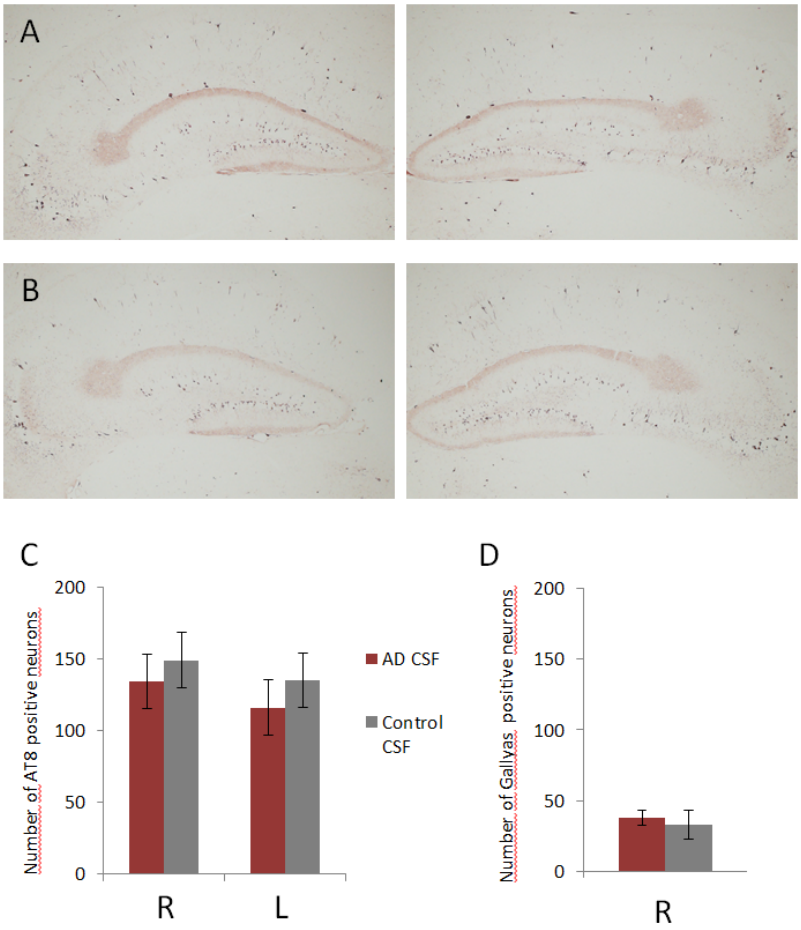

Figure 3. Injection of human CSF from AD (A, n=10 mice) or control (B, n=8 mice) patients did not result in an increase of AT8 pathology in the whole hippocampus, or between injected (R, left panels) and non-injected (L, right panels) hippocampal side as shown by immunohistochemistry (A, B) and quantification (C). There was no difference in the number of Gallyas positive neurons between the injected sides (D). Error bars indicate SEMs.

However, there is a high variation in the endogenously present P301S mice pathology, and also a seeding effect can be very focal and hence not detectable in sections spanning the whole hippocampus. For this reason, next we looked at AT8 pathology at different Bregma levels and in between different subhippocampal regions of the injected versus non injected

sites. As a result, anterior/in proximity to the injection site we observed significant increase of AT8 pathology in the right CA3 region of AD CSF treated mice, compared to their contralateral CA3 region (Fig. 4 A, B). This effect was also present in control CSF seeded mice, even though with smaller effect size.

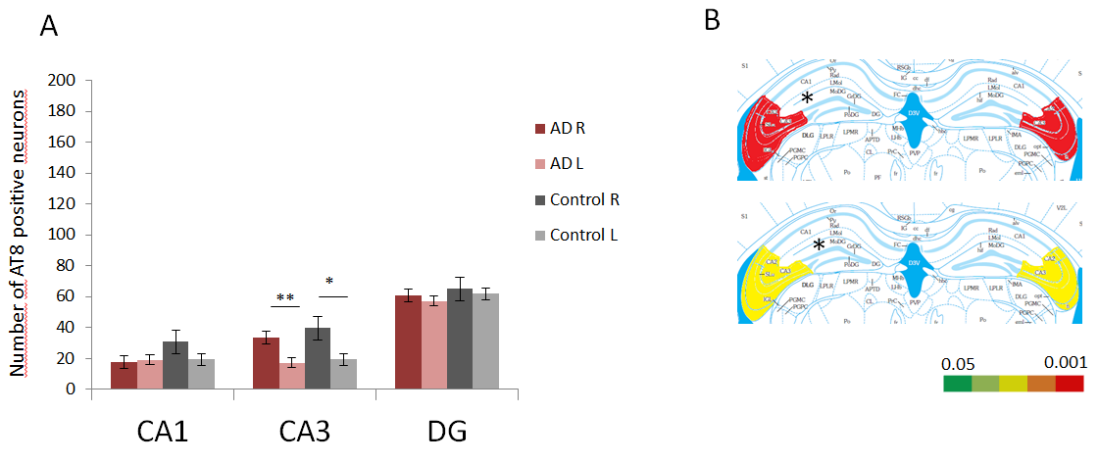

Figure 4. Quantification of AT8 tau pathology in the CA1, CA3 and DG hippocampal subregions at -2 to -2.2 from Bregma (A) revealed significantly more signal in the CA3 of the injected versus non-injected side, in both AD (n=10) and control (n=8) CSF seeded mice. The results are depicted using a heat map showing differences between the injected and non-injected hippocampus (B) in AD (top image) and Control patients (bottom image), as color grade depicts p-values. Star indicates the injection site, * indicates $p<0.05$, ** indicates $p<0.001$, as based on Student`s t-test. Error bars indicate SEMs.

However, even if total hippocampal AT8 load was above the baseline observed in non-treated injected mice for both AD and Control patients (see Fig. S3 in Skachokova et al., 2016), we did not find any significant difference between those 3 groups. Also, we observed different pathology in mice injected with CSF from the same patient that may be due to differences in injection site, and variation in mice endogenous tau pathology.

Additional analysis showed no correlation between tau levels in the CSF and AT8 or Gallyas pathology in the injected hippocampus, for both AD and control CSF seeded mice.

These results suggest that human CSF can harbor some seeding potential based on local AT8 increase. However, our assay is not sensitive enough to discriminate between AD and non-AD patients, and/or our control patients are not optimally selected, as we lack CSF derived from fully asymptomatic patients (e.g. patients' spouses). This could be addressed by the

use of a larger patient cohort and better control patients selection, that is currently ongoing.

Discussion

CSF Amyloid-β lack of seeding

We reported that APP23 mice injected with CSF derived from plaque-bearing APP23 mice for a period of up to 21 months did not show any increase in Aβ load at or close to the injection site, in contrast to brain homogenate seeded mice. This suggests a lower to absent seeding effect of amyloid-β in the CSF, as compared to the one in the brain. In a collaborative study the authors did not find any β-amyloidosis inducing activity as a result of injection of human AD CSF into APP23 mice, even though they observed some seeding activity in an *in vitro* assay (Fritschi et al. 2014). This demonstrates that seeding prone amyloid-β does not reach the CSF or is not detectable in an *in vivo* seeding model.

The lack of detectable *in vivo* Aβ-inducing activity in human CSF can be seen as a negative result in terms of developing an early Alzheimer's disease biomarker assay. However, it is reassuring that human CSF, being routinely handled in many laboratories, does not seem to contain the self-propagating Aβ seeds that have been shown to be transmissible under laboratory conditions (Jucker and Walker, 2013), and this knowledge could be used in laboratory safety regulations.

Potential prion-like behavior of CSF tau

By seeding P301S CSF into young P301S mice we demonstrated that mouse CSF tau exhibits seed like properties *in vivo*, as tau hyperphosphorylation was induced and transmitted along existing anatomical networks (Skachokova et al., 2016, *in preparation*). Using this knowledge and methodology, we looked at the seed like properties of human CSF, which would be of a diagnostic importance. Injection of human CSF into young P301S mice did not result in the same total hippocampal increase of tau pathology. However, we noted a local seeding effect when comparing the injected and non-injected sides, indicating that human CSF tau could also harbor some seeding potential. This, to our knowledge, is the first study so far to demonstrate that human CSF could induce tau pathology, even though
CSF obtained from AD patients was previously shown to enhance the fibril formation of another amyloidogenic protein, alpha-synuclein (Ono et al. 2007). Using this method, we were not able to differentiate between AD and control patients, possibly due to the small number of patients, the strong endogenously present tau pathology in the mice, and the limited sensitivity of our quantification. Furthermore, the selection of valid control patients is complicated by the fact that neuropathological changes (including tangles formation) may precede clinical symptoms, and so may remain undiagnosed (Jack et al. 2010). In order to check for potential diagnostic use of the human CSF seeding will be needed more patient samples and younger and/or healthier controls.
The pathology we observed as a result of tau propagation was different when induced by murine or human CSF, as based on a comparison of the injected and the non-injected hippocampus. This may be due to the lower concentrations of tau in human CSF, or there may be structural varieties in the tau strains they contain. P301S mice carry a mutation that

is typical of frontotemporal dementia, which is characterized by pathology different from AD. It has been suggested that brain samples from different tauopathy patients may seed tau aggregation in different structures/ cell types, and possibly propagate in distinctive ways, due to the presence of different tau strains (Boluda et al. 2014). It may be the case that AD and P301S derived CSF contains different tau variants, and hence the different spreading patterns (local versus the whole hippocampus).

CSF tau molecular structure has been studied with contradicting results, most probably due to the low tau concentration in CSF. Some studies report predominance of a mid-domain tau fragment, rather than C and N-terminal fragments or a full length tau (Barthélemy et al. 2016), but also N-terminal fragments have been identified, with no tau containing a microtubule binding site present (Meredith et al. 2013). It was shown that tau molecules containing the repeat domain are able to form fibrils at a different rate form P301L mutant tau mice *in vitro* (Shammas et al. 2015). It could be that human CSF and P301S CSF contain tau forms with different molecular structures, hence different propagation patterns. Further structural studies will be needed to shed more light into this, as well as between AD and control patients CSF. Our results suggest that CSF in both P301S mice and aged humans contains seeding competent tau species, however their exact structure is yet to be revealed.

How does pathological tau enter the CSF compartment? It has been shown that tau propagates via synaptically connected regions, via cell to cell transmission, however the exact mechanisms are still unknown (Pooler et al. 2014; Clavaguera et al. 2015). Using an *in vitro* cell model it was demonstrated that phosphorylated tau is actively secreted via exosomal release, and also found in vesicles in AD patients CSF (Saman et al. 2012), as well as in exosomes isolated from P301S mouse brains (Asai et al. 2015). Furthermore, infusion of tau antibodies into tau transgenic mice lateral ventricles reduced tau seeding activity by reducing tau hyperphosphorylation and aggregation, implicating extracellular tau in AD pathology as seed responsible (Yanamandra et al. 2013). Based on these evidences, it is possible that seed prone tau is released by the neurons and reaches the CSF (Fig. 13), however it is not known whether this parallels the intracellular pathology and further studies need to be done to test its diagnostic value.

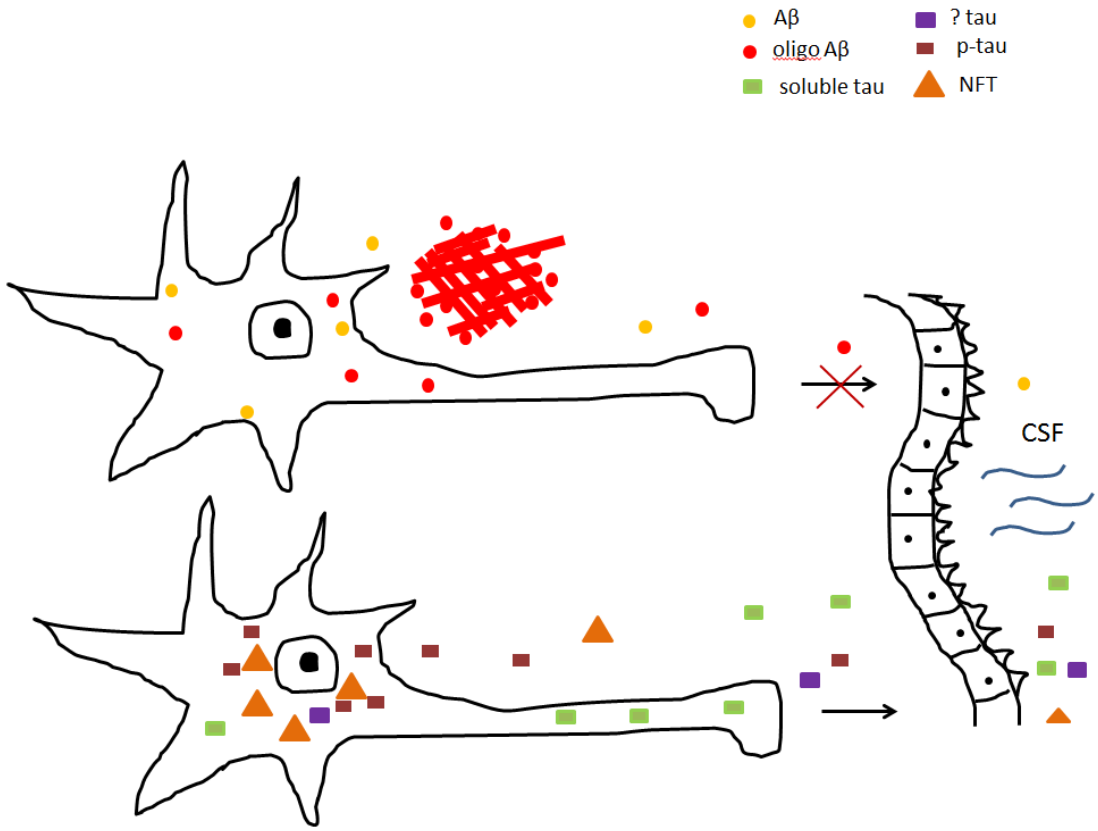

Figure 13. A hypothetical model of Aβ and tau secretion into the CSF. The proteins are normally released from the neurons into ISF and then, through the cells of the choroid plexus, into the CSF. In AD, aggregation prone, oligomeric Aβ is contained into plaques and does not reach the CSF. In contrast, pathogenic tau (aggregated, hyperphosphorylated (p-tau), truncated (? tau)), and soluble tau, possibly reach the CSF compartment, where they can be clinically accessed.

Another important question concerns the nature of the secreted, pathological tau. Previously, it has been reported that tau species harboring prion-like potential consist of large and aggregated hyperphosphorylated tau forms (Clavaguera et al. 2009; Jackson et al. 2016), but oligomeric tau has been implicated just as well (Lasagna-Reeves et al. 2012). However, immunization with an anti-phospho tau antibodies in tauopathy mice models reduced tau pathology (Bi et al. 2011; Boimel et al. 2010), indicating phosphorylated and/or aggregated tau as the seed inducing species. Phosphorylated tau is present in the CSF and used currently in diagnostics, however, so far there are no evidences for the presence of aggregated tau in there, even though the presence of aggregated amyloids in CSF from Parkinson`s disease patients has recently been shown (Horrocks et al. 2016). Further seeding studies using AD patients CSF and brain samples are needed to elucidate the nature of the seed inducing tau species, and possibly help the development of therapeutics to inhibit tau propagation.

The CSF of AD patients may contain fragmented forms of tau, that are not normally present in healthy individuals, as demonstrated by some studies (Jr et al. 2013; Barthélemy et al. 2016). In this sense, tau truncation as detected by its presence in the CSF may serve as indicator of early pathological changes associated with the disease.

Our additional results point to the importance of truncated tau in disease toxicity and neurodegeneration, especially when it is expressed together with full length tau (Ozcelik et al. 2016). It has been previously shown that truncation of tau increases its propensity to aggregate, and it has been suggested that cleaved tau may seed the aggregation of full length tau (Abraha et al. 2000; Spires-Jones 2011). It is possible that the seeding properties of P301S CSF are due to the presence of tau fragments, however more structural studies will be needed to elucidate this. In this light, we have injected P301S mice with brain homogenates from mice expressing fragmented tau and also both fragmented and full length tau, to see its effect on the host pathology. This analysis is currently ongoing.

The toxicity of truncated tau in combination with full length tau at molecular to behavior levels in our mice model is striking, however even more surprising is the fact that this effect is reversible. This study implicates oligomeric tau as a toxic mediator in tauopathy and points at inhibitors of tau oligomerization and truncation as possible therapeutic tools.

In conclusion, our results implicate CSF tau as a candidate for the development of future diagnostic bioassays based on its seeding properties. However, its clinical use in AD diagnosis and possibly presymptomatic diagnosis still remain to be clarified.
In addition, tau fragmentation plays an important role in tau mediated toxicity, and represents a promising target for the development of novel therapeutic tools.

Materials and methods

Mice

APP23 mice are expressing the human *APP* gene (751-aa isoform), containing the Swedish double mutation at positions 670/671 (KM->NL), under the control of the murine Thy-1.2 promoter. The APP_{751} cDNA was inserted into the blunt-ended *Xho*I site of the expression cassette containing the Thy-1.2 gene that was microinjected into pronuclei (Sturchler-Pierrat et al. 1997). Heterozygous APP23 mice were interbred with C57BL/6J mice and transgenic littermates were identified by genotyping.

P301S mice are expressing the shortest human four-repeat tau isoform (4R0N) containing the P301S mutation (Allen et al. 2002). The mouse line was generated by using a cDNA encoding a 383 amino acids isoforms of human tau, subclonied into a murine Thy 1.2 expression vector using a *Xho*I restriction site. Transgenic mice were generated by microinjection into pronuclei of (C57BL/6J x CBA/ca) F1 generation. The founders were identified via PCR analysis, and these were interbred with C57BL/6J mice. For seeding experiments, homozygous P301S were used. For investigating the role of fragmented tau, heterozygous P301S were used.

Tau62 mice expressing an inducible fragmented tau were generated by co-injection of two Thy 1.2 minigenes based constructs into C57BL/6J oocytes. The Thy 1.2-tTS construct was produced by replacing exon 2 of the mouse Thy 1.2 promoter by a tetracycline controlled transcription silencer element (tTS). The Thy 1.2-TRE-tau construct contained a tetracycline responsive element (TRE) upstream of the human wild-type tau cDNA encoding amino acids 151 to 421 of a 3-repeat domain spanning human wild-type tau fragment (Fig. 14). A total of 6 positive Tau62 founders were identified and the inducible expression of human tau was assessed by western blot and immunohistochemistry. Lines 62-2 and 62-48 exhibited comparable and robust fragmented tau expression only in the presence of doxycycline.

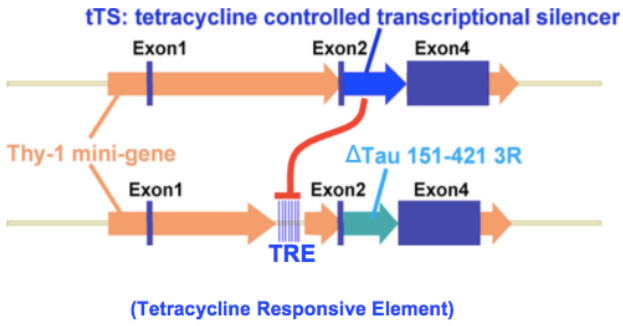

Figure 14. Genetic construct used for the generation of TAU62 mice.

P301SxTAU62 double transgenic mice have been obtained by crossing P301S mice with Tau62 line. All double transgenic mice were heterozygous for the transgenes of interest.

Chow containing 500mg/kg doxycycline was provided *ad libitum* to induce fragmented tau expression. All animal experiments were performed in compliance with protocols approved by the official local Committee for Animal Care and Animal Use of the Canton of Basel.

DNA isolation and Genotyping

Small pieces of mice toes or ears were incubated in lysis buffer containing 0.1 mg/ml Proteinase K (Macherey-Nagel, Germany) overnight in Eppendorf Thermomixer comfort shaker (700 rpm, 55°C). The solution was centrifuged (13000 rpm, 5 min) and 750 µl of the supernatant was mixed with 750 µl of isopropanol by inverting the tubes. Next, the mix was spun down (13000 rpm, 10 min), the supernatant was discarded and the pellet was washed with 75% ethanol and centrifuged again (13000 rpm, 10 min). The remaining pellet, containing the DNA, was dried on Eppendorf Thermomixer comfort shaker (55°C, 5-10 min) and finally resuspended in 250 µl dH_2O (50°C, 1h).

Lysis buffer composition: 100 mM Tris pH 8.0, 5 mM EDTA, 0.2% SDS, 200 mM NaCl, sterile H_2O.

Mice from the APP23 line were analyzed for the presence of the transgene by PCR. For the PCR mixture were used:
2µl of 10pmol/µl Forward primer (‘5-CCG ATG GGT AGT GAA GCA ATG GTT-3’)
2µl of 10pmol/µl Reverse primer (‘5-GAA TTC CGA CAT GAC TCA GG-3’), both primers from (Eurofins MWG, Germany)
12.5µl of TopTaq Master Mix (Qiagen, Germany)
6.5µl sterile H_2O
and 2µl of DNA

PCR program:

Temperature, °C	Time, s	Cycles
94	120	1
94	45	1
60	60	35
72	45	
94	45	
72	300	1
4	∞	

The program was run on a PTCM100 machine (MJ Research, Canada) and finally the PCR product was run on a 1.5% agarose gel using a 100bp DNA ladder (Roche, Switzerland) at 150 V. DNA was stained using SybrSafe (Thermo Fisher Scientific, USA).

Murine CSF collection and processing

For CSF sampling, mice were deeply anesthetized with a mixture of ketamine (10 mg/kg, Ketalar®, Pfizer, USA) and xylazine (20 mg/kg, Rompun® 2%, Bayer, Germany), placed ventrally on a tube holder rack and the hair around the neck was wet. Next, a vertical incision was made on the skin on the neck, and the visible splenius and rectus muscles were pulled aside until the pia mater surrounding the cisterna magna was visible. Secondly, the membrane was punctured using an injection needle (25 G Agani, Terumo, Belgium) and CSF was collected using a 10 µl pipette for an interval of 2 min. Finally, the liquor was spun down at 2500 rpm for 2 min and the supernatant was collected and immediately frozen. Visibly blood contaminated CSF was discarded.

Next, CSF from different mice was pooled together and concentrated by lyophilization at −80°C, 0.01 mbar vacuum pressure, overnight, using an Alpha 2-4 LSCplus Christ dryfreezer (Millrock, USA). The dried product was reconstituted in sterile H_2O with a 5-fold concentration ratio. CSF tau concentration was measured by ELISA.

Stereotaxic surgery

Three months-old P301S, APP23 or non-transgenic C57BL/6 control mice were anesthetised with a mixture of ketamine (10 mg/kg, Ketalar®, Pfizer, USA) and xylazine (20 mg/kg, Rompun® 2%, Bayer, Germany), and placed on a heating pad to maintain body temperature throughout the surgery (Harvard Apparatus, USA). Skin on the head was cut open by a vertical incision, and mice were head fixed on a stereotaxic frame (David Kopf Instruments, USA). Animals eyes were protected using Lacrinorm gel during the procedure (Bausch&Lomb, USA) Next, the precise injection site was determined and a hole was carefully drilled into the skull, avoiding any rupture of the pia mater. Mice were injected in the right (R) hippocampus (A/P, −2.5 mm from Bregma; L, − 2.0 mm; D/V, −1.8 mm) using a 10 µl glass syringe (701N, Hamilton, USA), as previously reported (Clavaguera et al. 2009). Each received a unilateral stereotaxic injection of 5 µl, at a speed of 1.25 µl/min. Following the injection, the needle was kept in place for additional 3 minutes before being withdraw. The surgical area was cleaned with sterile saline and the incision site closed using Prolene 6-0 C1 sutures (Ethicon, USA). Mice were monitored until recovery from anesthesia and checked regularly following surgery.

Perfusion and brain preparation

Following the previously specified seeding time, mice were deeply anaesthetized by an intraperitoneal injection with a mixture of 100 mg/kg ketamine (Ketalar®, Pfizer) and 10 mg/kg xylazine (Rompun® 2%, Bayer), followed by 100 mg/kg sodium pentobarbital (Pentothal® 0.5g, Ospedalia AG). Next they were transcardially perfused with 0.01M cold phosphate-buffered saline (PBS, Bichsel), followed by 4% paraformaldehyde in PBS. After perfusion, brain was quickly removed, cut in coronal plane anterior to the hippocampus, and both brain parts were immersion fixed in 4% paraformaldehyde overnight, and finally embedded in paraffin.

Immunohistochemical analysis

Following paraffin embedding, the brain containing the whole hippocampus was cut into 4 µm coronal sections (starting at -2 Bregma to -3 Bregma, as defined by the Mouse Brain Atlas by G. Paxinos and K. Franklin) in a serial manner using a sliding microtome (Leica SM2000R, Leica, Germany). Sections were shorty placed on a floating bath (60°C) to straighten and mounted on histological slides (Leica IP S, Leica, Germany), and finally let dry overnight at 37°C.

After drying, sections were deparaffinised by placing them subsequently in Xylol (20 min, from Biosystems, Switzerland), 100% EtOH (3 min), 96% EtOH (2x3 min) and in 70% EtOH (2x3 min), followed by washing in PBS. For 82E1 immunohistochemistry, pretreatment with 100% Formic acid for 5 min was applied. In order to mask antigenic sites, antigen retrieval was performed using Citric acid buffer pH=6.0 (Pro Taps) for 30 min at 90°C. After blocking in 2.5% normal horse serum (Vector Laboratories) for 30 min at room temperature, sections were incubated with primary antibody diluted in PBS at 4°C, overnight. The next day, sections were washed in Tris/PBS solution (3x5 min) and incubated with ImmPRES Reagent peroxidase (Vector Laboratories, USA) for 1h at RT. Next, sections were washed with Tris/PBS (3x5 min) and stained using chromogen ImmPACT NovaRED Peroxidase substrate kit (Vector Laboratories, USA), as reaction time was controlled under a microscope. Sections were then washed with H_2O to stop the reaction and, in some cases, slides were counterstained with hematoxyline (J.T. Baker). Finally, sections were dehydrated in 70% ethanol (1 min), 96% EtOH (2x1 min), 100% EtOH (2x1 min) and xylol, and mounted using Pertex® medium (Biosystems, Switzerland). Pictures of sections were taken using an Olympus DP73 (Olympus, USA) microscope.

For immunohistochemistry (IHC), immunofluorescence (IFL) and western blot (WB), the following primary antibodies were used:

Antibody	Species	Antigen	Concentration/Use	Source
82E1	mouse	Amyloid-β	1:1000/ IHC	Demeditec, Germany
AT8	mouse	PHF tau (Ser202/Thr205)	1:800/ IHC 1:1000/ WB	Thermo Scientific, USA
AT100	mouse	PHF tau (Ser212/Thr214)	1:1000/ IHC	Thermo Scientific, USA
HT7	mouse	Human $tau_{159-163}$	1:1000/ WB	Pierce, USA
TauC3	mouse	Truncated tau (Asp421)	1:1000/ IHC, WB	Santa Cruz Biotechnology, USA
MC1	mouse	tau_{5-15} and $tau_{312/322}$	1:1000/ IHC	P. Davies, Albert Einstein College of Medicine, NYC, USA
PHF1	mouse	$Phosphoresine_{396-404}$	1:1000/ IHC 1:2000/ WB	P. Davies, Albert Einstein College of Medicine, NYC, USA
RD3 (8E6/C11)	mouse	Human 3R $tau_{209-224}$	1:3000/ IHC 1:4000/ WB	Millipore, USA
RD4 (1E1/A6)	mouse	Human/mouse 4R $tau_{275-291}$	1:100/ IHC 1:4000/ WB	Millipore, USA

VAMP2	rabbit	Postsynaptic vesicles	1:1000/ IHC	Synaptic System, Germany
MG160	rabbit	Golgi apparatus	1:1000/ ICH, IFL	N. Gonatas, Univeristy of Pennsylvania, USA
Synaptophysin	mouse	Presynaptic vesicles	1:1000/ IHC	Millipore, USA
β-actin	mouse	Actin	1:5000/ WB	Sigma-Aldrich, USA
Cox1a	mouse	Mitochondrial protein	1:200/ IFL	Abcam, UK

Gallyas silver staining

Sections were silver-impregnated following the method of Gallyas-Braak to visualize filamentous tau pathology (Gallyas 1971; Braak et al. 1988). After deparaffinisation and rehydration as previously described, sections were incubated in 3% Periodic Acid (Sigma-Aldrich, USA) for 30 min at room temperature. Second, slides were washed in d H_2O for 2 min and incubated in 1% Alkaline Silver solution (1M sodium hydroxide, 0.6M potassium iodide, 1% silver nitrate solution, all from Merck, Germany), for 10 min at room temperature. Third, slides were incubated in ABC solution, shaking occasionally, and reaction time (tangles colored form brown to black) was controlled under a microscope.

ABC solution:

Solution	Composition	Concentration, %	Producer
A	Sodium carbonate anhydrous	5	Merck, Germany
B	Ammonium nitrate	0.14	Merck, Germany
	Silver nitrate	0.2	Merck, Germany
	Tungstosilicic acid	1	Sigma-Aldrich, USA
C	Ammonium nitrate	0.14	Merck, Germany
	Silver nitrate	0.2	Merck, Germany
	Tungstosilicic acid	1	Sigma-Aldrich, USA
	37% formaldehyde solution	0.74	Merck, Germany

Fourth, reaction was stopped by incubation in 0.5% Acetic Acid (Merck, Germany) for 30 min at room temperature. Fifth, slides were washed in dH_2O and incubated in 5 % Sodium thiosulfate (Merck, Germany) for 5 min at room temperature. Next slides were washed in cold tap water, followed by hematoxylin eosin staining, dehydration in EtOH and mounting,

as previously described.

Hematoxylin and Eosin Staining

After deparaffinisation and rehydratation, sections were rinsed in cold tap water and stained in hematoxylin for 5 to 8 min. After washing in cold tap water and decolorizing shortly in alcohol-HCl, the slides were washed again in cold tap water and placed for 10 min in warm water until blue. Next sections were immersed in 1% erythrosine B solution (RAL diagnosis) for 2-3 min, washed shortly in cold tap water, dehydrated in EtOH concentration gradient and finally placed in xylol before mounting.

Immunofluorescence and confocal microscopy

After deparaffinisation and rehydration, followed by antigen retrieval and blocking, sections were incubated with primary antibody overnight at 4°C. Next day, after washing with PBS (3x5 min), secondary anti-mouse Alexa Fluor 488 or 594 antibody (Invitrogen, USA) was added in concentration 1:1000 in dark for 2h, at room temperature. Finally, slides were washed again in PBS (3x5 min), mounted with Dapi containing medium (ProLong®, Invitrogen, USA) and kept in dark at 4°C.
Sections were observed using a fluorescent Olympus BX43F (Olympus, USA) microscope and images were acquired using an A1 confocal microscope (Nikon, USA). All images were acquired at the same exposure and were automatically aligned using the stitching tool in the Axiovision LE software. Once acquired, all images were opened in ImageJ (NIH, USA) and were normalized and the threshold was set automatically.

Human CSF collection and patient characteristics

CSF was collected within a clinical trial set up at the Memory Clinic of the University Hospital Basel. The trial was approved by the local Ethics Commission of the Canton of Basel, and recruitment was limited to patients with a Mini Mental Score >19/30 for reasons of informed consent (Pachet et al. 2010). Subsequent patients examined for potential neurodegenerative dementia at the Memory Clinic were included in the study. Up to 15 ml of CSF per patient were collected by lumbar puncture after obtaining written informed consent of the patient and a care-giver. Final clinical diagnosis was based on multimodal assessments including neuropsychological testing, brain MRI imaging, CSF tau and Aβ level measurements, and, in selected cases, rbf-SPECT imaging.
For purpose of inoculation into mice, CSF samples derived from the patients with the highest ("AD CSF" group, n=5) and the lowest ("Control CSF" group, n=4) probability of AD-related cognitive decline were selected. AD-CSF samples were obtained from 2 patients fulfilling the actual criteria for "Probable AD dementia with high biomarker probability of AD etiology" (McKhann et al. 2011), one patient with "Probable AD dementia based on clinical criteria" as well as one patient with "MCI core clinical data" (Albert et al. 2011), both with high evidence for neuronal injury. The 4 patients attributed to the "Control-CSF" group fulfilled the criteria for "Dementia-unlikely due to AD" or "MCI-unlikely due to AD" without biomarker evidence for AD" (McKhann et al. 2011; Albert et al. 2011) . Cognitive decline of

control patients was related to non-neurodegenerative causes (e.g. vascular dementia or alcohol abuse). For the ongoing human CSF study, we are collecting samples from cognitively healthy spouses of demented patients.

Human CSF processing

Freshly collected human CSF was spun down at 3000 rpm for 30 min to separate cell debris. The supernatant was collected and frozen at −80° C. In order to obtain reasonable tau levels in the small volumes that could be injected into mouse brains, human CSF samples were concentrated. To this end, 10 ml of human CSF per patient was lyophilized at −80° C, 0.01 mbar vacuum pressure, overnight, using an Alpha 2-4 LSC plus lyophilizer (Millrock, USA). The dried product was reconstituted in 1 ml sterile H_2O and dialyzed in order to decrease salts content using Float-A-Lyzer® G2 (Spectrum Labs, USA) during 24h with 3 buffer changes, again lyophilized, and finally reconstituted in H_2O. The final concentration was measured by ELISA.

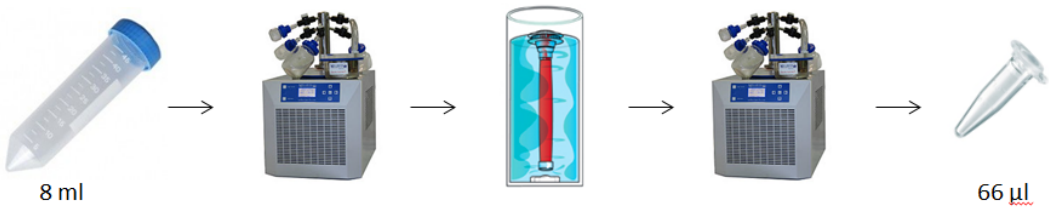

Figure 1. Human CSF was collected by a lumbar puncture (10ml on average), and 8ml were used for subsequent lyophilisation, dialysis, and lyophilisation again, and finally dissolved in 66µl sterile water, with a theoretical concentration factor of 120x.

ELISA

Tau and phospho-tau levels were measured using the MSD Phospho (Thr231)/Total Tau Multi-Spot assay (Meso Scale Discovery, USA) and analyzed using Sector Imager (Meso Scale Discovery, USA), according to the manufacturer's guidelines.
Amyloid-beta$_{40}$ and APP levels were measured using Human 6E10 and APPalpha/sAPPbeta Kits respectively (Meso Scale Discovery, USA) according to the manufacturer's instructions.

Western blot

Following perfusion with PBS, one half of the mouse brain was dissected into forebrain and brain stem and immediately frozen in liquid nitrogen or on dry ice. The brain tissue was homogenized using Ultraturrax T8 (IKA Labortechnik) in 1:10 weight:volume of TBS-Complete buffer containing 20 mM Tris pH 7.5 (Biomol), 137 mM NaCl (Merck) and 1 tablet complete mini protease inhibitor cocktail (Roche, Switzerland). This was followed by sonication (90% power, 10% cycle and 10 pulses) using Sonopuls (Bandelin, Germany). The homogenized samples were spun down at 5000 rpm for 30 min and the supernatant was collected and aliquoted.

7% Nupage® Bis Tris gel (Thermo Scientific, USA) was loaded with 5 µl Precision Plus Protein All Blue standard (Bio Rad, USA) and with the sample mix containing the protein, 4 µl Nupage LDS sample buffer, and sterile water up to 20 µl final volume. The gel was run at 125 V for 90 min. Next, samples were transferred on a PVDF membrane with the iblot gel transfer stack (Novex®, Life Technologies, USA) using the iblot (Invitrogen, USA) for 7 min. Next, unspecific binding epitopes were blocked with 5% non-fat milk in PBS-T for 1h at room temperature, followed by incubation with primary antibody overnight at 4°C on a shaker. After washing with PBS-T (3x5 min), the membrane was incubated with horseradish peroxidase (HRP) conjugated secondary antibody for 1h at room temperature. Then, membranes were washed three times with PBS-T (3x5 min), and detected by electrochemiluminescence (ECL) (GE Healthcare, USA) using Azure c300 Western blot imager (Azure Biosystems, USA). Images were analyzed using ImageJ (NIH, USA)

Quantification and statistical analysis

For quantification we used 8 to 10 brain sections, depending on the tissue quality. Sections were selected for each animal from the injected right (R) and lateral left (L) hemisphere at corresponding Bregma levels, spanning the hippocampus (starting anterior to the injection site at -1.8 mm and extending to -3.1 mm posterior), with at least 50 µm distance in between.

The hippocampal Aβ-plaque burden (the area occupied by all plaques as percent of the total area) was estimated for each section using ImageJ software. Pictures were transformed into 8-bit images, hippocampus was selected as a region of interest, threshold was set automatically and the area and mean grey value were measured. In order to analyse the effect of CSF inoculation on Aβ-plaque-burden, linear mixed-effects models were used. We thereby compared the injected to the non-injected hippocampal side. Aβ-plaque burden served as dependent variables, independent variables were hippocampal sides (injected vs. non-injected). Subject was treated as a random factor. Side was nested within time point and group. To achieve approximately normal distribution, Aβ-plaque burden values were log-transformed (zeros were replaced by half the smallest value). Results were expressed as geometric mean ratios (GMR) with corresponding 95% confidence intervals and p-values. A p-value < 0.05 was considered as significant. All analyses were done using R version 3.0.1 (R Foundation for Statistical Computing, Vienna, Austria).

For quantification of tau pathology, the number of AT8, AT100 and Gallyas positive NFTs was counted using the Cell counter plugin in ImageJ. Then average score from all sections per animal and per group was made. For the AT8 heatmap average tau pathology per Bregma level per group was calculated and manually colour graded using the Windows Paint program. The amounts of granular tau pathology in 3 hippocampal regions (CA1, CA3, dentate gyrus) at varying Bregma levels were qualitatively assessed by two independent researchers and an average score was obtained. Brain images that were used and modified are from the Mouse Brain Atlas (Franklin and Paxinos, Elsevier 2007). All group scores were compared using unpaired Student t-test. P values are reported when significant.

Grid test

Testing of the mice grid reflex and motor strength was performed on the grid test. For this purpose, animals were placed on a vertical mesh grid and the latency to fall off was measured during a maximum time of 180s. Mice were tested 3 times with at least 5 min interval in between trials, and an average score per day was made.

Object recognition test

To assess the impact of fragmented tau on short term memory, mice were tested in the object recognition test. After handling the animals first for a couple of days to reduce their stress level, they were placed in a squared open field box (48x48x40cm) under dim light conditions, and let freely explore it. Because the animals displayed initially some freezing behavior, the habituation phase was extended during 3 consecutive days for 15 min, until no signs of stress were present and they were freely moving into the box. The behavior was recorded using a video camera placed above the box. During the following two days, two identical objects were introduced at diagonal corners of the field, and mice were let explore them until a 20s exploration criteria for each was reached (Leger et al. 2013), for a maximum training duration of 10 min. Next day the animals' short term memory was tested by replacing one of the familiar objects with a novel one, and the time spent exploring each object during a period of 6 min was video recorded. Video scoring was done manually by a researcher blind to the genotype using VLC media player (VideoLAN, France), and as exploration criteria was used nose sniffing/touching of the object at a distance of 2 cm or less (Leger et al. 2013). For both training and test phases were used 10 cm high objects composed of the same material (Lego Duplo®, Billund, Denmark), and the position of the novel and familiar objects were randomized across groups.

References

Abraha, a et al., 2000. C-terminal inhibition of tau assembly in vitro and in Alzheimer's disease. *Journal of cell science*, 113 Pt 21, pp.3737–3745.

Ahmed, Z. et al., 2014. A novel in vivo model of tau propagation with rapid and progressive neurofibrillary tangle pathology: the pattern of spread is determined by connectivity, not proximity. *Acta neuropathologica*, 127(5), pp.667–83. Available at: http://www.pubmedcentral.nih.gov/articlerender.fcgi?artid=4252866&tool=pmcentrez&rendertype=abstract [Accessed December 22, 2014].

Albert, M.S. et al., 2011. The diagnosis of mild cognitive impairment due to Alzheimer's disease: recommendations from the National Institute on Aging-Alzheimer's Association workgroups on diagnostic guidelines for Alzheimer's disease. *Alzheimer's & dementia : the journal of the Alzheimer's Association*, 7(3), pp.270–279.

Allen, B. et al., 2002. Abundant Tau Filaments and Nonapoptotic Neurodegeneration in Transgenic Mice Expressing Human P301S Tau Protein. , 22(21), pp.9340–9351.

Alzheimer, A. et al., 1995. An English translation of Alzheimer's 1907 paper, "Uber eine eigenartige Erkankung der Hirnrinde". *Clinical anatomy (New York, N.Y.)*, 8(6), pp.429–431.

Asai, H. et al., 2015. Depletion of microglia and inhibition of exosome synthesis halt tau propagation. *Nature Neuroscience*, (October). Available at: http://www.nature.com/doifinder/10.1038/nn.4132.

Augustinack, J.C. et al., 2002. Specific tau phosphorylation sites correlate with severity of neuronal cytopathology in Alzheimer's disease. *Acta Neuropathologica*, 103(1), pp.26–35.

Barthélemy, N.R. et al., 2016. Tau Protein Quantification in Human Cerebrospinal Fluid by Targeted Mass Spectrometry at High Sequence Coverage Provides Insights into Its Primary Structure Heterogeneity. *Journal of Proteome Research*, p.acs.jproteome.5b01001. Available at: http://pubs.acs.org/doi/10.1021/acs.jproteome.5b01001.

Bi, M. et al., 2011. Tau-targeted immunization impedes progression of neurofibrillary histopathology in aged P301L tau transgenic mice. *PloS one*, 6(12), p.e26860.

Blennow, K. et al., 2010a. Cerebrospinal fluid and plasma biomarkers in Alzheimer disease. *Nature Reviews Neurology*, pp.1–14. Available at: http://dx.doi.org/10.1038/nrneurol.2010.4.

Blennow, K. et al., 2010b. Cerebrospinal fluid and plasma biomarkers in Alzheimer disease. *Nature Publishing Group*, 6(3), pp.131–144. Available at: http://dx.doi.org/10.1038/nrneurol.2010.4.

Blennow, K. et al., 2014. Clinical utility of cerebrospinal fluid biomarkers in the diagnosis of early Alzheimer's disease. *Alzheimer's & dementia : the journal of the Alzheimer's Association*, pp.1–12. Available at: http://www.ncbi.nlm.nih.gov/pubmed/24795085.

Blennow, K. et al., 1995. Tau protein in cerebrospinal fluid: a biochemical marker for axonal degeneration in Alzheimer disease? *Molecular and chemical neuropathology / sponsored by the International Society for Neurochemistry and the World Federation of Neurology and research groups on neurochemistry and cerebrospinal fluid*, 26(3), pp.231–245.

Blennow, K., Zetterberg, H. & Fagan, A.M., 2015. Fluid Biomarkers in Alzheimer Disease.

Blennow, K., Zetterberg, H. & Fagan, A.M., 2012. Fluid biomarkers in Alzheimer disease. *Cold Spring Harbor perspectives in medicine*, 2(9), p.a006221.
Bohm, K.J. et al., 1990. Effect of MAP 1, MAP 2, and tau-proteins on structural parameters of tubulin assemblies. *Acta histochemica. Supplementband*, 39, pp.357–364.
Boimel, M. et al., 2010. Efficacy and safety of immunization with phosphorylated tau against neurofibrillary tangles in mice. *Experimental neurology*, 224(2), pp.472–485.
Boluda, S. et al., 2014. Differential induction and spread of tau pathology in young PS19 tau transgenic mice following intracerebral injections of pathological tau from Alzheimer's disease or corticobasal degeneration brains. *Acta Neuropathologica*, 129, pp.221–237. Available at: http://link.springer.com/10.1007/s00401-014-1373-0.
Braak, H. et al., 2013. Intraneuronal tau aggregation precedes diffuse plaque deposition, but amyloid-?? changes occur before increases of tau in cerebrospinal fluid. *Acta Neuropathologica*, 126(5), pp.631–641.
Braak, H. et al., 1988. Silver impregnation of Alzheimer's neurofibrillary changes counterstained for basophilic material and lipofuscin pigment. *Stain technology*, 63(4), pp.197–200.
Braak, H. & Braak, E., 1997. Diagnostic criteria for neuropathologic assessment of Alzheimer's disease. *Neurobiology of aging*, 18(4 Suppl), pp.S85–8.
Braak, H. & Braak, E., 1991. Neuropathological stageing of Alzheimer-related changes. *Acta neuropathologica*, 82(4), pp.239–259.
Braak, H. & Del Tredici, K., 2015. The preclinical phase of the pathological process underlying sporadic Alzheimer's disease. *Brain : a journal of neurology*, 138(Pt 10), pp.2814–2833.
Brys, M. et al., 2009. Magnetic resonance imaging improves cerebrospinal fluid biomarkers in the early detection of Alzheimer's disease. *Journal of Alzheimer's disease : JAD*, 16(2), pp.351–362.
Bugiani, O. et al., 1999. Frontotemporal dementia and corticobasal degeneration in a family with a P301S mutation in tau. *Journal of neuropathology and experimental neurology*, 58(6), pp.667–677.
de Calignon, A. et al., 2012. Propagation of tau pathology in a model of early Alzheimer's disease. *Neuron*, 73(4), pp.685–97. Available at: http://www.pubmedcentral.nih.gov/articlerender.fcgi?artid=3292759&tool=pmcentrez&rendertype=abstract [Accessed July 22, 2014].
Cappai, R. & White, A.R., 1999. Amyloid beta. *The international journal of biochemistry & cell biology*, 31(9), pp.885–889.
Castellani, R.J. et al., 2004. Cerebral amyloid angiopathy : major contributor or decorative response to Alzheimer ' s disease pathogenesis. , 25, pp.599–602.
Castellano, J.M. et al., 2011. Human apoE isoforms differentially regulate brain amyloid-beta peptide clearance. *Science translational medicine*, 3(89), p.89ra57.
Chartier-Harlin, M.C. et al., 1991. Early-onset Alzheimer's disease caused by mutations at codon 717 of the beta-amyloid precursor protein gene. *Nature*, 353(6347), pp.844–846.
Ciryam, P. et al., 2013. Widespread Aggregation and Neurodegenerative Diseases Are Associated with Supersaturated Proteins. *Cell Reports*, 5(3), pp.781–790. Available at: http://dx.doi.org/10.1016/j.celrep.2013.09.043.
Clavaguera, F. et al., 2013. Brain homogenates from human tauopathies induce tau inclusions in mouse brain. *Proceedings of the National Academy of Sciences of the*

United States of America, 110(23), pp.9535–40. Available at: http://www.pubmedcentral.nih.gov/articlerender.fcgi?artid=3677441&tool=pmcentrez&rendertype=abstract [Accessed December 11, 2014].
Clavaguera, F. et al., 2015. Invited review : Prion-like transmission and spreading of tau pathology. , pp.47–58.
Clavaguera, F. et al., 2009. Transmission and spreading of tauopathy in transgenic mouse brain. , (June).
Clavaguera, F., Grueninger, F. & Tolnay, M., 2014. Intercellular transfer of tau aggregates and spreading of tau pathology: Implications for therapeutic strategies. *Neuropharmacology*, 76 Pt A, pp.9–15. Available at: http://www.ncbi.nlm.nih.gov/pubmed/24050961 [Accessed January 14, 2015].
Correas, I., Diaz-Nido, J. & Avila, J., 1992. Microtubule-associated protein tau is phosphorylated by protein kinase C on its tubulin binding domain. *The Journal of biological chemistry*, 267(22), pp.15721–15728.
Cummings, J.L., Disorders, C. & As-, R.D., 2004. Alzheimer's Disease. , pp.56–67.
Dickson, D.W. et al., 1992. Identification of normal and pathological aging in prospectively studied nondemented elderly humans. *Neurobiology of aging*, 13(1), pp.179–189.
Eisele, Y.S. et al., 2010. Peripherally Applied A β -Containing Inoculates Induce Cerebral β -Amyloidosis. , (October).
Fasulo, L. et al., 2000. The Neuronal Microtubule-Associated Protein Tau Is a Substrate for Caspase-3 and an Effector of Apoptosis.
Filipcik, P. et al., 2009. Cortical and hippocampal neurons from truncated tau transgenic rat express multiple markers of neurodegeneration. *Cellular and molecular neurobiology*, 29(6-7), pp.895–900. Available at: http://www.ncbi.nlm.nih.gov/pubmed/19263214.
Frisoni, G.B. et al., 2010. The clinical use of structural MRI in Alzheimer disease. *Nature reviews. Neurology*, 6(2), pp.67–77.
Fritschi, S.K. et al., 2014. Highly potent soluble amyloid-?? seeds in human Alzheimer brain but not cerebrospinal fluid. *Brain*, 137(11), pp.2909–2915.
Frost, B. & Diamond, M.I., 2009. Prion-like mechanisms in neurodegenerative diseases. Available at: http://dx.doi.org/10.1038/nrn2786.
Gallyas, F., 1971. Silver staining of Alzheimer's neurofibrillary changes by means of physical development. *Acta morphologica Academiae Scientiarum Hungaricae*, 19(1), pp.1–8.
García-Sierra, F. et al., 2012. Ubiquitin is associated with early truncation of tau protein at aspartic acid(421) during the maturation of neurofibrillary tangles in Alzheimer's disease. *Brain pathology (Zurich, Switzerland)*, 22(2), pp.240–50. Available at: http://www.ncbi.nlm.nih.gov/pubmed/21919991 [Accessed January 14, 2015].
Genin, E. et al., 2011. APOE and Alzheimer disease: a major gene with semi-dominant inheritance. *Molecular psychiatry*, 16(9), pp.903–907.
Goedert, M. et al., 1989. Multiple isoforms of human microtubule-associated protein tau: sequences and localization in neurofibrillary tangles of Alzheimer's disease. *Neuron*, 3(4), pp.519–526.
Goedert, M., Clavaguera, F. & Tolnay, M., 2010. The propagation of prion-like protein inclusions in neurodegenerative diseases. *Trends in neurosciences*, 33(7), pp.317–25. Available at: http://www.ncbi.nlm.nih.gov/pubmed/20493564 [Accessed October 27, 2014].
Götz, J. et al., 1995. Somatodendritic localization and hyperphosphorylation of tau protein in transgenic mice expressing the longest human brain tau isoform. *The EMBO journal*,

14(7), pp.1304–1313.
Guerreiro, R. & Hardy, J., 2014. Genetics of Alzheimer's disease. *Neurotherapeutics : the journal of the American Society for Experimental NeuroTherapeutics*, 11(4), pp.732–737.
Hardy, J. & Selkoe, D.J., 2002. The amyloid hypothesis of Alzheimer's disease: progress and problems on the road to therapeutics. *Science (New York, N.Y.)*, 297(5580), pp.353–356.
Harper, J.D. & Lansbury, P.T.J., 1997. Models of amyloid seeding in Alzheimer's disease and scrapie: mechanistic truths and physiological consequences of the time-dependent solubility of amyloid proteins. *Annual review of biochemistry*, 66, pp.385–407.
Holtzman, D.M. et al., 2011. Mapping the road forward in Alzheimer's disease. *Science translational medicine*, 3(114), p.114ps48.
Horowitz, P.M. et al., 2004. Early N-terminal changes and caspase-6 cleavage of tau in Alzheimer's disease. *The Journal of neuroscience : the official journal of the Society for Neuroscience*, 24(36), pp.7895–902. Available at: http://www.ncbi.nlm.nih.gov/pubmed/15356202 [Accessed January 14, 2015].
Horrocks, M.H. et al., 2016. Single-molecule imaging of individual amyloid protein aggregates in human biofluids. *ACS Chemical Neuroscience*, p.acschemneuro.5b00324. Available at: http://pubs.acs.org/doi/abs/10.1021/acschemneuro.5b00324.
Iba, M. et al., 2013. Synthetic tau fibrils mediate transmission of neurofibrillary tangles in a transgenic mouse model of Alzheimer's-like tauopathy. *The Journal of neuroscience : the official journal of the Society for Neuroscience*, 33(3), pp.1024–37. Available at: http://www.pubmedcentral.nih.gov/articlerender.fcgi?artid=3575082&tool=pmcentrez&rendertype=abstract [Accessed January 8, 2015].
Jack, C.R. et al., 2010. Hypothetical model of dynamic biomarkers of the Alzheimer's pathological cascade. *The Lancet Neurology*, 9(1), pp.119–128.
Jackson, S.J. et al., 2016. Short Fibrils Constitute the Major Species of Seed-Competent Tau in the Brains of Mice Transgenic for Human P301S Tau. , 36(3), pp.762–772.
Jaunmuktane, Z. et al., 2015. Evidence for human transmission of amyloid-β pathology and cerebral amyloid angiopathy. *Nature*, 525(7568), pp.247–50. Available at: http://www.ncbi.nlm.nih.gov/pubmed/26354483.
Jr, J.E.M. et al., 2013. Characterization of Novel CSF Tau and ptau Biomarkers for Alzheimer ' s Disease. , 8(10), pp.1–14.
Jucker, M. & Walker, L.C., 2011. Pathogenic protein seeding in Alzheimer disease and other neurodegenerative disorders. *Annals of neurology*, 70(4), pp.532–40. Available at: http://www.pubmedcentral.nih.gov/articlerender.fcgi?artid=3203752&tool=pmcentrez&rendertype=abstract [Accessed December 11, 2014].
Jucker, M. & Walker, L.C., 2013a. Self-propagation of pathogenic protein aggregates in neurodegenerative diseases. *Nature*, 501(7465), pp.45–51. Available at: http://www.pubmedcentral.nih.gov/articlerender.fcgi?artid=3963807&tool=pmcentrez&rendertype=abstract.
Jucker, M. & Walker, L.C., 2013b. Self-propagation of pathogenic protein aggregates in neurodegenerative diseases. *Nature*, 501(7465), pp.45–51. Available at: http://www.pubmedcentral.nih.gov/articlerender.fcgi?artid=3963807&tool=pmcentrez&rendertype=abstract [Accessed July 13, 2014].
Kahle, P.J. & De Strooper, B., 2003. Attack on amyloid. *EMBO reports*, 4(8), pp.747–751.
Kane, M.D. et al., 2000. Evidence for Seeding of [illegible] -Amyloid by Intracerebral Infusion of

Alzheimer Brain Extracts in ␣ -Amyloid Precursor Protein- Transgenic Mice. , 20(10), pp.3606–3611.
Kang, J.H. et al., 2013. Clinical utility and analytical challenges in measurement of cerebrospinal fluid amyloid-??1-42 and ?? proteins as alzheimer disease biomarkers. *Clinical Chemistry*, 59(6), pp.903–916.
Karch, C.M., Jeng, A.T. & Goate, A.M., 2012. Extracellular tau levels are influenced by variability in tau that is associated with tauopathies. *Journal of Biological Chemistry*, 287(51), pp.42751–42762.
Kelly, P.H. et al., 2003. Progressive age-related impairment of cognitive behavior in APP23 transgenic mice. *Neurobiology of aging*, 24(2), pp.365–378.
Klein, W.L., Krafft, G.A. & Finch, C.E., 2001. Targeting small Abeta oligomers: the solution to an Alzheimer's disease conundrum? *Trends in neurosciences*, 24(4), pp.219–224.
Lahiri, D.K., 2012. edited by Jennifer Sills Prions : A Piece of the Puzzle ? , 337(September), pp.1172–1173.
Lambert, M.A. et al., 2014. Estimating the burden of early onset dementia; systematic review of disease prevalence. *European journal of neurology*, 21(4), pp.563–569.
Langer, F. et al., 2011. Soluble Aβ seeds are potent inducers of cerebral β-amyloid deposition. *The Journal of neuroscience : the official journal of the Society for Neuroscience*, 31(41), pp.14488–95. Available at: http://www.pubmedcentral.nih.gov/articlerender.fcgi?artid=3229270&tool=pmcentrez&rendertype=abstract [Accessed January 9, 2015].
Lasagna-Reeves, C. a et al., 2012. Alzheimer brain-derived tau oligomers propagate pathology from endogenous tau. *Scientific reports*, 2, p.700. Available at: http://www.pubmedcentral.nih.gov/articlerender.fcgi?artid=3463004&tool=pmcentrez&rendertype=abstract [Accessed January 8, 2015].
Leger, M. et al., 2013. Object recognition test in mice. *Nature Protocols*, 8(12), pp.2531–2537. Available at: http://www.nature.com/doifinder/10.1038/nprot.2013.155.
Liu, L. et al., 2012. Trans-synaptic spread of tau pathology in vivo. *PloS one*, 7(2), p.e31302. Available at: http://www.pubmedcentral.nih.gov/articlerender.fcgi?artid=3270029&tool=pmcentrez&rendertype=abstract [Accessed November 3, 2014].
Maia, L.F. et al., 2013. Changes in Amyloid- b and Tau in the Cerebrospinal Fluid of Transgenic Mice Overexpressing Amyloid Precursor Protein. , 5(194).
Mandelkow, E.M. & Mandelkow, E., 2011. Biochemistry and cell biology of Tau protein in neurofibrillary degeneration. *Cold Spring Harbor Perspectives in Biology*, 3(10), pp.1–25.
Marchant, N.L. et al., 2012. Cerebrovascular disease, beta-amyloid, and cognition in aging. *Neurobiology of aging*, 33(5), pp.1006.e25–36.
Masters, C.L. et al., 1985. Amyloid plaque core protein in Alzheimer disease and Down syndrome. *Proceedings of the National Academy of Sciences of the United States of America*, 82(12), pp.4245–4249.
Masters, C.L. et al., 2006. Molecular mechanisms for Alzheimer's disease: implications for neuroimaging and therapeutics. *Journal of neurochemistry*, 97(6), pp.1700–1725.
McKhann, G.M. et al., 2011. The diagnosis of dementia due to Alzheimer's disease: recommendations from the National Institute on Aging-Alzheimer's Association workgroups on diagnostic guidelines for Alzheimer's disease. *Alzheimer's & dementia : the journal of the Alzheimer's Association*, 7(3), pp.263–269.

Mena, R. et al., 1996. Staging the pathological assembly of truncated tau protein into paired helical filaments in Alzheimer's disease. *Acta neuropathologica*, 91(6), pp.633–641.
Meredith, J.E. et al., 2013. Characterization of novel CSF Tau and ptau biomarkers for Alzheimer's disease. *PloS one*, 8(10), p.e76523. Available at: http://www.pubmedcentral.nih.gov/articlerender.fcgi?artid=3792042&tool=pmcentrez&rendertype=abstract [Accessed January 14, 2015].
Meyer-Luehmann, M. et al., 2006. Exogenous induction of cerebral beta-amyloidogenesis is governed by agent and host. *Science (New York, N.Y.)*, 313(2006), pp.1781–1784.
Meyer-luehmann, M. et al., 2006. Exogenous Induction of Cerebral by Agent and Host. , 313(September), pp.1781–1784.
Mondragón-Rodríguez, S. et al., 2008. Cleavage and conformational changes of tau protein follow phosphorylation during Alzheimer's disease. *International journal of experimental pathology*, 89(2), pp.81–90. Available at: http://www.pubmedcentral.nih.gov/articlerender.fcgi?artid=2525766&tool=pmcentrez&rendertype=abstract [Accessed January 12, 2015].
Mouton, P.R. et al., 1998. Cognitive decline strongly correlates with cortical atrophy in Alzheimer's dementia. *Neurobiology of aging*, 19(5), pp.371–377.
Muller, U., Winter, P. & Graeber, M.B., 2013. A presenilin 1 mutation in the first case of Alzheimer's disease. *The Lancet. Neurology*, 12(2), pp.129–130.
Nelson, P.T. et al., 2012. Correlation of Alzheimer disease neuropathologic changes with cognitive status: a review of the literature. *Journal of neuropathology and experimental neurology*, 71(5), pp.362–381.
Neumann, M. et al., 2009. Abundant FUS-immunoreactive pathology in neuronal intermediate filament inclusion disease. *Acta Neuropathologica*, 118(5), pp.605–616.
Ono, K. et al., 2007. Cerebrospinal fluid of Alzheimer's disease and dementia with Lewy bodies patients enhances alpha-synuclein fibril formation in vitro. *Experimental neurology*, 203(2), pp.579–83. Available at: http://www.ncbi.nlm.nih.gov/pubmed/17011551.
Ozcelik, S. et al., 2016. Co-expression of truncated and full-length tau induces severe neurotoxicity. *Mol Psychiatry*. Available at: http://dx.doi.org/10.1038/mp.2015.228.
Ozcelik, S. et al., 2013. Rapamycin Attenuates the Progression of Tau Pathology in P301S Tau Transgenic Mice. *PLoS ONE*, 8(5), p.e62459. Available at: http://dx.doi.org/10.1371%2Fjournal.pone.0062459.
Pachet, A., Astner, K. & Brown, L., 2010. Clinical utility of the mini-mental status examination when assessing decision-making capacity. *Journal of geriatric psychiatry and neurology*, 23(1), pp.3–8.
Perani, D. et al., 2014. Validation of an optimized SPM procedure for FDG-PET in dementia diagnosis in a clinical setting. *NeuroImage. Clinical*, 6, pp.445–454.
Pooler, A.M. et al., 2013. Propagation of tau pathology in Alzheimer's disease: identification of novel therapeutic targets. *Alzheimer's research & therapy*, 5(5), p.49. Available at: http://alzres.com/content/5/5/49.
Pooler, A.M., Noble, W. & Hanger, D.P., 2014. A role for tau at the synapse in Alzheimer's disease pathogenesis. *Neuropharmacology*, 76(PART A), pp.1–8. Available at: http://dx.doi.org/10.1016/j.neuropharm.2013.09.018.
Prince, M. et al., 2013. The global prevalence of dementia: a systematic review and metaanalysis. *Alzheimer's & dementia : the journal of the Alzheimer's Association*, 9(1), pp.63–75.e2.

Rohn, T.T. et al., 2002. Caspase Activation in the Alzheimer's Disease Brain: Tortuous and Torturous. *Drug news & perspectives*, 15(9), pp.549–557.
Rosen, R.F. et al., 2010. SDS-PAGE / Immunoblot Detection of Aβ Multimers in Human Cortical Tissue Homogenates using Antigen-Epitope Retrieval Part 1 : Preparation of clarified tissue homogenates Part 2 : SDS-PAGE Sample preparation Part 3 : SDS-PAGE Gel electrophoresis Part 4 : T. , pp.4–7.
Saman, S. et al., 2012. Exosome-associated tau is secreted in tauopathy models and is selectively phosphorylated in cerebrospinal fluid in early Alzheimer disease. *Journal of Biological Chemistry*, 287(6), pp.3842–3849.
Samgard, K. et al., 2010. Cerebrospinal fluid total tau as a marker of Alzheimer's disease intensity. *International journal of geriatric psychiatry*, 25(4), pp.403–410.
Scheltens, P. et al., 2016. Alzheimer's disease. *Lancet (London, England)*.
Scheuner, D. et al., 1996. Secreted amyloid beta-protein similar to that in the senile plaques of Alzheimer's disease is increased in vivo by the presenilin 1 and 2 and APP mutations linked to familial Alzheimer's disease. *Nature medicine*, 2(8), pp.864–870.
Selkoe, D.J. et al., 1986. Isolation of low-molecular-weight proteins from amyloid plaque fibers in Alzheimer's disease. *Journal of neurochemistry*, 46(6), pp.1820–1834.
Shammas, S.L. et al., 2015. A mechanistic model of tau amyloid aggregation based on direct observation of oligomers. *Nature communications*, 6, p.7025. Available at: http://www.nature.com/ncomms/2015/150430/ncomms8025/full/ncomms8025.html.
Shaw, L.M. et al., 2009. Cerebrospinal fluid biomarker signature in Alzheimer's disease neuroimaging initiative subjects. *Annals of neurology*, 65(4), pp.403–413.
Skachokova, Z. et al., 2015. Amyloid-beta in the Cerebrospinal Fluid of APP Transgenic Mice Does not Show Prion-like Properties. *Current Alzheimer research*, 12(9), pp.886–891.
Small, S.A. & Duff, K., 2008. Linking Abeta and tau in late-onset Alzheimer's disease: a dual pathway hypothesis. *Neuron*, 60(4), pp.534–542.
Stamer, K. et al., 2002. Tau blocks traffic of organelles, neurofilaments, and APP vesicles in neurons and enhances oxidative stress. *The Journal of cell biology*, 156(6), pp.1051–1063.
Stancu, I.-C. et al., 2015. Templated misfolding of Tau by prion-like seeding along neuronal connections impairs neuronal network function and associated behavioral outcomes in Tau transgenic mice. *Acta Neuropathologica*. Available at: http://link.springer.com/10.1007/s00401-015-1413-4.
Sturchler-Pierrat, C. et al., 1997. Two amyloid precursor protein transgenic mouse models with Alzheimer disease-like pathology. *Proceedings of the National Academy of Sciences of the United States of America*, 94(24), pp.13287–13292.
Tagliavini, F. et al., 1988. Preamyloid deposits in the cerebral cortex of patients with Alzheimer's disease and nondemented individuals. *Neuroscience letters*, 93(2-3), pp.191–196.
Takashima, A., 2013. Tauopathies and tau oligomers. *Journal of Alzheimer's disease : JAD*, 37(3), pp.565–568.
Tapiola, T. et al., 2009. Cerebrospinal fluid {beta}-amyloid 42 and tau proteins as biomarkers of Alzheimer-type pathologic changes in the brain. *Archives of neurology*, 66(3), pp.382–389.
Terry, R.D. et al., 1991. Physical basis of cognitive alterations in Alzheimer's disease: synapse loss is the major correlate of cognitive impairment. *Annals of neurology*, 30(4), pp.572–580.

Wallin, a K. et al., 2006. CSF biomarkers for Alzheimer's Disease: levels of beta-amyloid, tau, phosphorylated tau relate to clinical symptoms and survival. *Dementia and geriatric cognitive disorders*, 21(3), pp.131–8. Available at: http://www.ncbi.nlm.nih.gov/pubmed/16391474 [Accessed January 14, 2015].

Wang, Y. et al., 2012. Will Posttranslational Modifications of Brain Proteins Provide Novel Serological Markers for Dementias ? , 2012.

Watts, J.C. et al., 2014. Serial propagation of distinct strains of Abeta prions from Alzheimer's disease patients. *Proceedings of the National Academy of Sciences of the United States of America*, 111(28), pp.10323–10328.

Weingarten, M.D. et al., 1975. A protein factor essential for microtubule assembly. *Proceedings of the National Academy of Sciences of the United States of America*, 72(5), pp.1858–1862.

Winkler, D.T. et al., 2010. Rapid cerebral amyloid binding by Aβ antibodies infused into β-amyloid precursor protein transgenic mice. *Biological psychiatry*, 68(10), pp.971–4. Available at: http://www.ncbi.nlm.nih.gov/pubmed/20359696 [Accessed January 14, 2015].

Yamada, K. et al., 2011. In vivo microdialysis reveals age-dependent decrease of brain interstitial fluid tau levels in P301S human tau transgenic mice. *The Journal of neuroscience : the official journal of the Society for Neuroscience*, 31(37), pp.13110–7. Available at: http://www.ncbi.nlm.nih.gov/pubmed/21917794 [Accessed January 9, 2015].

Yanamandra, K. et al., 2013. Anti-tau antibodies that block tau aggregate seeding invitro markedly decrease pathology and improve cognition in vivo. *Neuron*, 80(2), pp.402–414. Available at: http://dx.doi.org/10.1016/j.neuron.2013.07.046.

Zilka, N. et al., 2006. Truncated tau from sporadic Alzheimer's disease suffices to drive neurofibrillary degeneration in vivo. *FEBS letters*, 580(15), pp.3582–8. Available at: http://www.ncbi.nlm.nih.gov/pubmed/16753151 [Accessed January 5, 2015].

List of abbreviations

aa	amino acids
Aβ	amyloid beta
Aβ 40	amyloid beta 40
Aβ 42	amyloid beta 42
AD	Alzheimer's disease
APP	amyloid precursor protein
Asp	aspartic acid
C-terminal	carboxy terminal
CAA	cerebral amyloid angiopathy
CBD	corticobasal degeneration
CSF	cerebrospinal fluid
DNA	deoxyribonucleic acid
ECL	enhanced chemiluminescence
g	gram
GA	golgi apparatus
GSK3	glycogen synthase kinase 3
FTD	frontotemporal dementia
H	hour
IHC	immunohistochemistry
IFL	immunofluorescence
ISF	interstitial fluid
kDa	kilo daltons
MAPK	microtubule associated protein kinase
MAPT	microtubule associated protein tau
µm	micrometer(s)
mm	millimeter(s)
MCI	mild cognitive impairment
MTBR	microtubule binding region (of tau)
N-terminal	amino terminal
nm	nanometer(s)
nmol	nanomolar
NFTs	neurofibrillary tangles
PBS	phosphate buffered saline
PCR	polymerase chain reaction
PiD	Pick's disease
PSEN1	presenelin 1
PSP	progressive supranuclear palsy
s	second(s)
Tau62	transgenic mice expressing truncated tau
tTs	tetracycline controlled transcriptional silencer element
VAMP2	vesicle associated membrane protein 2

Acknowledgements

I would like to thank David Winkler for his guidance, help and support throughout the 4 years of my PhD.
Many thanks to Markus Rüegg and Bernhard Bettler for taking part in my thesis committee, and taking their time to evaluate my performance.
I am grateful to Markus Tolnay and Stephan Frank for their support, and to our collaborator Andreas Monsch for providing us with CSF samples.
I also thank my colleagues Sefika, Freddy, Lisa, Gabriel, Björn, Jürgen, Florence, Alphonse, Sabine, Christian and many more from the Institute of Pathology for their help and advices, and providing me with a really enjoyable work environment.
I am grateful to the animal caretakers at USB for their dedication and good work.
A big благодаря to my parents for their support in my endless education.
Merci, danke, grazias, dziekuje to all my old and new Basel friends, to the Engelberg ski crew, and the Ticino hiking group. I hope that the Swiss Alps will never stop inspiring people in their quest for knowledge and advancement!